From the
Institute for Cardiovascular Prevention
of the Ludwig-Maximilians-Universität München
Director: Univ.-Prof. Dr. med. Christian Weber

The impact of the circadian clock on myeloid cell recruitment during atherosclerosis

DISSERTATION
zum Erwerb des Doctor of Philosophy (Ph.D.)
an der Medizinischen Fakultät der
Ludwig-Maximilians-Universität München

submitted by

Carla Winter

from

Geesthacht, Germany

2018

Supervisor:	Univ.-Prof. Dr. Dr. med. Oliver Soehnlein
Second evaluator:	Prof. Dr. Christoph Scheiermann
Dean:	Prof. Dr. med. dent. Reinhard Hickel
Date of oral defence:	19.11.2018

Abstract

Cardiovascular complications, as a consequence of atherosclerosis, are the leading cause of mortality worldwide. Their onset exhibits a circadian incidence with a peak in the morning hours, thus indicating a circadian susceptibility to cardiovascular diseases. Circadian rhythmicity is controlled by the circadian clock and comprises rhythmic changes in physiological processes, immune cell functionality, and immune cell trafficking, hence leading to time-dependent susceptibilities to diseases and its outcomes.

Here, we hypothesized a circadian control of leukocyte recruitment during early atherosclerotic lesion development. We observed rhythmic myeloid cell recruitment to atherosclerotic lesions in hypercholesterolemic *Apoe*$^{-/-}$ mice with elevated myeloid cell recruitment primarily during the transition from the activity to the resting phase. This phenotype was abolished in mice lacking the clock gene *Bmal1* in myeloid but not endothelial cells, highlighting a leukocyte-intrinsic regulatory mechanism. Specifically, myeloid cell derived CCL2 exhibited diurnal rhythmicity and blockage of CCL2-CCR2 signaling abrogated rhythmicity in arterial leukocyte recruitment. In contrast, myeloid cell recruitment in the microcirculation peaked during the early activity phase and CCL2-CCR2 signaling blockage had only minor effects. Subsequently, timed pharmacological CCR2 neutralization during the activity phase ameliorated atherosclerosis without disturbing microvascular recruitment, while timed treatment during the resting phase did not affect the development of atherosclerotic lesions.

Overall, we discovered a time-dependent leukocyte recruitment pattern to atherosclerotic lesions and with the identification of its underlying mechanism successfully established a novel chrono-pharmacological treatment strategy (Figure 1).

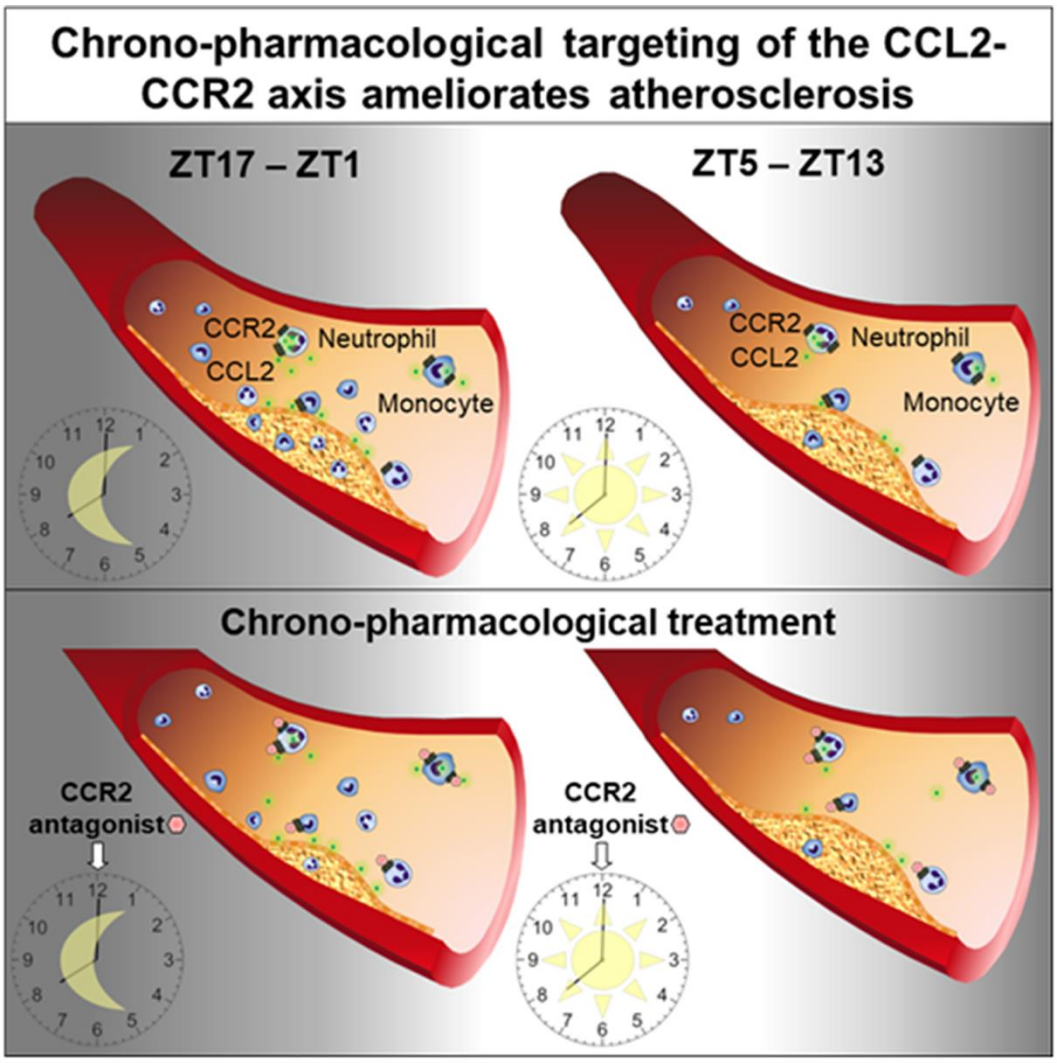

Figure 1: **Chrono-pharmacological targeting of the CCL2-CCR2 axis ameliorates atherosclerosis**

Myeloid cell recruitment to atherosclerotic lesions exhibited rhythmicity with a peak between ZT17 and ZT1 and a through between ZT5 and ZT13. Timed activation of the CCL2-CCR2 axis regulated its rhythmicity. Blockage of CCR2 signaling, when leukocyte recruitment was at its highest, successfully ameliorated atherosclerosis, while treatment when leukocyte recruitment was at its lowest had no effect. ZT: Zeitgeber time. (Illustration from Winter et al. 2018)

Table of contents

Table of figures and tables

Abbreviations

µl	microliter
ACTH	adrenocorticotropic hormone
adr.rec.ant.	α-adrenergic receptor antagonists
ALDH	aldehyde dehydrogenase
Apoe	apolipoprotein E
bHLH	basic-helix-loop-helix
BMAL1	brain and muscle ARNTL-like protein 1
BMX	bone marrow x promoter
BSA	bovine serum albumin
CAD	coronary artery disease
CCG	clock controlled genes
CCR	CC chemokine receptor
CD	circadian time
CD	cluster of differentiation
CLOCK	circadian locomotor output cycles kaput
CRY	cryptochrome
CT	circadian time
CTX	cyclophosphamide
CXCR	CXC chemokine receptor
DAMP	damage-associated molecular pattern
DBP	albumin D-box binding protein
DC	dendritic cell

DMSO	dimethyl sulfoxide
DNA	deoxyribonucleic acid
EDTA	ethylenediaminetetraacetic acid
FBS	fetal bovine serum
FSC	forward scattered
GR	glucocorticoid receptors
GRE	glucocorticoid-response elements
h	hours
HBSS	hank‘s balanced salt solution
H&E	hematoxylin and eosin staining
HEPES	4-(2-hydroxyethyl)-1-piperazineethanesulfonic acid
HFD	high fat diet
HPA axis	hypothalamic-pituitary-adrenal axis
HRP	horseradish peroxidase
HSC	haematopoietic stem cell
HSPC	haematopoietic stem and progenitor cell
ICAM1	intercellular adhesion molecule-1
IFN-γ	interferon- γ
IL	interleukin
i.p.	intraperitoneal
LC-MS	liquid chromatography–mass spectrometry
LDL	low-density lipoprotein
LDLR	low density lipoprotein (LDL) receptor

LFA1	lymphocyte function-associated antigen 1
LPS	lipopolysaccharide
Lyz2	lysozyme 2
Mac1	macrophage antigen 1
min	minutes
ml	milliliter
MMP	matrix metalloproteinase
NETs	neutrophil extra-cellular traps
NFIL3	nuclear factor interleukin 3
ng	nanogram
NTP	nucleotide triphosphates
oxLDL	oxidized LDL
PAI-1	plasminogen activator inhibitor-1
PAMP	pathogen-associated molecular pattern
PAS	period-ARNT-single-minded
PBS	phosphate-buffered saline
PER	period
PFA	paraformaldehyd
PSGL1	P-selectin glycoprotein ligand 1
REV-ERBα	reverse erythroblastosis virus-α
ROREs	receptor-related orphan receptor response elements
RORα	retinoic acid receptor-related orphan receptor-α
ROS	reactive oxygen species

rpm	rounds per minute
RPMI	roswell park memorial Institute
RT	room temperature
S	seconds
SCN	suprachiasmatic nuclei
SEM	standard error of mean
SSC	side scattered
Timp	tissue inhibitor of metalloproteinases
Tlr	toll like receptor
TNF α	tumor necrosis factor-α
VCAM1	vascular cell adhesion molecule-1
VLA4	very late antigen 4
vsmc	vascular smooth muscle cells
vWF	von-willebrand-factor
ZT	Zeitgeber time

1. Introduction

1.1 Atherosclerosis

Atherosclerosis, the most common type of arteriosclerosis, describes a chronic inflammatory disorder leading to cardiovascular diseases. The main clinical manifestations are coronary artery disease (CAD) and cerebrovascular disease whose clinical outcome has severe life-threatening consequences. Although treatment and prevention of associated risk factors such as hyperlipidemia, smoking, hypertension, diabetes, and obesity aim to reduce the development of the disease, CAD associated to atherosclerosis are still the leading cause of mortality worldwide (Roth et al. 2015).

Atherosclerosis affects large and medium-sized arteries. Arteries consist of three major layers. The outermost layer is the tunica adventitia and it is characterized by loose connective tissue, nerves, and blood vessels. The external elastic layer separates the tunica adventitia from the middle layer called tunica media. Multiple layers of smooth muscle cells embedded in elastic tissue form the tunica media and allow vasoconstriction or vasodilation. The internal elastic layer separates the innermost layer tunica intima from the tunica media (Figure 2). Development of atherosclerosis occurs in the tunica intima, which consists of endothelial cells and some individual smooth muscle cells located within the intimal extracellular matrix. Atherogenesis is initiated by disturbed blood flow at regions of curvature, bifurcation, and branching points of arterial vessels. Disturbed blood flow induces low or high oscillatory shear stress on endothelial cells and modifies endothelial gene expression. Hence, the resulting altered endothelial structure and function favors the development of atherosclerosis (Chiu et al. 2011). Activated and dysfunctional endothelial cells express adhesion molecules and different chemokines to facilitate adhesion of leukocytes, lymphocytes, and activated platelets (Iiyama et al. 1999; Sakai et al. 1997; Hansson et al. 2011; Huo et al. 2003; Zernecke et al. 2008). Additionally, the permeability of blood vessels for lipid components in the plasma, such as low-density lipoproteins (LDL), increases. LDL particles function as cholesterol transporters in the

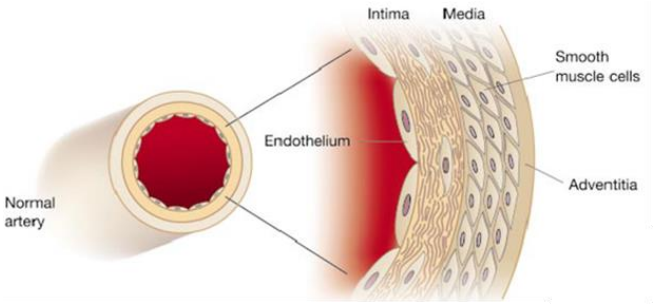

Figure 2: Structure of arterial walls

Arterial walls are surrounded by supportive tissue called adventitia. The following media regulates vasoconstriction or vasodilation. Subsequently, the intima, the innermost layer, defines the barrier to the blood. (modified illustration from Libby et al. 2002)

circulation. They contain esterified cholesterol and triglycerides surrounded by phospholipids, free cholesterol, and apolipoproteins. Their components bind to proteoglycans of the extracellular matrix in the subendothelial space through ionic interactions, hence facilitating LDL particle accumulation (Tabas et al. 2007). Glycation or oxidative modifications by myeloperoxidases or lipoxygenases derived from neutrophils or macrophages alter retained LDL particles. Modified LDL particles activate endothelial cells and macrophages, thus upregulating expression of adhesion molecules and chemokines to promote further leukocyte recruitment to atherosclerotic lesions.

Leukocytes recruited to atherosclerotic lesions contribute to lesion development in distinct ways (Figure 3). Neutrophils release their granule proteins such as myeloperoxidase, azurocidin, and proteinase-3 upon stimulation, thus triggering monocyte recruitment, endothelial dysfunction, macrophage polarization, and foam cell formation (Taekema-Roelvink et al. 2001). Recruited monocytes enter lesions, reside within the intima and differentiate into macrophages upon stimulation with the macrophage-colony stimulating factor. Macrophages uptake modified LDL particles by scavenger receptors (such as CD204 and CD36), whose cholesterol esters and free cholesterol content gets hydrolyzed in their lysosomes (Kunjathoor et al. 2002). The intracellular accumulation of the resulting lipids promotes accumulation of lipid droplets, thus turning macrophages into foam cells (Moore et al. 2011). This commonly known process describes the transition from early atherosclerotic lesions into so called fatty streaks.

Over a longer period of time these fatty streaks progress into mature atherosclerotic lesions with accumulating inflammatory-cell subsets and extracellular lipids in their central region surrounded by a subendothelial fibrous cap. Smooth muscle cells form the fibrous cap and promote plaque stability by producing elastin, collagen, and other matrix components. Subsequently, the pro-inflammatory environment triggers cell death of macrophages and smooth muscle cells (Kyaw et al. 2013). Continuous accumulation of free cholesterol in macrophages causes cellular stress, thus leading to the induction of apoptosis. Phagocytes clear apoptotic cell bodies in a process defined as efferocytosis. However, during advanced atherosclerosis apoptotic cells undergo secondary necrosis due to impaired efferocytosis. Hence, elevated apoptosis and necrosis in combination with impaired efferocytosis contribute to the necrotic core formation and expansion. Furthermore, apoptosis of smooth muscle cells induced by pro-inflammatory cytokines reduces the production of extracellular matrix components and leads to fibrous cap thinning (Clarke et al. 2006). Further mechanical weakening of the fibrous cap due to extracellular matrix degradation by metalloproteinases induces the degradation of the fibrous cap, thus favoring plaque rupture. During plaque rupture released pro-coagulant and pro-thrombotic contents from the lesion trigger thrombus

formation. Subsequently, oxygen and nutrient supply of the surrounding tissue is disrupted and can induce clinical outcomes such myocardial infarction, stroke or peripheral artery disease.

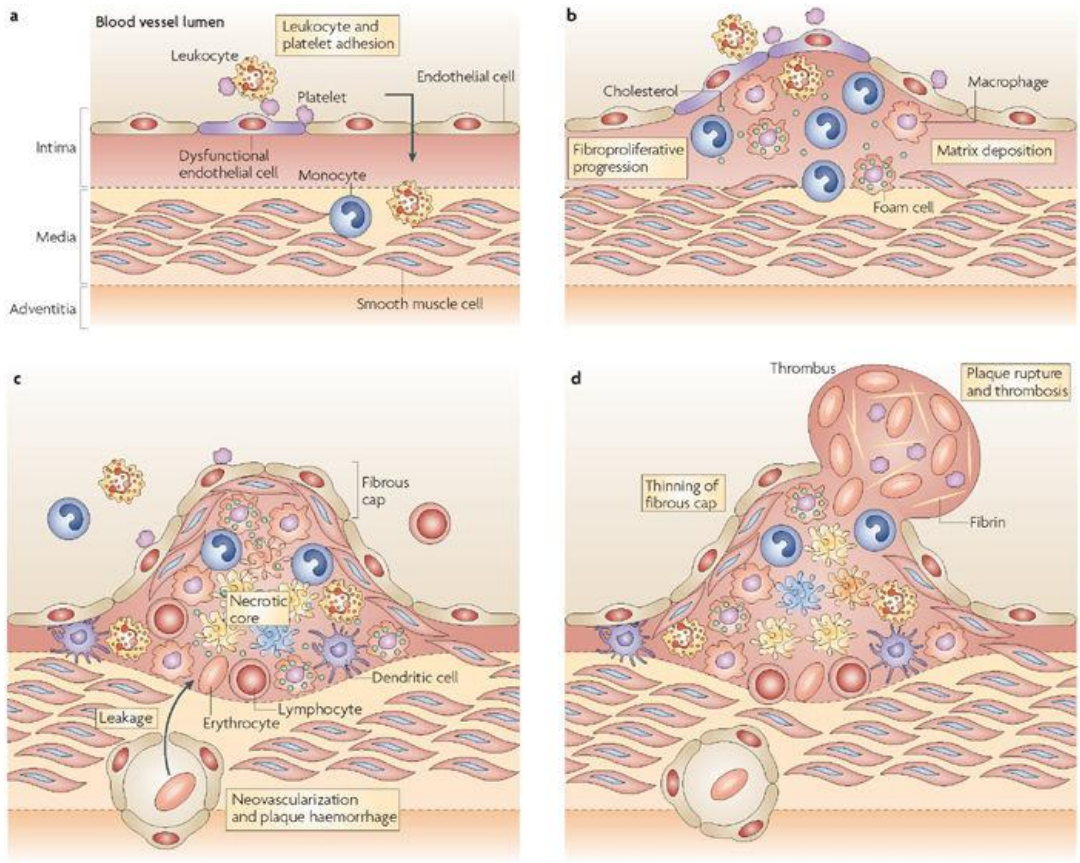

Figure 3: Development of atherosclerosis

a) Atherogenesis is initiated by recruitment of leukocytes and platelets to activated endothelial cells. b) Lesional monocytes uptake lipids and give rise to foam cells. Further immune cells transmigrate into the lesion area and consistently produce pro-inflammatory cytokines, thus triggering matrix deposition and fibroproliferative progression. c) A fibrous cap containing matrix and smooth muscle cell layer forms. Underneath has been established a necrotic core due to macrophage and smooth muscle cell apoptosis as well as impaired efferocytosis. Furthermore, neovascularization might occur within the plaque and rupture of these neovessels leads to plaque haemorrhage. d) Excessive expansion of the necrotic core and thinning of the fibrous reduce the stability of the atherosclerotic plaque. Eventually, the plaque ruptures and the resulting thrombus formation might cause myocardial infarction or stroke. (Illustration from Weber et al., 2008)

1.2 Myeloid cell recruitment to inflamed tissue

1.2.1 Myeloid cells

Myeloid cells are the most abundant haematopoietic cells in the human body. They originate from multipotent haematopoietic stem cells (HSCs) in the bone marrow and comprise granulocytes, monocytes, mast cells, erythrocytes, megakaryocytes or macrophages.

1.2.1.1 Monocytes

Monocytes are mononuclear cells of myeloid origin, functioning as immune effector cells of the innate immune response. In mice, monocytes represent up to 4 %, and in humans up to 10 % of leukocytes in blood (Auffrey et al. 2009). Two functionally distinct subsets of monocytes exist in mice, known as inflammatory/classical ($Ly6C^{high}$) and anti-inflammatory/non-classical ($Ly6C^{low}$) monocytes.

Classical monocytes are described as inflammatory cells due to their high expression of tumor necrosis factor (TNF)-α and interleukin (IL)-1 during inflammation. At site of inflammation they act as precursors of peripheral mononuclear phagocytes, including inflammatory dendritic cells (DCs) or macrophages (Ginhoux et al. 2014). Upon stimulation, classical monocytes secrete inflammatory cytokines resulting in immune activation, bacterial clearance, and induction of tissue damage (Graham et al. 2015).

In contrast, non-classical monocytes are known as patrolling cells of the vasculature and participate in resolution of inflammation (Nahrendorf et al. 2007). Their patrolling behavior allows them to rapidly invade damaged or infected tissue (Auffray et al. 2007). At site of inflammation non-classical monocytes initiate the innate immune response but also resolution of inflammation by promoting myofibroblast accumulation, angiogenesis, and deposition of collagen (Auffrey et al. 2007; Nahrendorf et al. 2007).

1.2.1.2 Neutrophils

Neutrophils are short-lived, polymorphonuclear leukocytes and represent the most abundant immune cell population in human blood. In mice, about 10-25% of circulating leukocytes are neutrophils (Doeing et al. 2003). They act in the first line of host defense against invading pathogens but also as key mediators of sterile tissue injury. During terminal granulopoiesis in the bone marrow up to 700 proteins including serine proteases, myeloperoxidase or matrix metalloproteinases (MMPs) are produced and stored in granules of neutrophils (Rorvig et al.

2013). Neutrophils exhibit an antimicrobial activity through the production and release of reactive oxygen species (ROS), antimicrobial peptides or DNA structures named neutrophil extra-cellular traps (NETs), which are covered with granule proteins and histones to trap and eliminate bacteria. Besides their microbicidal function, activated neutrophils release inflammatory signals (alarmins) to initiate an inflammatory response, thus contributing to the recruitment and activation of monocytes, macrophages, and dendritic cell subsets.

1.2.2 Leukocyte recruitment cascade

Leukocyte recruitment during inflammation depends on the ability of leukocytes to track, adhere, and transmigrate into inflamed tissue. A multistep cascade including capturing, rolling, arrest, crawling, and transendothelial migration guides leukocytes across the barrier of the blood vessel wall (Vestweber et al. 2015). Adhesion molecules expressed on endothelial cells or leukocytes play an essential role during this leukocyte recruitment cascade (Figure 4).

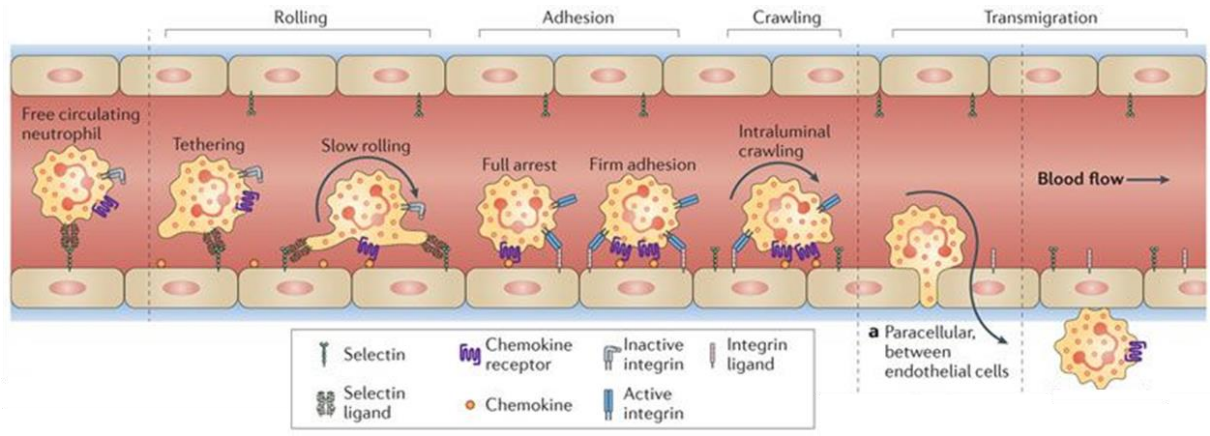

Figure 4: Leukocyte recruitment cascade. Distinct adhesion molecules regulate rolling, adhesion, crawling, and finally transmigration of leukocytes into tissue. (Illustration from Kolaczkowska et al. 2013)

1.2.2.1 Leukocyte rolling

The first step of myeloid cell recruitment involves recognition of signals released from inflamed or infected tissues by circulating leukocytes. Pathogens or damaged cells in the inflamed tissue release pathogen-associated molecular patterns (PAMPs) or damage-associated molecular patterns (DAMPs), thus activating resident immune cells. Production of cytokines and other pro-inflammatory mediators stimulates endothelial cells and induces

upregulation of E-selectins and P-selectins on their cell surface. Leukocytes express P-selectin glycoprotein ligand 1 (PSGL1) that binds to selectins expressed on endothelial cells to mediate leukocyte rolling (Spertini et al. 1996). Additionally, L-selectin on leukocytes facilitates leukocyte-leukocyte and leukocyte-endothelium interactions by binding to PSGL1 expressed on already adherent leukocytes or endothelial cells, a process known as secondary leukocyte capturing (Da Costa Martins et al. 2007; Ley et al. 2007).

Furthermore, leukocyte rolling is mediated by integrins. Integrins consist of transmembrane heterodimers with one α-subunit and one β-subunit. Up to today, 24 different integrin receptors formed by combinations out of 18 α-subunits and 8 β-subunits are known (Campdell et al. 2011). The most important integrins involved in leukocyte recruitment are lymphocyte function-associated antigen 1 (LFA1, αLβ2), macrophage antigen 1 (Mac1, αMβ2), and very late antigen 4 (VLA4, α4β1) (Vestweber et al. 2015).
Binding of PSGL1 to selectins triggers integrin activation. Subsequently, activated VLA4 and LFA1 switch to their intermediate affinity conformation, thus promoting leukocyte rolling by binding to members of the immunoglobulin superfamily, such as intercellular adhesion molecule-1 (ICAM1) or vascular cell adhesion molecule-1 (VCAM1), on endothelial cells.

1.2.2.2 Leukocyte arrest

Rolling leukocytes are able to sense immobilized chemokines on endothelial cells by their chemokine receptors. Chemokines and other chemoattractants are produced by inflammatory cells or endothelial cells. While endothelial cells directly release or deposit their chemokines on their cell surface, chemoattractants, produced by inflammatory cells in the surrounding tissue, are transported via transcytosis through endothelial cells to their cell surface (Mordelet et al. 2005). On the cell-surface, chemokines bind selectively to subsets of glycosaminoglycans, thus locally defined glycosaminoglycan patterns determine side specific chemokine presentation (Witt et al. 1994; Kuschert et al. 1999; de Paz et al. 2007). Furthermore, distinct patterns of chemokine presentation define functionality and hierarchy of chemokines and their receptors during leukocyte arrest (Weber et al. 1999). Overall, chemokine binding to their chemokine receptor on leukocytes activates integrins via inside-out signaling. Integrins undergo a transition from low affinity conformation to high affinity conformation, thus facilitating cell arrest by binding to ICAM1 or VCAM1. Furthermore, integrin clustering and adhesion strengthening prevent leukocyte detachment.

1.2.2.3 Leukocyte transmigration

Adherent leukocytes start to crawl along the endothelium until reaching exit sites to transmigrate. During transmigration leukocytes have to penetrate the endothelial-cell barrier, basement membrane, and pericytes. Transcellular migration is observed at “thin” parts of the endothelium and regulated by forming an intracellular channel, through which a leukocyte can transmigrate. Endothelial cells guide leukocytes to exit sites by forming ICAM1, VCAM1, and cytoplasmic molecules rich structures, so called “docking structures” (Barreiro et al. 2002). These structures occur around adherent leukocytes, which either enter by a transcellular or paracellular route into surrounding tissues. Leukocyte membrane protrusions spread into the endothelial-cell body (transcellular) or endothelial-cell junctions (paracelullar) by ICAM1-Mac1 binding (Schenkel et al. 2004; Phillipson et al. 2006), thereby opening interendothelial contacts. Subsequently, leukocytes pass the endothelium and basement membrane to enter the surrounding tissue.

1.2.3 Myeloid cell recruitment during atherogenesis

Initiation of atherosclerotic lesion development is promoted by the accumulation of neutrophils and monocytes in the vessel wall. Monocytes and macrophages were identified as the first cells associated with atherosclerosis (Napoli et al. 1997). The number of circulating classical monocytes is dramatically increased in hypercholesterolemic *Apoe*$^{-/-}$ mice (Swirski et al. 2007, Tacke et al. 2007). Within the atherosclerotic lesion, monocytes differentiate into macrophages or dendritic cells. Upon uptake of modified LDL particles via micropinocytosis or scavenger-receptor mediated pathways, macrophages give rise to foam cells, whose release of pro-inflammatory cytokines amplifies the inflammatory response.

Neutrophils, as the most abundant white blood cell, play an important role during early stages of atherosclerosis (Drechsler et al. 2010). Hypercholesterolemia triggers neutrophilia due to enhanced granulopoiesis and mobilization from the bone marrow (Drechsler et al. 2010). Recruited neutrophils into atherosclerotic lesions aggravate endothelial dysfunction by releasing their granule proteins. The granule proteins Proteinase-3 and α-defensin stimulate endothelial expression of adhesion molecules and chemokines, hence inducing leukocyte recruitment (Taekema-Roelvink et al. 2001; Chaly et al. 2000). Furthermore, neutrophils activate macrophages and promote their development into foam cells. Azurocidin and α-defensin stimulate the formation of reactive oxygen species in macrophages, thus leading to enhanced pro-inflammatory cytokine release and phagocytic activity (Soehnlein et al. 2008b; Soehnlein et al. 2008c). In addition, LDL particles bind to neutrophil derived α-defensin,

which triggers retention of lipoproteins in the vessel wall and finally the development of foam cells (Bdeir et al. 1999).
The recruitment of monocytes and neutrophils to atherosclerotic lesions depends on the classical steps of the recruitment cascade but also the cooperative and sequential function of different cell subsets.

Different studies in mouse models of atherosclerosis identified a major role of distinct adhesion molecules, chemokines, and chemokine receptors during atherogenesis. On the one hand, upregulation of adhesion molecules on endothelial cells in atheroprone regions associates with atherosclerosis. Next to low or oscillatory shear stress the risk factor hypercholesterolemia induces upregulation of adhesion molecules VCAM-1 and ICAM-1 on endothelial cells of regions predisposed to atherosclerotic lesion development (Iiyama et al. 1999; Nakashima et al. 1998). Furthermore, P- and E-selectin-double deficient mice with low density lipoprotein (LDL) receptor (*Ldlr)*- deficient background developed five times smaller atherosclerotic lesions compared to its respective control mouse strain after being 8 weeks on atherogenic diet (Dong et al. 1998).
On the other hand, adhesion molecules expressed on leukocytes contribute to their own recruitment. *In vivo* experiments gave evidence of the important role of VLA-4 and LFA-1 in the initiation of atherosclerotic lesion development (Shih et al. 1999; Watanabe et al. 1998).
Besides adhesion molecules, leukocytes express chemokine receptors whose signaling triggers leukocyte adhesion. The chemokine receptors CX_3CR1 and CCR5 play a major role during atherosclerosis, thus blocking its signaling is associated with reduced atherosclerotic lesion size (Poupel et al. 2013; Zernecke et al. 2006). Furthermore, the CCR2-CCL2 axis contributes to the development of atherosclerosis; hence genetic deficiency of *Ccl2* or its receptor *Ccr2* resulted in less development of atherosclerotic lesions (Boring et al. 1998; Gu et al. 1998). Moreover, overexpression of CCL2 by leukocytes increased progression of atherosclerosis (Aiello et al. 1999). Next to CCL2, several other chemokines have been found to be involved in atherosclerotic lesion development, such as CCL5, CCL3, CCL4, CXCL1 or CX3CL1 (Reape et al. 1999; Saederup et al. 2008; Zhou et al. 2011).
Taken together, distinct adhesion molecules, chemokine receptors, and chemokines expressed on endothelial cells or leukocytes contribute to atherosclerotic lesion development by guiding myeloid cell recruitment.

Myeloid cells are the first cells entering atherosclerotic lesions and their recruitment pathway has been intensively studied. Neutrophils are recruited early to activated endothelial cells and play a major role in early lesion development. Leukotriene B4, platelet activating factor, CXCL8, and other distinct chemotactic agents released by macrophages or by already

infiltrated leukocyte subsets promote neutrophil attraction (Soehnlein et al. 2010). Their recruitment is regulated in a CCR1, CCR2, CCR5, and CXCR2 dependent manner (Drechsler et al. 2010). Expression of CD11b and CD18 on neutrophils facilitates binding to P-selectin, intracellular adhesion molecules-1 (ICAM1) and intracellular adhesion molecules-2 (ICAM2) on endothelial cells (Ley et al. 2007). Once neutrophils emigrate into tissue, they sequentially release granule proteins including azurocidin, α-defensins, proteinase G, cathepsin G or cathelicidin (Doering et al. 2012; Soehnlein et al. 2010; Ortega-Gomez et al. 2016). These granule proteins bind to endothelial proteoglycans or activate endothelial cells, thus promoting further synthesis of chemokines. Different studies performed in macro- and microcirculation point out the important role of neutrophils in monocyte recruitment. Depletion of neutrophils in hypercholesterolemic *Apoe*$^{-/-}$ mice reduced the number of infiltrated classical monocytes into aortic tissue (Drechsler et al. 2010). In agreement with this previous study, less adhesion and extravasation of classical monocytes was observed in the microcirculation of neutropenic mice. Interestingly, this deficiency could be rescued by the application of supernatant derived from activated neutrophils (Soehnlein et al. 2008a). Further examination, identified the granule proteins cathelicidin, proteinase 3, proteinase G, and azurocidin from neutrophils as major triggers for classical monocyte recruitment (Doering et al. 2012; Soehnlein et al. 2010; Ortega-Gomez et al. 2016). Next to these proteins, neutrophil derived human neutrophil peptide 1 (HNP1) forms a heterodimer with platelet-derived CCL5 and stimulates recruitment of monocytes by binding to CCR5 (Alard et al. 2015). Hence, neutrophils induce classical monocyte recruitment to sites of inflammation.

Classical monocytes express different adhesion molecules including PSGL-1, CD62L (L-selectin), and distinct integrins (Soehnlein et al. 2013). The chemokine receptors CCR1, CCR2, and CCR5 together with their respective chemokines have been identified to regulate classical monocyte recruitment during atherogenesis (Soehnlein et al. 2012, Tacke et al. 2007). Recruitment of non-classical monocytes to atherosclerotic lesions occurs less frequently and seems to be of minor importance compared to classical monocyte accumulation (Tacke et al. 2007). Thus, depletion of non-classical monocytes in hypercholesterolemic *Apoe*$^{-/-}$ mice did not impact on lesion size, whereas lack of classical monocytes interfered with early lesion development (Soehnlein et al. 2012). However, a previous study investigated increased non-classical monocyte patrolling activity under hypercholesterolemia. The uptake of oxidized LDL (oxLDL) in the vasculature by the scavenger receptor CD36 on non-classical monocytes triggered their patrolling activity. Hence, indicating an atheroprotective role of non-classical monocytes during early atherogenesis (Marcovecchio et al. 2017).

In summary, neutrophil and monocyte recruitment is guided through different adhesion molecules, chemokine receptors, and their respective chemokines. Communication between neutrophils and monocytes as well as with endothelial cells regulates their recruitment to athero-prone regions.

1.3 Circadian rhythms

Many aspects in plants, humans or bacteria display temporal rhythmicity, which is controlled by an internal biological clock. These rhythms describe endogenous and entrainable oscillations, whose frequency range from seconds to years. Cycles with a short period length of seconds to about 20 h, such as heart rate, pulse or respiratory oscillations in yeast, are considered as ultradian rhythms (Gachon et al. 2004; Murray et al. 2001). In contrast, menstruation or circannual mating cycles describe infradian rhythms with a period from 30 h to decades. Circadian rhythms have a period length of approximately 24 h. The term *circadian* is derived from the Latin word *circa diem*, which means “for about a day” (Scheiermann et al. 2013). The first circadian rhythm was described in 1729, when the french geophysicist Jean Jacques d'Ortous de Mairan discovered a circadian rhythmicity in the folding and unfolding of leaves from *Mimosa pudica* (de Mairan 1729).

In mammals, almost each cell has a cell autonomous clock, which is regulated by a central clock and peripheral clocks. Such regulatory mechanisms ensure synchronization of rhythms throughout the body and to the environment. Alignment of circadian rhythms with the environment is controlled by Zeitgebers (i.e. time givers). For instance, light represents one of the major Zeitgebers and is recognized by the central clock, thus followed adjustment of internal rhythms leads to an overlap with the earth´s rotation cycle. Additionally, food intake, body temperature, hormones, and autonomic innervation are able to regulate synchronization (Brown et al. 2002). However, circadian rhythms oscillate independent of Zeitgebers and are characterized by even functioning under constant darkness. Whereas, rhythms only observed under a 12 h light/dark cycle are considered as diurnal rhythms.

1.3.1 Molecular circadian clock

Each cell autonomous clock is regulated by the rhythmic expression of the main core clock proteins circadian locomotor output cycles kaput (CLOCK) and brain and muscle ARNTL-like protein 1 (BMAL1, also known as ARNTL). BMAL1 and CLOCK belong to the family of basic-helix-loop-helix (bHLH) and period-ARNT-single-minded (PAS) domain-containing transcription factors. Both proteins form a heterodimer and bind to DNA E-boxes, the most frequent promoter elements of clock controlled genes (CCGs) (King et al. 1997; Bunger et al. 2000). Clock controlled genes can encode proteins involved in the regulation of the immune system or other transcription factors leading to up to 43% of clock controlled genes in mammals (Zhang et al. 2014).

Their cell autonomous circadian expression is regulated by at least three transcriptional-translational feedback loops (Figure 5). The central feedback loop is formed by BMAL1 and CLOCK. These proteins regulate their own expression and furthermore the expression of their own repressors PER1-3 and CRY1-2. When PER and CRY accumulate in the cytoplasma, they form a heterodimer and translocate back to the nucleus to interrupt the interaction of the heterodimer BMAL1:CLOCK with the gene promoter. This feedback loop controls rhythmic expression of *bmal1*, *clock*, *per* and *cry* (Anne M. Curtis et al. 2014).

The nuclear receptors retinoic acid receptor-related orphan receptor-α (RORα) and reverse erythroblastosis virus-α (REV-ERBα) form a second feedback loop. These transcription factors bind to receptor-related orphan receptor response elements (ROREs) in the *Bmal1* promoter region to regulate its expression. While RORα functions as a transcriptional activator, REV-ERBα represses *Bmal1* expression (Preitner et al., 2002; Sato et al. 2004).

Additionally, this second loop regulates expression of the repressor nuclear factor interleukin 3 (NFIL3). NFIL3 and the transcriptional activator albumin D-box binding protein (DBP) regulate a third feedback loop. Both transcription factors bind to the D-box of promoter regions to control expression of *Per* (Anne M. Curtis et al. 2014). Furthermore, post-translational modifications ensure the maintenance of circadian rhythms. Thus, phosphorylation, acetylation, and ubiquitylation modulate clock proteins to regulate their activity and degradation (Bellet et al., 2010).

Besides controlling their own rhythmic expression, core clock proteins were identified to bind to promoters of other genes, including proteins involved during inflammation. Nguyen et al. identified BMAL1 as a recruiter of the histone complex polycomb repressive complex 2 to the E-box binding site in the promoter region of *Ccl2*, thus regulating its rhythmic expression (Nguyen et al. 2013). Similar results were obtained for *Ccl8*, *S100a8*, *Timp4,* and *Tlr9* (Silver et al. 2012; Lutshumba et al. 2018).

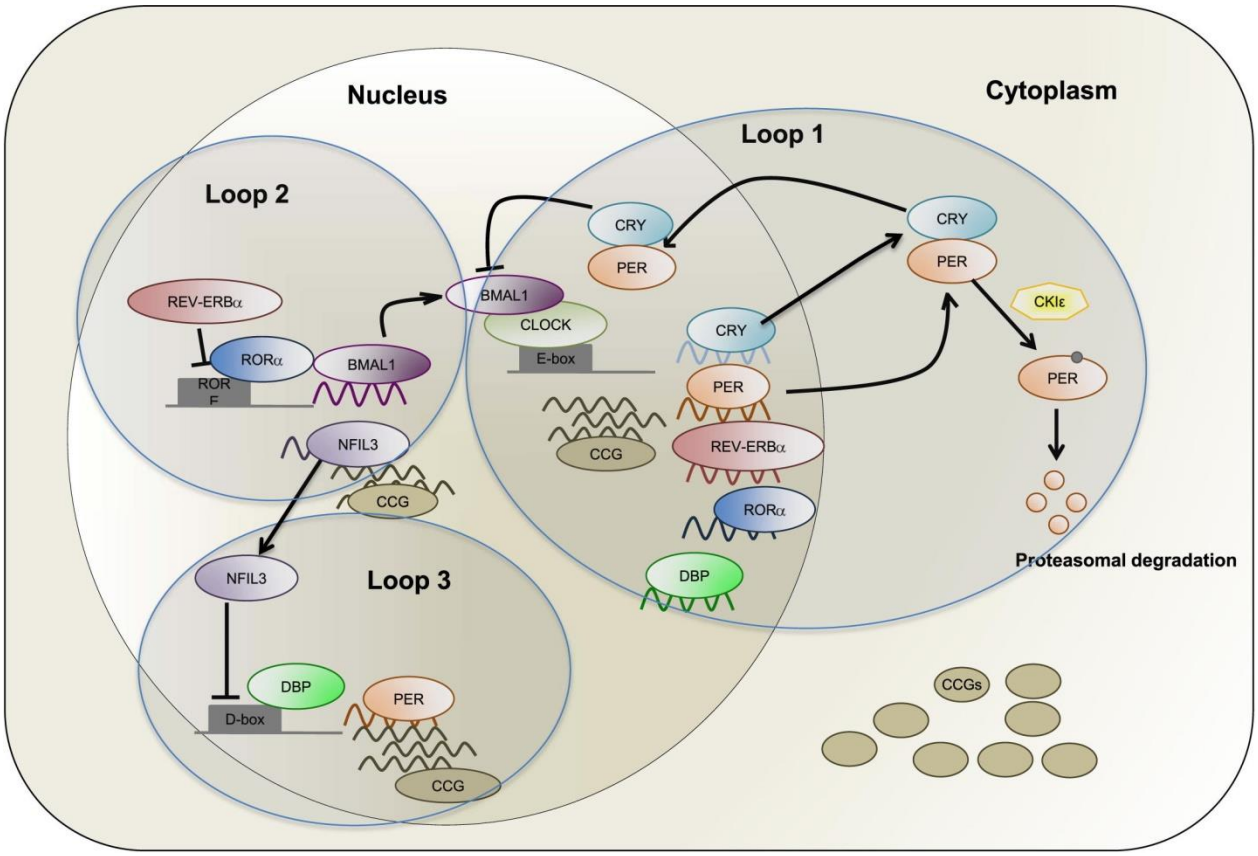

Figure 5: Molecular circadian clock

Oscillations in the expression of the central circadian clock genes Bmal1 and Clock are regulated by three connected transcriptional-translational feedback loops. BMAL1 and CLOCK bind to E-box binding sites within promoter regions to regulate the expression of cry, per, clock controlled genes (CCG) and other genes involved in further feedback loops. CRY and PER inhibit their expression by interfering with the heterodimer BMAL1 and CLOCK. Proteins derived from the first feedback loop are involved in other feedback loop to control oscillations in circadian clock gene expression. (Illustration from Anne M. Curtis et al. 2014)

1.3.2 Regulatory mechanism of the circadian clock

Circadian rhythms require regulatory mechanisms to ensure synchronized and effectively working circadian systems. A circadian pacemaker functions with a 24-hour rhythmicity even in the absence of environmental timing cues and it is also able to entrain oscillations according to the environment, thus functioning as the central clock (Herzog et al. 2007).
The suprachiasmatic nuclei (SCN) have been identified as the master circadian pacemaker of daily rhythms in mammals (Ralph et al. 1990). It is located in the anterior part of the hypothalamus and can transmit environmental signals to the organisms due to nerve signals directly received from the retina. Loss of the SCN had no impact on the presence of circadian rhythms in peripheral tissues; however, the rhythms were desynchronized among tissues and animals (Yoo et al. 2004). Peripheral clocks are not only regulated by the central clock but also by local regulatory mechanisms. Evidence for a local regulatory mechanism was given by a study of Kornmann et al., demonstrating robust rhythmicity in a subset of transcripts, while most other hepatic transcripts became arrhythmic in the absence of a functional liver clock (Kornmann et al. 2007). Furthermore, parabiosis experiments between intact and SCN-lesioned mice indicate that circadian oscillations are controlled by non-humoral and humoral pathways (Mohawak et al. 2012; Guo et al. 2005).
Therefore, distinct peripheral clock entrainment pathways have been identified, such as the autonomic nervous system, body temperature, food intake or humoral signals (e.g. glucocorticoids).

As the central clock, the SCN regulates many different body functions via humoral and neuronal signals. Light signals from the eye are forwarded via the retinohypothalamic tract to the SCN where the signal can either be translated by the hypothalamic-pituitary-adrenal axis (HPA axis) or by sympathetic innervation (Figure 6).
According to the HPA axis, the hypothalamus controls the release of adrenocorticotropic hormone (ACTH) from the pituitary gland into the bloodstream, thus being transported to the adrenal gland. In the adrenal gland ACTH stimulates the release of steroid hormones, such as glucocorticoids from the adrenal cortex or catecholamines from the adrenal medulla. The effect of noradrenaline and adrenaline is mediated via seven-transmembrane-segment receptors. These receptors are classified into α_1, α_2 and β adrenergic receptors and have multiple impacts on immune cells (Cosentino et al. 2015). Glucocorticoids bind to intracellular glucocorticoid receptors (GR) that function as ligand-dependent transcription factors via glucocorticoid-response elements (GRE) in promoter regions, thus upregulating the expression of anti-inflammatory proteins (Barnes et al. 1998). Interestingly, the core clock

proteins CLOCK/BMAL1 were identified as negative regulator of glucocorticoid activity due to modification of the ligand binding domain of GRs by CLOCK (Nader et al. 2009). Additionally, sympathetic innervation of distinct tissues regulates oscillations by local release of noradrenaline (Scheiermann et al. 2012).

In summary, the pacemaker of the circadian clock consists of the SCN, which regulates synchronization of peripheral clocks. Nevertheless, other entrainment pathways have been identified to affect circadian clocks, thus building up a complex feedback relationship.

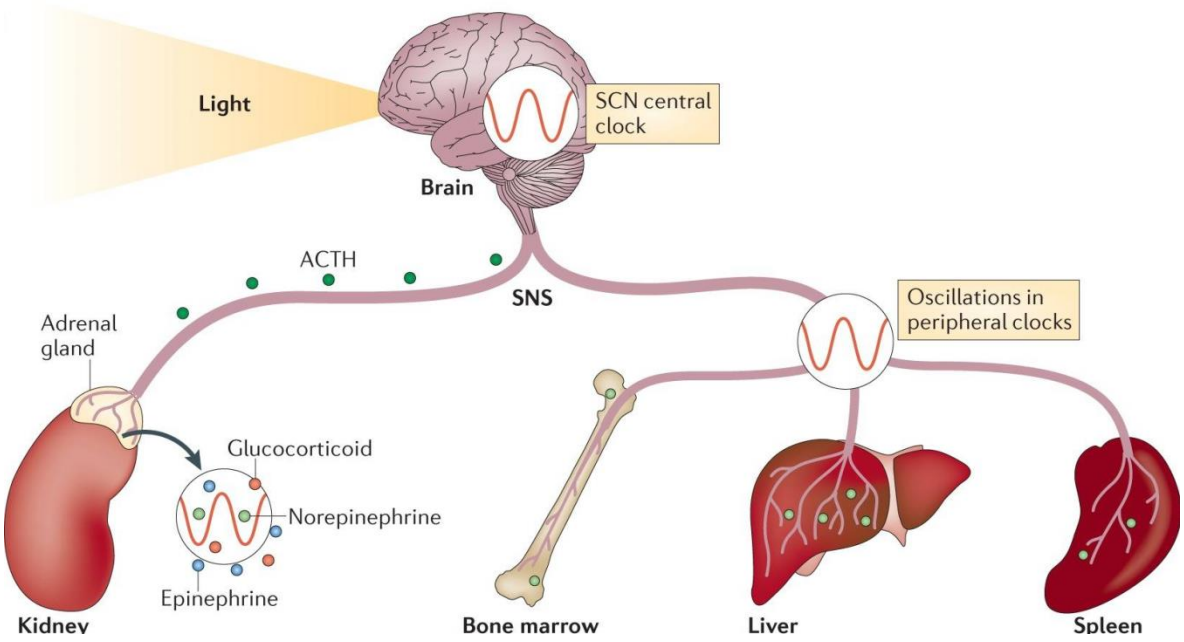

Figure 6: Regulatory mechanisms leading to entrainment and synchronization of peripheral clocks

The suprachiasmatic nuclei (SCN) represent the central clock and regulate peripheral clocks by distinct pathways. Light can be sensed through the eye and provides an entrainment mechanism to align peripheral rhythms with the light cycle. The SCN regulates the release of different hormones from the adrenal gland as well as local sympathetic innervation of peripheral tissues to influence their circadian rhythmicity. (Illustration from Scheiermann et al. 2013)

1.3.3 Rhythmic immune cell trafficking

Immune cell trafficking under steady state exhibits circadian rhythmicity. Rhythmic expression of adhesion molecules, chemokines, and their chemokine receptors regulates oscillatory lymphocyte and leukocyte trafficking from the bone marrow to peripheral tissues. In the light of disease outcome and mortality, previous research highlights the importance of understanding the circadian control of immune cell mobilization and recruitment.

Under steady state circulating hematopoietic stem and progenitor cells (HSPCs) oscillate with a peak during the resting phase and a through during the activity phase. Rhythmic activation of β3-adrenergic receptors via local sympathetic innervation promotes oscillatory expression of the chemokine CXCL12 in stromal cells of the bone marrow, thus regulating HSPC egress or homing (Méndez-Ferrer et al. 2008). Additionally, rhythmic leukocyte trafficking to the bone marrow and peripheral tissues peaked during the activity phase and has been described as a consequence of rhythmic expression of adhesion molecules and chemokines by local sympathetic nervous system activation (Scheiermann et al. 2012). While oscillatory expression of *Selp*, *Sele*, and *Vcam1* regulates leukocyte egress into the bone marrow, rhythmic expression of *Icam1* and *Ccl2* in endothelial cells of the skeletal muscle promotes leukocyte recruitment. Both described phenotypes were regulated by photic cues. Changes in light input disturbed rhythmic release of HSPCs or leukocytes from the bone marrow. These results point out light as an important entrainment factor being able to influence immune cell trafficking.

In addition, monocyte and neutrophil trafficking to different tissues revealed rhythmicity under physiological conditions. Monocyte numbers in blood, spleen, and bone marrow exhibit diurnal oscillations. Monocyte numbers in blood and spleen peaked between ZT4-ZT8, while an opposing phenotype was observed in their cell number in the bone marrow (Ngyuen et al. 2013). Circulating granulocytes in C57BL/6J mice peaked at ZT5 and were at their lowest level at ZT13. In contrast, neutrophil numbers in the heart represented a peak at ZT13 and a through at ZT5 (Schloss et al. 2016). Homeostatic clearance of neutrophils follows daily cycles by regulating their trafficking between blood and bone marrow. Circulating aged $CD62^{low}$ and $CXCR4^{high}$ neutrophils infiltrate back to the bone marrow at the end of the resting phase. In the bone marrow, macrophages phagocyte aged neutrophils, thus triggering a feedback mechanism by promote rhythmic egress of hematopoietic progenitors into the circulation (Casanova-Acebes et al. 2013).

Furthermore, lymphocyte trafficking to lymph nodes exhibited circadian rhythmicity. Lymphocyte homing and egress was regulated by time-dependent clock-controlled

expression of the receptors *Ccr7* and *S1pr1* (Druzd et al. 2017). In addition, oscillations in the number of T cells were observed in human blood. While naive cells exhibited a peak at night, effector CD8 T cells peaked during daytime (Dimitrov et a. 2009). Interestingly, cortisol and epinephrine levels have been identified as regulators of T cell trafficking by regulating CXCR4 and CX3CR1 expression (Dimitrov et a. 2009).

In summary, distinct regulatory components of the circadian clock were identified as influencers of leukocyte recruitment during steady state with predicted consequences on immune responses.

1.3.4 Circadian clock controls inflammation

The immune system consists of the innate and adaptive immune response. It protects the organism against pathogens such as bacteria, viruses or parasites with a complex interplay of different cell subsets and inflammatory/anti-inflammatory molecules.

Monocytes and macrophages play a central role in the innate immune response. They contribute to initiation and resolution of inflammation by phagocytosis, activation of the adaptive immune system and release of inflammatory cytokines and reactive oxygen species. Circadian clock genes oscillate in circulating monocytes and macrophages from the spleen, lymph node, and peritoneum, thus influencing expression of downstream genes involved in inflammatory innate immune functions. Gene expression profiling in macrophages revealed that approximately 8% of the macrophage transcriptome is under circadian control (Keller et al. 2009). In detail, rhythmic expression of *Ccl2* and *Ccl8* was observed in myeloid cells (Nguyen et al. 2013). Furthermore, TNF-α and IL-6 secretion exhibited circadian rhythms in lipopolysaccharide (LPS) – challenged spleen macrophages (Keller et al. 2009). During inflammation myeloid cells recognize pathogens via pattern-recognition receptors (PRRs), such as TLR4 and TLR9. While there is no circadian rhythmicity in TLR4 expression, components of the downstream signaling pathway exhibit circadian oscillations, which promote time-dependent immune responses (Keller et al. 2009). In contrast, *Tlr9* expression oscillates and regulates improved immune responses, when its expression is at its highest level (Silver et al. 2012). Additionally, the rhythmicity of blood monocytes impacts on Ly6C^{high} inflammatory monocyte recruitment to sites of inflammation. Mice that were intraperitoneally infected with *Listeria monocytogenes* at a time with increased circulating Ly6C^{high} monocyte numbers showed improved bacterial clearance (Nguyen et al. 2013).

Neutrophils are the most abundant circulating white blood cells and the first cells at sites of inflammation. They support host defense by phagocytosis of pathogens and release of antimicrobial agents. Rhythmic neutrophil recruitment has been described to be involved in outcomes of different diseases. Responses to pulmonary infections induced by lipopolysaccharide differed between distinct time points with the highest infiltration of neutrophils at CT0. These observations relied on epithelial club (clara), cells which promote neutrophil recruitment to injured lung tissue by rhythmic *Cxcl5* expression (Gibbs et al. 2014). Furthermore, circadian neutrophil recruitment to the heart during myocardial infarction (MI) defined infarct size, healing, and cardiac function. Depletion of neutrophils when their recruitment was at its highest level at ZT13 revealed an improved cardiac function and infarct size (Schloss et al. 2016). In addition, other disease models, such as sickle cell disease and septic shock, are affected by circadian neutrophil recruitment. Overall survival in mouse models of sickle cell disease challenged with TNFα and in C57BL/6 mice challenged with LPS (septic model) was reduced at night (Scheiermann et al. 2012). Interestingly, a recent study describes circadian rhythmicity in parasite infection by *Leishmania major* with a daytime-dependent neutrophil and anti-inflammatory macrophage infiltration induced by rhythmic expression of chemokines (Kiessling et al. 2017).

Next to myeloid cells, natural killer cells express clock genes and exhibit circadian rhythmicity in their cytotoxicity characterized by oscillations of granzyme B, perforin, and IFN-γ (Fernandez et al. 1969; Arjona et al. 2004). Disruption of the circadian clock by chronic shift-lag revealed attenuated natural killer cell cytotoxicity and promoted tumor growth (Logan et al. 2012).

In light of the adaptive immune system, lymphocytes contain a functional molecular clockwork (Silver et al. 2012; Bollinger at al. 2011). Recent research illustrated a time-of-day dependence in adaptive immune responses to immunization and pathogens. Elevated numbers of activated T cells and dendritic cells were present in lymph nodes at night onset. In the autoimmunity model of EAE, mice immunized at ZT8, when cell counts were high in lymph nodes, showed an accelerated disease severity compared to a control group immunized at ZT20 (Druzd et al. 2017). Similar results were obtained in mice infected with *Helicobacter pylori* or influenza A virus and highlight the importance of circadian rhythms in adaptive immune responses (Druzd et al. 2017). Furthermore, antibody levels due to vaccination were elevated after morning administration compared to afternoon vaccination (Long et al. 2016).

Taken together, circadian rhythms influence inflammation and disease outcomes due to oscillations in leukocyte recruitment and rhythmicity in the expression of inflammatory molecules.

1.3.5 Circadian clock in atherosclerosis

Increasing evidence points out the critical role of circadian rhythmicity in the pathogenesis of atherosclerosis. Different aspects of cardiovascular functions as well as major clinical consequences of atherosclerosis, such as myocardial infarction or stroke, exhibit diurnal variations in their frequency (Mueller et al. 1985). Regarding the influence of rhythmic gene expression on inflammation, expression profile analysis of aortic tissue discovered 330 transcripts with circadian rhythmicity (Rudic et al. 2005). Further evidence is given by the discovery of cell-intrinsic molecular clocks in different cell types involved in atherosclerosis including leukocytes, macrophages, endothelial cells, and smooth muscle cells. About 8% of the macrophage transcriptome from isolated macrophages from spleen, lymph node, and peritoneum is under circadian control (Keller et al. 2009). In murine smooth muscle cells rhythmic gene expression occurred for the tissue inhibitor of metalloproteinase 1 and 3, collagen 3a1, transgelin, and calponin (Chalmers et al. 2008).

Distinct studies emphasize the role of circadian clock genes in the pathogenesis of atherosclerosis. By comparing conventional and inducible core clock gene deficiency in *Ldlr*$^{-/-}$ mice, constitutive lack of *Bmal1* revealed accelerated atherogenesis, whereas inducible *Bmal1* knockout mice developed less atherosclerotic lesions (Yang et al. 2016). In addition, human studies obtained a lower *Cry1* mRNA expression in atherosclerotic patients (Yang et al. 2015). Its atheroprotective role was further investigated in mice. *Cry1* overexpression by adenovirus-mediated gene transfer revealed a lower expression of proinflammatory cytokines, adhesion molecules, and improved hyperlipidemia (Yang et al. 2015). Similarly, specific lentiviral-mediated knockdown of *Rev-erb* in hematopoietic cells in *Ldlr*$^{-/-}$ mice enhanced atherosclerotic lesion development, while pharmacological activation of REV-ERB decreased atherosclerotic plaque size (Ma et al. 2013; Sitaula et al. 2015).

Disruption of a functional circadian clock in tissue or specific cell types has pathophysiological relevance on key risk factors of cardiovascular diseases. Deficiency of *Per2* in mice promotes endothelial dysfunction by reduced production of vasodilators and increased release of vasoconstrictors, thus Per2 maintains normal cardiovascular functions

(Viswambharan et al. 2007). Furthermore, *in vivo* models deficient of the core clock gene *Bmal1* have a dramatic prothrombotic phenotype including elevated levels of circulating vWF, fibrinogen, and PAI-1 (Somanath et al. 2011). Risk factors of cardiovascular diseases are altered by circadian clock deficiency, but considering the opposite, risk factors have also been shown to change rhythmicity of molecular clocks. Hyperlipidemia induced altered rhythmicity and expression of circadian genes in *Apoe*$^{-/-}$ mice (Hou et al. 2009). Additionally, human plaque-derived vascular smooth muscle cells (VSMCs) exhibited different circadian rhythmicity from that of normal carotid VSMCs (Lin et al. 2014).

Tissue intrinsic circadian clocks contribute to arteriosclerotic diseases. A study from 2011 demonstrates the influence and importance of tissue clocks versus extrinsic clocks. Aortic grafts from *Bmal1*$^{-/-}$ or *Per2,3*$^{-/-}$ mice transplanted into WT mice developed arteriosclerotic disease, while aortic grafts from WT mice transplanted into clock disrupted mice revealed no lesion development, thus highlighting the importance of functional tissue intrinsic clocks (Cheng et al. 2011). Furthermore, cell intrinsic clocks promote the pathogenesis of atherosclerosis. Specific myeloid *Bmal1* deletion affected lesion development. An increased lesion development was observed with a higher number of lesional macrophages and preferential differentiation of Ly6C^{high} inflammatory monocytes into M1 macrophages (Huo et al. 2017).

As a conclusion, much evidence has been given that the circadian clock influences the pathogenesis of atherosclerosis. However, the impact of the circadian clock on myeloid cell recruitment during atherogenesis and its regulatory mechanism is still unknown.

1.4 Research objective

The circadian clock controls distinct components of the immune system, thus regulating inflammatory processes and susceptibility to diseases in a time-dependent manner. The higher incidence of myocardial infarction early in the morning together with previous studies on the atherogenic effect of core clock proteins already give indications of rhythmic inflammatory processes during atherosclerotic lesion development. However, these studies focused on the importance of the circadian clock proteins BMAL1 and CLOCK on the development of atherosclerosis without identifying circadian rhythmicity in leukocyte recruitment (Pan et al. 2013; Yang et al. 2016; Huo et al. 2017). Leukocyte recruitment to site of activated arterial endothelium plays a major role during the initiation of atherosclerotic lesion development. In regard that distinct components of the immune system exhibit circadian rhythmicity, thus modulating leukocyte recruitment during acute inflammation in a time-dependent manner, we questioned whether rhythmic leukocyte recruitment occurs during atherogenesis (Scheiermann et al. 2012; Nguyen et al. 2013). Therefore, the aim of this study was to investigate to what extent the circadian clock orchestrates leukocyte recruitment during the development of atherosclerosis and to identify its regulatory mechanisms for generating a chronopharmacological treatment strategy.

2. Materials and Methods

Table 1: Buffers and Media

Red blood cell lysis buffer	150 mM NH_4Cl; 10 mM $KHCO_3$; 0.1 mM diNaEDTA, pH 7.4
Hank's buffer	1X Hank's buffered salt solution (HBSS), 0,06 % BSA, 0.5 mM diNaEDTA
Digestion medium	RPMI + 10% FBS (Thermo Fisher Scientific, Waltham, USA)
Antibody staining solution	50 µl PBS supplemented with 1,6 % BSA and 15,9 µl/ml mouse serum,rabbit serum and human serum (Sigma, Sigma-Aldrich, St. Louis, USA) + 50 µl Hank's buffer
Static adhesion buffer	RPMI + 0.5% BSA (SERVA, Heidelberg, Germany)
Oil red O staining solution	1g Oil-red-o (Sigma, Sigma-Aldrich, St. Louis, USA) in 200 ml 2-propanol (Merck, Darmstadt, Germany)
Antigen retrieval solution	12,6 ml Solution A (21,01g Citric Acid, 1 l Aqua dest.), 57,4 ml Solution B (29,4g Sodium Citrate, 1 l Aqua dest.), 350µl Tween20 (Merck, Darmstadt, Germany)
Blocking solution	6 ml PBS + 1% BSA (1%) + 3 drops horse serum (VECTA laboratories, Burlingame, USA)

2.1 *In vivo* experiments

2.1.1 Mice

8 weeks old *Apoe*$^{-/-}$, *Cx*$_3$*cr1*$^{gfp/WT}$*Apoe*$^{-/-}$, *Lyz2CreBmal1*$^{fl/fl}$*Apoe*$^{-/-}$, *Lyz2CreApoe*$^{-/-}$, *Bmal1*$^{fl/fl}$*Apoe*$^{-/-}$, *BmxCre*^{ERT2}*Bmal1*$^{fl/fl}$*Apoe*$^{-/-}$, C57BL/6J and *Ldlr*$^{-/-}$ mice were used to study circadian oscillations in the pathogenesis of atherosclerosis. All mice were housed at a 12-hour light/ 12-hour dark cycle (Lights on at 7 am, i.e. ZT0; lights off at 7 pm, i.e. ZT12) or 24-hour dark cycle during the last two weeks before sacrifice. Starting at the age of 8 weeks mice were fed a high-fat diet (HFD) containing 21% fat and 0.15% cholesterol (ssniff, Soest, Germany) for four weeks to induce a hypercholesterolemia and the development of atherosclerotic lesions.

Inducible knockout mouse strains were injected i.p. with 1 mg tamoxifen (T5648, Sigma-Aldrich, St. Louis, USA) dissolved in coconut oil, daily for 5 days before initiation of HFD feeding. All animal experiments were approved by the local ethical committee for animal experimentation.

2.1.2 Genotyping

C57BL/6J mice and *Ldlr*$^{-/-}$ mice were purchased from Janvier labs (Le Genest Saint Isle, France). The rest of strains derived from our own animal facility and was genotyped as described in the following section. For genotypic analysis a tail biopsy was obtained and incubated overnight at 56°C in 250 µl tissue lysis buffer supplemented with proteinase k solution (0,2 mg/ml, Qiagen, Hilden, Germany) for tissue digestion (Qiagen, Hilden, Germany). Afterwards, DNA was isolated with a QIAxtractor (Qiagen, Hilden, Germany) according to the manufacturer's instructions.

PCR reagent mixes were prepared for all genes as described below:

Reaction component	**Final concentration**
5X Green Gotaq Flexi buffer (Promega, Fitchburg, USA)	1X
25 mM MgCl2 (Sigma-Aldrich, St. Louis, USA)	1,5 mM
dNTPs (Sigma-Aldrich, St. Louis, USA)	0,2 mM
Forward Primer (Sigma-Aldrich, St. Louis, USA)	0,5 µM
Reverse Primer (Sigma-Aldrich, St. Louis, USA)	0,5 µM
GoTaq DNA polymerase (Promega, Fitchburg, USA)	0,05 U/µl
Genomic DNA (Promega, Fitchburg, USA)	200 ng

PCR reagent mixes were prepared containing either wildtype- or mutant allele-detecting primer pairs and the following PCR reaction programs were used. Afterwards, PCR products were analyzed by gel electrophoresis with a QIAxcel Advanced System (Qiagen, Hilden, Germany) according to the manufacturer's instructions. In every set of samples, a reaction with wildtype and mutant material as well as water was included as positive and negative controls, respectively.

PCR reaction programs:

Apoe

Primer	
Apoe common forward	5' GCC TAG CCG AGG GAG AGC CG 3'
Apoe wildtype reverse	5' TGT GAC TTG GGA GCT CTG CAG C 3'
Apoe mutant reverse	5' GCC GCC CCG ACT GCA TCT 3'

Cycling

Step	Temperature °C	Time
1	94	5 min
2	94	30 sec
3	60	30 sec
4	72	30 sec
5	Repeat steps 2-4 for 35 cycles	
6	72	5 min
7	21	5 min

Cx_3cr1

Primer	
Cx_3cr1 common forward	5’ GGT TCC TAG TGG AGC TAG GG 3’
Cx_3cr1 wildtype reverse	5’ TTC ACG TTC GGT CTG GTG GG 3’
Cx_3cr1 mutant reverse	5’ GAT CAC TCT CGG GAT GGA CG 3’

Cycling

Step	Temperature °C	Time
1	94	5 min
2	94	30 sec
3	60	30 sec
4	72	1 min
5	Repeat steps 2-4 for 35 cycles	
6	72	5 min
7	21	5 min

Lyz2Cre

Primer	
Lyz2Cre common forward	5’ CTT GGG CTG CCA GAA TTT CTC 3’
Lyz2Cre wildtype reverse	5’ TTA CAG TCG GCC AGG CTG AC 3’
Lyz2Cre mutant reverse	5’ CCC AGA AAT GCC AGA TTA CG 3’

Cycling

Step	Temperature °C	Time
1	94	3 min
2	94	30 sec

3	60	30 sec
4	72	50 sec
5	Repeat steps 2-4 for 37 cycles	
6	72	3 min
7	21	5 min

Bmal1

Primer	
Bmal1 forward	5’ ACT GGA AGT AAC TTT ATC AAA CTG 3’
Bmal1 reverse	5’ CTG ACC AAC TTG CTA ACA ATT A 3’

Cycling

Step	Temperature °C	Time
1	94	3 min
2	94	30 sec
3	60	60 sec
4	72	60 sec
5	Repeat steps 2-4 for 35 cycles	
6	72	5 min
7	21	5 min

BmxCre

Primer	
BmxCre forward	5’ AAA TAC CTT CAG TTT TCA TCT 3’
BmxCre reverse	5’ TTG CGA ACC TCA TCA CTC GTT 3’

Cycling

Step	Temperature °C	Time
1	94	2 min
2	94	30 sec
3	60	30 sec
4	72	1 min
5	Repeat steps 2-4 for 35 cycles	
6	72	5 min
7	21	5 min

2.1.3 *In vivo* CCR2-CCL2 inhibition

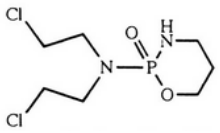

Figure 7: *Structure of CCR2 antagonist RS102895*

The spiropiperidine compound RS102895 (Figure 7) is a small molecule antagonist of the CCR2 receptor. CCL2-CCR2 signaling was interrupted in hypercholesterolemic *Apoe*$^{-/-}$ mice by injecting daily a single dose of 5 mg/kg CCR2 antagonist (RS102895, Sigma-Aldrich, St. Louis, USA) or vehicle control at ZT5 or ZT17 during a period of four weeks. The CCR2 antagonist was dissolved in DMSO and diluted in PBS before the injection. The same concentration of DMSO in PBS served as a vehicle control. Because RS102895 has a short half-life, a dose of 5 mg/kg is not detectable in plasma beyond 9 hours after administration (Mitchell et al., 2013), thus avoiding a long-lasting CCR2 blockage. During the short term inhibition of CCR2-CCL2 signaling a single dose of 5 mg/kg CCR2 antagonist (RS102895, Sigma-Aldrich, St. Louis, USA) or vehicle control was injected 30 min before imaging.

2.1.4 *In vivo* leukocyte depletion

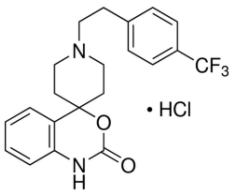

Figure 8: *Structure of cyclophosphamide*

The medical substrate cyclophosphamide is used for chemotherapy and suppresses the immune system. Upon administration of cyclophosphamide the toxic metabolite phosphoramide mustard accumulates specifically in cells with low levels of aldehyde dehydrogenase (ALDH). Due to the formation of crosslinks between phosphoramide mustard and DNA strands, cells undergo apoptosis. High levels of ALDHs, as observed in bone marrow stem cells, prevent the formation of toxic metabolites and protect the cells from cell death. Peripheral leukocyte depletion was induced in hypercholesterolemic *Apoe*$^{-/-}$ mice by i.p. administration of 160 mg/kg cyclophosphamide (CTX) (pharmacy of the LMU Munich, Germany) (Figure 8). Successful leukopenia was verified by quantifying leukocyte numbers in the blood with flow cytometry as described below (see section “2.4.1 Flow cytometry”).

2.1.5 *In vivo* glucocorticoid receptor inhibition

Mifepristone inhibits the activity of progesterone and glucocorticoid receptor signaling. The glucocorticoid receptor belongs to the nuclear receptor superfamily by functioning as a ligand-dependent transcription factors. Mifepristone binds to the glucocorticoid receptor and prevents the translocation to the nucleus, thus inhibiting its function as a transcription factor. The glucocorticoid receptor activity was blocked by injecting 30 mg/kg Mifepristone i.p. (Sigma-Aldrich, St. Louis, USA) 24 hours and 12 hours before imaging. Mifepristone was dissolved in DMSO and diluted in PBS shortly before administration. The same concentration of DMSO diluted in PBS was used as a vehicle control.

2.1.6 *In vivo* adrenergic receptor inhibition

Adrenergic receptor signaling was inhibited by injecting 5 mg/kg of a β3-adrenergic receptor antagonist (Sigma-Aldrich, St. Louis, USA), 10 mg/kg of the β1/2-adrenergic receptor antagonist propranolol (Sigma-Aldrich, St. Louis, USA) and 5 mg/kg of the α-adrenergic receptor antagonist phentolamine (Sigma-Aldrich, St. Louis, USA) i.p. shortly before imaging. All antagonists were dissolved in DMSO and diluted in PBS before the injection. The same concentration of DMSO diluted in PBS was used as a vehicle control.

2.1.7 LPS-induced lung injury

Acute lung injury induced by LPS is a neutrophil-dependent lung disease model characterized by increased permeability of the alveolar-capillary endothelium and epithelium leading to edema formation and recruitment of neutrophils (Grommes et al. 2011).

C57BL/6 mice (Janvier labs, Le Genest Saint Isle, France) were exposed to aerosolized LPS (500 µg/ml) from *Salmonella enteritidis* (Sigma-Aldrich, St- Louis, Germany) for 30 min. Two hours later 5 µl Gr1-FITC (RB6-8C5, BioLegend, San Diego, USA) was applied by tail vein injection to label intravascular neutrophils. Afterwards mice were sacrificed and non-adherent cells were removed by flushing the pulmonary vasculature with 20 ml PBS. Lungs were removed and processed according to the protocol described in section “2.4.1.1 Organ preparation protocol”. Neutrophils were labeled as described in section “2.4.1.2 Staining protocol”. Intravascular neutrophils were identified as $CD45^+$, $CD11b^+$, $Ly6G^+$ and $Gr1^+$ cells whereas interstitial neutrophils were characterized as $CD45^+$, $CD11b^+$, $Ly6G^+$ and $Gr1^-$ cells.

2.2 Intravital microscopy

Intravital microscopy enables live imaging of leukocyte-endothelial cell interactions along the carotid artery and in the microcirculation of the cremaster muscle. Intravital microscopy was performed by Oliver Soehnlein.

2.2.1 Macrocirculation

First, a catheter (PE10, Becton Dickinson, Franklin Lakes, USA) was placed into the right jugular vein for injecting a PE-conjugated antibody to Ly6G (1 µg, 1A8, Thermo Fisher Scientific, Waltham, USA) and a FITC-conjugated antibody to Ly6C (1 µg, HK1.1, BioLegend, San Diego, USA) to visualize myeloid cells. Application of a Ly6C antibody was not necessary for already GFP labeled monocytes in the *Cx$_3$cr1$^{egfp/WT}$Apoe$^{-/-}$* mice. Second, the external carotid artery was imaged using an Olympus BX51 microscope equipped with a Hamamatsu 9100-02 EMCCD camera, and a 10× saline-immersion objective. The interaction of labeled myeloid cells with endothelial cells was imaged for 30 s. Afterwards one video per mouse was analyzed by counting the number of adherent myeloid cells.

2.2.2 Microcirculation

Live imaging of adherent or interstitial cells in the microcirculation was obtained by injecting antibodies as described above via a catheter in the right jugular vein and exposing the cremaster muscle for imaging. Videos were taken with an Olympus BX51 microscope equipped with a Hamamatsu 9100-02 EMCCD camera, and a 20× water-dipping objective. Cremasteric arterioles were discriminated from postcapillary venules by flow direction. Adherent myeloid cells were imaged for 30 s and finally the number of adherent cells was obtained by analyzing 5 different videos of each cremaster muscle per mouse.

2.2.3 CCL2 rescue experiment

Intravital microscopy in the carotid artery was used to study changes in the number of adherent cells after injecting the chemokine CCL2. Antibodies to visualize myeloid cells were injected via a jugular catheter as described in section “2.2.1 Macrocirculation”. The number of adherent myeloid cells to the carotid artery endothelium was recorded for baseline levels. Next, 300 ng CCL2 (Peprotech, Rocky Hill, NJ, USA) were injected via the jugular vein catheter and 30 min later the number of adherent myeloid cells to the carotid artery was recorded again.

2.3 Tracking intravascular leukocytes into tissues

Trafficking of intravascular leukocytes was assessed by intravenous injection of a specific antibody to stain circulating leukocytes. Then, pre-labeled intravascular-derived cells were tracked into tissues. In order to establish the method, the antibody leakage through the endothelium of atherosclerotic lesions was tested to confirm that the intravenous injected antibodies labeled circulating but not tissue-resident leukocytes in atherosclerotic lesions. For that purpose, an antibody against collagen type IV alpha 1 (Novus Biologicals, Littleton, USA), a component of the endothelial basement membrane, was intravenously injected. The fenestrated endothelium in glomerular capillaries of the kidney served as a positive control for antibody leakage. Furthermore, the staining efficiency of the antibody, which was used to labeled circulating leukocytes (rat anti-CD45 antibody conjugated to APC-Cy7, clone: 30-F11), was analyzed by flow cytometry of blood samples shortly after the intravenous injection. Sample preparation was performed according to the protocol "2.4.1.1 Organ preparation protocol". Staining efficiency was analyzed by determining the percentage of pre-labeled CD45 APC-Cy7 positive cells in the blood.

After establishing the experimental set-up, *Apoe*$^{-/-}$ mice were fed with a HFD for 4 weeks and the amount of immigrated leukocytes into tissues was analyzed by labeling intravascular leukocytes two hours before harvesting at either ZT1 or ZT13 (Figure 9). Aorta and blood were analyzed by flow cytometry to determine the staining efficiency of circulating cells and the amount of intravascular-derived leukocytes (see protocol "2.4.1 Flow cytometry"). Intravascular-derived and tissue-resident leukocytes were discriminated by being positive or negative for the intravascular injected CD45 antibody, respectively. Neutrophils and monocytes were stained according to the protocol "2.4.1.2 Staining protocol". The heart was taken for staining intravascular-derived leukocytes in atherosclerotic lesions of aortic root sections. Processing and staining of the heart was performed in accordance to the protocol "2.7. Histology and Immunohistochemistry". Visualization of infiltrated intravascular-derived leukocytes (pre-labeled with anti-CD45 APC-Cy7 antibody) in atherosclerotic lesions was performed by an additional staining with a secondary anti-rat antibody conjugated to Dylight550.

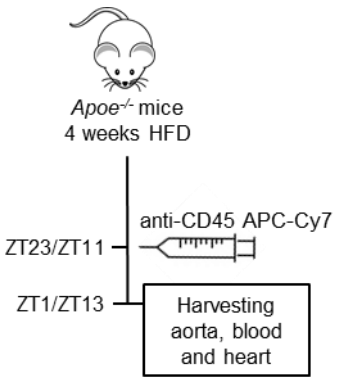

Figure 9: Experimental layout
Mice have been injected with an anti-CD45 antibody conjugated with APC-Cy7 to label blood leukocytes two hours before harvesting. ZT=Zeitgeber time, HFD=high fed diet. Apoe= Apolipoprotein E

2.4 Protein assays

2.4.1 Flow cytometry

Flow cytometry is a laser-based method to determine the expression of cell-surface and intracellular molecules by using specific fluorescent-labeled antibodies. This technique allows to distinguish cell types within a cell population and to analyze the expression of interest such as chemokines or chemokine receptors. During flow cytometry analysis, fluorescently labeled single cells of a cell suspension pass through a laser beam. Thereby, forward and side scattered light, as well as fluorescence signals are measured by several detectors (Figure 10). Measurements of forward scattered (FSC) light provide information about cell size, whereas side scattered (SSC) light allows discrimination by cell granularity. Fluorescence measurements enable to determine molecule expression according to the fluorescence intensity.

The number of red blood cells and platelets were calculated by an automated blood cell counter (Scil ABC Vet Blood Counter).

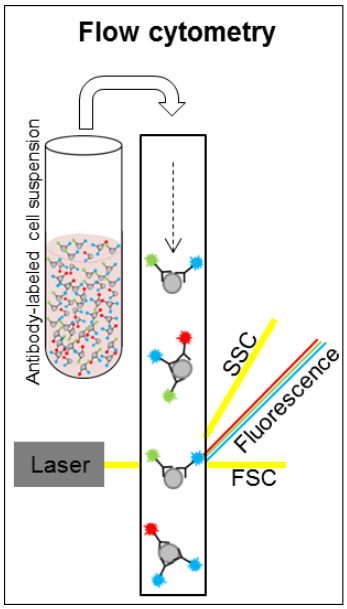

Figure 10: Flow cytometry principle *Single cells labeled with cell type specific markers are analyzed by their side scattered (SSC) light, forward scattered (FSC) light, and fluorescence signals.*

2.4.1.1 Organ preparation protocol

***Blood**:* Blood was taken by punctuation of the retrobulbar venous plexus and collected in tubes containing Ethylenediaminetetraacetic acid (EDTA) to avoid coagulation by chelating calcium ions. Afterwards, red blood cell lysis was performed using 3 ml of red blood cell lysis buffer (Table 1) per 100 µl of blood for 15 min at room temperature (RT). The lysis was stopped by adding 10 ml of HANKs buffer. After spinning down at 300 x g for 5 min, cells were suspended in antibody staining solution (see section 2.4.1.2 Staining protocol).

***Bone marrow**:* The bone marrow for cell type analysis was extracted from the femur, which was stored on ice, in a petri dish containing HANKs buffer until tissue processing. To obtain the bone marrow both ends of the femur were cut with a scalpel before being flushed with 3 ml of cold HANKs buffer out of a syringe (size: 5 ml and a 23G needle). Afterwards, cell suspension was spun down for 5 min at 300 x g and 1 ml of red blood lysis buffer was added for 1 min at RT. Lysis was stopped by adding 10 ml of HANKs buffer. After spinning down for

5 min at 300 x g the cell pellet was suspended in 1 ml HANKs buffer. 100 µl of cell suspension were used for staining (see section 2.4.1.2 Staining protocol).
For analyzing bone marrow stromal cells, cleaned and crushed tibias were washed with 1X HBSS supplemented with 2% BSA and 10 mM HEPES. Afterwards, fragmented bones were digested in DMEM+0.2% collagenase D for 1 h at 37°C. After washing twice, filtering through a 70 µm cell strainer (70 µm, Sysmex, Norderstedt, Germany) and red blood cell lysis, cell staining was performed (see section 2.4.1.2 Staining protocol).

***Lung**:* The right lung was taken, cut into small pieces and added to 300 µl of digestion medium supplemented with 1,25 mg/ml liberase (Roche, Rotkreuz, Switzerland). The digestion of lung tissues occurred at 37°C for 1 hour. Afterwards, 1 ml of HANKs buffer was added and the lysate was filtered through a 50 µm cell strainer (70 µm, Sysmex, Norderstedt, Germany). The filtered cell suspension was spun down for 10 min at 300 x g. The supernatant was carefully removed and the cell pellet was dissolved in 2 ml of HANKs buffer. 100 µl of cell suspension were additionally filtered through a 35 µm cell strainer cap, washed with 500 µl of HANKs buffer (5 min at 300 x g) and finally suspended in antibody staining solution (see section 2.4.1.2 Staining protocol).

***Spleen**:* After harvesting, spleens were stored on ice, in a petri dish containing HANKs buffer until further tissue processing. A cell suspension was obtained by smashing 1/3 of the spleen through a 30 µm filter with 3 ml of HANKs buffer. Afterwards, the sample was spun down at 300 x g for 5 min. For red blood cell lysis the cell pellet was dissolved in 1 ml of lysis buffer and incubated for 1 min at RT. Red blood cell lysis was stopped by adding 10 ml of HANKs buffer. Then, cells were spun down for 5 min at 300 x g. The cell pellet was dissolved in 1 ml HANKs buffer and only 50 µl of cell suspension were used for staining (see section 2.4.1.2 Staining protocol).

***Aorta**:* Whole aorta was collected in 300 µl of digestion medium (Table 1) and cut into small pieces. After adding 1,25 mg/ml liberase (Roche, Rotkreuz, Switzerland) aortic tissues were incubated at 37°C for 1 hour to allow tissue digestion. The digestion was stopped by adding 500 µl of HANKs buffer. Cell suspension was filtered through a 35 µm cell strainer cap and spun down for 5 min at 300 x g. Whole cell pellet was suspended in antibody staining solution (see section 2.4.1.2 Staining protocol).

2.4.1.2 Staining protocol

Each cell suspension was labeled with 100 µl of antibody staining solution supplemented with the antibodies of interest at the indicated concentrations:

cell marker antibody	**clone**	**company**	**amount/sample**
CD45	30-F11	ThermoFisher Scientific	0.5 µg
CCL2	eH5	ThermoFisher Scientific	
CD140b	APB5	BioLegend	
CD31	MEC13.3	BioLegend	
CD45	I3/2.3	BioLegend	
Ly6C	HK1.4	BioLegend	
TER-119	APC/Cy7	BioLegend	
CD11b	M1/70	BioLegend	0.2 µg
Gr1	RB6-8C5	BioLegend	
CD115	AFS98	BioLegend	
Ly6G	1A8	ThermoFisher Scientific	
CD11a	M17/4	BioLegend	
CD62L	MEL-14	ThermoFisher Scientific	
CD18	M18/2	ThermoFisher Scientific	1 µg
CCR5	HM-CCR2 (7A4)	ThermoFisher Scientific	
CCR2	#475301	R&D Systems	10 µl/1 million cells
CXCR2	#242216	R&D Systems	
CXCR4	#247506	R&D Systems	

Cell surface staining was performed for 20 min on ice and the tubes were protected from light. After staining, non-bound antibodies were washed away by adding 500 µl of HANKs buffer and spinning down for 5 min at 300 x g. Supernatant was removed and cell pellet was suspended in 400 µl of HANKs buffer. Samples were kept on ice until analysis by flow cytometry.

Intracellular staining was performed after cell surface staining. First, the cells were fixed with Fixation buffer (BioLegend, San Diego, USA) for 15 min at RT, then permeabilized by adding 2 ml of PermWash buffer (BioLegend, San Diego, USA) and finally washed for 10 min at 300 x g. This step was repeated two times. Finally, the sample were stained with an antibody to CCL2 (eH5, Thermo Fisher Scientific, Waltham, USA) in PermWash buffer for 1 hour at RT in

the dark. After staining, the cells were washed with PermWash buffer and resuspended in HANKs buffer. The sample was kept on ice until analysis by flow cytometry.

Certain surface markers (CD45, CD11b, Gr1, CD115, Ly6C and Ly6G) were used to discriminate among myeloid cell populations; classical monocytes, non-classical monocytes, neutrophils and macrophages. In addition, stromal cells in bone marrow were identified by being positive for PDGF receptor β and negative for cell lineage markers. The following cell surface markers were used to differentiate the above mentioned cell types in distinct organs:

	Blood/Bone marrow/Spleen	**Aorta/Lung**
Neutrophils	$CD45^{+}$,$CD11b^{+}$,$Gr1^{high}$,$CD115^{-}$	$CD45^{+}$,non-autofluoresent cells, $CD11b^{+}$,$Gr1^{high}$, $Ly6G^{+}$,SSC^{high}
Classical monocytes	$CD45^{+}$,$CD11b^{+}$,$Gr1^{high}$,$CD115^{+}$	$CD45^{+}$,non-autofluoresent, $CD11b^{+}$,$Gr1^{high}$,$Ly6C^{high}$,SSC^{low}
Non classical monocytes	$CD45^{+}$,$CD11b^{+}$,$Gr1^{low}$,$CD115^{+}$	$CD45^{+}$,non-autofluoresent, $CD11b^{+}$,$Gr1^{low}$, $Ly6C^{low}$,SSC^{low}
Macrophages	$CD45^{+}$,autofluoresent cells	$CD45^{+}$,autofluoresent cells
Bone marrow stromal cells	$CD45^{-}$,$TER119^{-}$,$CD31^{-}$,PDGF receptor β^{+} (CD140b)	-

2.4.1.3 Analysis

Flow cytometry was performed with a FACSCanto II (BD Bioscience, San Jose, CA, USA). CountBright™ absolute counting beads (Invitrogen, Carlsbad, CA, USA) were used to assess the absolute cell number in each analyzed organ. Flow cytometry data were analyzed with FlowJo Software (10.1 Flowjo LLC, Ashland, USA). The expression levels of non-lineage markers are presented in geometrical mean fluorescence intensity (MFI).

2.4.2 Quantification of plasma chemokines

Screening of plasma chemokines levels was performed by using the Luminex Multiplex Immunoassay ProcartaPlex™ (ThermoFisher Scientific, Waltham, USA) while further single analysis of CCL2 (MCP-1) plasma levels was performed by using a mouse MCP-1 ELISA kit (Sigma-Aldrich, Hilden, Germany).

2.4.2.1 Plasma generation

Blood samples were collected in EDTA tubes and spun down at 3000 x g for 15 min at 4°C to separate the plasma from blood cells. Plasma samples were collected and frozen at -80°C until measurement.

2.4.2.2 Luminex Multiplex Immunoassay ProcartaPlex™

ProcartaPlex™ Immunoassays (ThermoFisher Scientific, Waltham, USA) allows to detect and quantify multiple proteins simultaneously in a single sample by *xMAP®* technology. Thereby, proteins are labeled with fluorescent-dyed beads and analyzed according to their bead size.

During processing each plasma sample was spun down at 10,000 x g for 10 min at 4 °C to separate plasma from lipid and platelet contaminations. First, the standard series was generated by preparing a 4-fold serial dilution with the "sample type-specific standard buffer" and the reconstituted antigen standard. Second, 50 µl of each antibody magnetic bead was added per well to a 96-well plate, fixed on a handheld magnetic washer, and washed with 150 µl of wash buffer. After allowing the beads to accumulate on the bottom of each well the wash buffer was removed by inverting the plate. Next, 25 µl of each standard and sample were added into dedicated wells. The plate was sealed, removed from the handheld magnetic washer and incubated for 120 min at RT, rocking at 500 rpm. Afterwards, the plate was fixed again on the handheld magnetic washer, the solution in each well was removed by inverting the plate and 150 µl of wash buffer was added into each well. After allowing beads to accumulate on the bottom of each well for 30 sec the wash buffer was removed by inverting the plate. This washing step was repeated 5 times. In the next step, 25 µl of detection antibodies was added into each well and the plate was removed from the handheld magnetic washer, sealed and placed on a shaker at 500 rpm for 30 min at room temperature. Then, the plate was fixed on the handheld magnetic washer and each well was washed again as described above before adding 50 µl of Streptavidin-PE solution into each well. After sealing and removing it from the handheld magnetic washer, the plate was incubated at 500 rpm for 30 min at room temperature. Afterwards, the plate was fixed again on the handheld magnetic washer and washed as described above. In the last step, 120 µl of reading buffer was added into each well. The plate was sealed, fixed on the magnetic handheld washer and incubated for 5 min at room temperature, rocking at 500 rpm. Finally, the analysis was performed with an Infinite 200 PRO plate reader (TECAN, Männedorf, Switzerland).

2.4.2.3 CCL2 (MCP-1) ELISA

A solid-phase sandwich Enzyme-Linked Immunosorbent Assay was used to detect plasma CCL2 levels. During the first step the standard was reconstituted in standard diluent buffer to generate a stock solution at a concentration of 5000 pg/ml. This standard stock solution was further diluted to generate seven standards at concentrations ranging from 39 pg/ml to 2500 pg/ml. Next, 100 µl of standard and plasma samples were added to the wells and incubated for 2 hours at RT to allow CCL2 to bind the antibodies on the well surface. Afterwards, non-bound proteins were removed by washing wells six times with 1X Wash buffer. Then, 100 µl of mouse anti-CCL2 biotin conjugate solution was added into each well and incubated for 45 min at RT. This solution contains biotin conjugated antibodies that recognize bound CCL2 on captured antibodies. Afterwards, non-bound antibodies were removed by washing wells six times with 1X Wash buffer. During the next step 100 µl of 1X streptavidin-HRP was added and incubated for 45 min at RT. This detection antibody is linked to the enzyme horseradish peroxidase (HRP) and binds to the biotin of the previous added antibody. Non-bound antibodies were removed by washing wells six times with 1X Wash buffer. In the last step 100 µl of stabilized chromogen substrate (TMB) was added to each well and incubated for 30 min at RT in the dark. The enzyme HRP catalyzes the conversion of TMB into a blue product, which turns yellow after adding 100 µl of stop solution. The absorbance was measured at 450 nm with an Infinite 200 PRO plate reader (TECAN, Männedorf, Switzerland).

2.5 Confocal imaging

Confocal microscopy is an optical imaging method that captures two-dimensional images at different depths to achieve the three-dimensional structure.

2.5.1 Imaging of CCR2 and intracellular CCL2 expression

Whole blood cells were lysed with 3 ml lysis buffer/100 µl blood. Afterwards, cells were suspended in cell culture medium RPMI-1460 supplemented with 0.5% bovine serum albumin (BSA) (ThermoFisher Scientific, Waltham, USA) and added to a Poly-L-Lysine coated slide (ThermoFisher Scientific, Waltham, USA) for 15 min at 37°C. Non adherent cells were removed by washing with RPMI-1640+0.5% BSA. Adherent cells were fixed with 4% paraformaldehyde for 30 min at RT and stained with an antibody to CCR2 (EPR19698, abcam) and to Ly6G (1A8, BD Bioscience, San Jose, CA, USA) or Ly6C (HK1.4, BioLegend, San Diego, USA) for monocytes or neutrophils identification. Nuclei were counterstained with

4',6-Diamidino-2-phenylindol (DAPI, ThermoFisher Scientific, Waltham, USA). Secondary staining was performed with anti-rabbit Dylight550 (ThermoFisher Scientific, Waltham, USA) and anti-rat Dylight488 (ThermoFisher Scientific, Waltham, USA).
For the intracellular CCL2 staining cells were fixed with 4% paraformaldehyde and stained with an antibody to Ly6G (1A8, BD Bioscience, San Jose, CA, USA) or Ly6C (HK1.4, BioLegend, San Diego, USA). The sample was then permeabilized with 0,05% TritonX-100 (Sigma-Aldrich, St- Louis, USA) for 10 min at RT. Afterwards, the cells were washed three times before adding an antibody to CCL2 (2H5, ThermoFisher Scientific, Waltham, USA) and DAPI (ThermoFisher Scientific, Waltham, USA). Secondary staining was performed with anti-rat Dylight488 (ThermoFisher Scientific, Waltham, USA) and anti-armenian hamster Cy3 (Jackson ImmunoResearch, Cambridgeshire, UK). The samples were imaged with a Leica TCS SP8 3X microscope in confocal mode. Image acquisition and processing was performed using LasX software (Leica, Wetzlar, Germany).

2.6 Static adhesion assay

Static adhesion assays aim to quantify adhesion of cells to an immobilized substrate under static conditions. In our experiment setup, isolated murine blood cells were either suspended in static adhesion buffer or plasma obtained from different mouse strains. Isolated blood cells suspended in static adhesion buffer were added to a well coated with immobilized murine proteins while isolated blood cells suspended in plasma were added to wells coated with a murine endothelial cell monolayer.

2.6.1 Murine endothelial SVECs

Murine endothelial cells SVEC4-10 (#CRL-2181, ATCC) were cultured in Dulbecco's modified Eagle's medium (DMEM) supplemented with 10% FCS in a 75 cm^2 Cellstar® flask with a specific surface-treatment to improve cell adhesion (Greiner bio-one, Kremsmünster, Austria). The cells were kept at 37°C with a concentration of 5 % CO_2 and they were split every three days with a subculture ratio of 1:8. To cover wells with a murine endothelial cell layer, SVEC4-10 cells were detached from the flask by adding 0,05% of Trypsin-EDTA. Trypsin is a serine protease that hydrolyzes surface adhesion molecules while EDTA removes calcium that is necessary for cell adhesion. One day before the experiment, wells of a 96 well plate were coated with 40 µg/ml collagen (Merck, Darmstadt, Germany) for 30 min at 37°C. Afterwards, 40.000 SVECs were seeded into each well and incubated overnight at 37°C with a concentration of 5 % CO_2.

2.6.2 Protein coating of wells

The wells of a 96 well plate were coated with immobilized proteins by adding 2 µg/ml of murine VCAM1, ICAM1, E-selectin, and P-selectin (R&D Systems, Minneapolis, USA) in 50 µl of PBS supplemented with 1 mM calcium and 1 mM magnesium into each well. To allow coating of the well surface, plates were incubated for 2 hours at 37°C with a concentration of 5 % CO_2. Afterwards non-specific binding sites were blocked by adding 50 µl of PBS supplemented with 5% BSA. Coated plates were kept at 4°C overnight before performing the static adhesion assay.

2.6.3 Cell adhesion and analysis

Whole blood cells were isolated from hypercholesterolemic *Apoe*$^{-/-}$ mice or hypercholesterolemic *Lyz2CreBmal*$^{flox/flox}$*Apoe*$^{-/-}$ mice. Blood cell lysis was performed by using 3 ml of red blood cell lysis buffer per 100 µl of blood for 15 min at RT. Cells were washed with HBSS and spun down at 300 x g for 5 min. Afterwards cells were either suspended in static adhesion buffer, plasma or plasma supplemented with the CCR2 antagonist (RS102895, 100 ng/ml) before being added to the wells. Cells were allowed to adhere for 15 min at 37°C. Non-adherent cells were carefully removed by washing the wells with PBS three times. After each washing step PBS was carefully removed by turning the plate and slowly blotting it on several paper towels. Thereafter, adherent cells were fixed with 4% paraformaldehyde (PFA). To visualize adherent monocytes and neutrophils, cells were stained with directly conjugated anti-Ly6G (1A8, BioLegend, San Diego, USA) and anti-Ly6C (HK1.4, BioLegend, San Diego, USA) for 15 min at room temperature. To quantify number of adherent cells images of each well were acquired with an Olympus IX81 inverted microscope with a 10x/0.3 objective. Number of adherent cells was counted in 5 pictures per well using ImageJ software.

2.7 Histology and Immunohistochemistry

Histology is used to study microstructure of tissue whereas immunohistochemistry is an antibody-based method for imaging proteins of interest in tissue sections.

2.7.1 Tissue preparation:

Mice were euthanatized and their circulation was flushed with PBS to remove blood cells. Hearts and kidneys were dissected and prepared by fixation with 4 % PFA for 24 hours and subsequently, samples were incubated in 30 % sucrose for 24 hours at 4°C. Afterwards,

hearts and kidneys were embedded in Tissue-Tek® O.C.T. Compound (A.Hartenstein, Würzburg, Germany) snap frozen and stored at -20°C until further processing. Sections of the aortic root were generated with a thickness of 4 µm with a cryostat (Leica, Wetzlar, Germany) and three sections from each mouse were analyzed.

2.7.2 Histology:

Lesion size was assessed in aortic root cross-sections by staining for lipid deposition with oil red O (Sigma-Aldrich, St. Louis, USA) and hematoxylin and eosin (H&E) staining.

H&E staining is used to visualize tissue types and morphological changes. Hematoxylin binds to basophilic substances, such as DNA, while Eosin stains acidophilic substances, such as positively charged amino acids of proteins. At the beginning of the staining procedure, the sections were washed by dipping them three times into aqua destillata. Then, sections were stained in a hematoxylin solution (Merck, Darmstadt, Germany) for 5 min. Afterwards, sections were washed in tap water for 5 min and stained with eosin (Carl Roth, Karlsruhe, Germany) for additonal 5 min. The sections were again washed in tap water for 5 min. Dehydration of the sections was performed by dipping or incubating the sections in distinct solutions according to the following protocol:

Solution	**Procedure**
EtOH 50%	dip 3x
EtOH 70%	dip 3x
EtOH 96%	dip 5x
EtOH 100%	dip 10x
EtOH 100%	dip 10x
Xylene 1	2 min
Xylene 2	2 min

Finally, sections were mounted with in Roti Histokitt II medium (Carl Roth, Karlsruhe, Germany) and stored at RT before imaging.

Oil red O is a fat-soluble dye, which stains neutral triglycerides and lipids in frozen sections. First, sections were washed in PBS for 5 min and dipped 10 times in 60% 2-propranol. The staining was performed in the oil red O staining solution (see Table 1) for 15 min at RT. Afterwards, sections were washed again by dipping the sections 10 times in 60% 2-

propranol, incubating them in tap water for 5 min and aqua destillata for 30 sec. Nuclei were counterstained by incubating the sections in the hematoxylin solution for 30 sec. After a final washing step for 5 min in tap water, the sections were mounted in Shandon-Mount™ medium (ThermoFisher Scientific, Waltham, USA).

All images were taken with a Leica DM4000 microscope (Leica Microsystems, Wetzlar, Germany) followed by computerized image analysis and quantification (Leica Qwin Imaging software, Wetzlar, Germany).

2.7.3 Immunohistochemistry:

Antigen retrieval was performed for every fixed tissue section. The sections were washed in PBS. Afterwards, the antigen retrieval solution (see Table 1) was warmed up in a microwave at maximum power. As soon as the antigen retrieval solution cooled down, the sections were placed into the solution and warmed up at 90 Watt for 10 min. Then, the sections were washed in PBS for 5 min at RT. Before performing specific stainings, unspecific binding sides were blocked with the blocking solution (see Table 1) for 30 min at RT. Specific antibody staining solutions with the following antibody concentrations were added afterwards. The content of macrophages in atherosclerosic lesions was analyzed by staining aortic root sections with 2,5 µg/ml anti-Mac2 (CL8942AP, Cedarlane, Burlington, USA). Adhesion molecules on endothelial cells were stained with antibodies to VCAM1 (429, BD Bioscience, San Jose, CA, USA), ICAM1 (3E2, BD Bioscience, San Jose, CA, USA), P-Selectin (RB40.34, BD Bioscience, San Jose, CA, USA) or E-Selectin (10E9.6, BD Bioscience, San Jose, CA, USA) at a concentration of 10 µg/ml. Expression of CCL2 on endothelial cells was measured by staining with an antibody to CCL2 (eH5, ThermoFisher Scientific, Waltham, USA) and endothelial cells were counterstained with an antibody to CD31-Alexa Fluor647 (MEC13.3, BioLegend, San Diego, USA) at a concentration of 5 µg/ml of each antibody. Expression of CCL2 in lesional macrophages of aortic root cross-sections was obtained by staining with an antibody to CCL2 (eH5, ThermoFisher Scientific, Waltham, USA) at a concentration of 5 µg/ml and an antibody to Mac2 (M3/38, Cedarlane, Burlington, USA) at a concentration of 2,5 µg/ml. Secondary antibody staining was performed with a donkey anti-Rat IgG-Dylight488 (1 µg/ml, ThermoFisher Scientific, Waltham, USA) and an anti-armenian hamster IgG-Cy™3 antibody (1 µg/ml, Jackson ImmunoResearch, Cambridgeshire, UK). To visualize CD45 pre-labeled leukocytes the sections were stained with donkey anti-rat IgG-Dylight550 (1 µg/ml, ThermoFisher Scientific, Waltham, USA). Nuclei were counterstained with 4',6-Diamidino-2-phenylindol (DAPI, ThermoFisher Scientific, Waltham, USA). A Leica DM4000 microscope with a 20x objective (Leica Microsystems, Wetzlar, Germany) and a

Leica DFC 365FX camera were used to capture images. Leica Qwin Imaging software (Leica, Wetzlar, Germany) was employed for image analysis.

2.8 Plasma cholesterol and triglyceride measurement

Blood samples were collected in EDTA tubes to avoid coagulation. Plasma separation was obtained by spinning it down at 3000 x g for 15 min at 4°C. Afterwards, plasma samples were collected and frozen at -80°C until measurement.
Plasma cholesterol and triglyceride levels were quantified in murine plasma by an enzymatic reaction that uses these compounds as a substrate and generates H_2O_2. The byproduct H_2O_2 is then used in a reaction catalyzed by the peroxidase, leading to a product whose absorbance can be measured at 500 nm to determine indirectly the concentration of cholesterol and triglycerides.

Total cholesterol was measured according to the following reaction sequence:

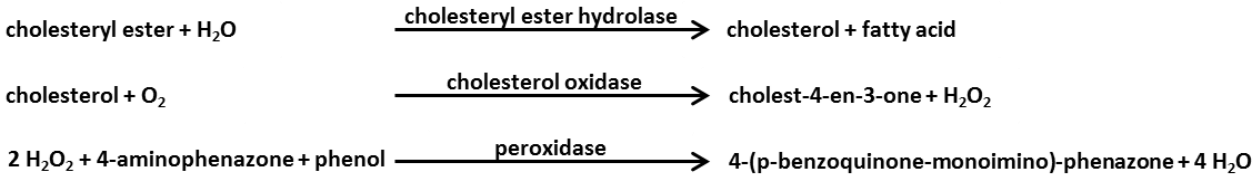

Triglyceride levels were quantified according to the following reaction:

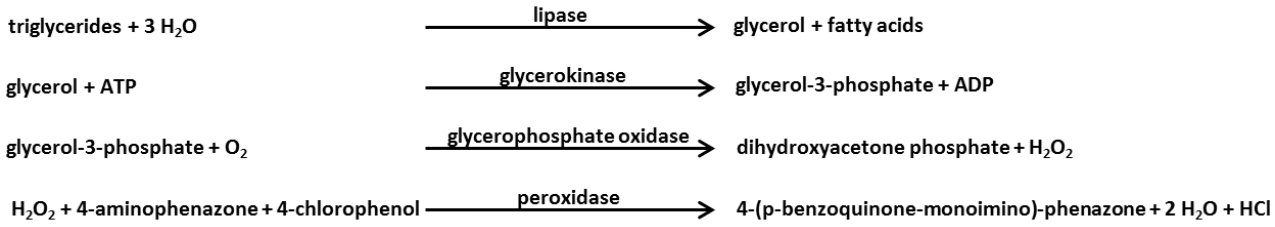

First, plasma samples were thawed on ice. A standard solution series was generated for cholesterol (0,05 µg/µl - 1,56 µg/µl) and triglycerides (0,04 µg/µl – 1,35 µg/µl) and added to a 96 well plate. Plasma samples for cholesterol measurements were diluted 1:5 while plasma samples for triglyceride measurements were used undiluted and 5 µl of each sample or standard were added to the plate. Finally, 200 µl of the reaction solution including all substrates necessary for the enzymatic reaction to analyze cholesterol and triglyceride levels

were added to each well. The plate was incubated for 30 min in the dark at RT before measuring the absorbance at 505-510 nm with a Thermo Scientific Multiskan Ex plate reader (ThermoFisher Scientific, Waltham, USA).

2.9 mRNA expression analysis

2.9.1 Isolation of primary cells

Blood was collected into EDTA tubes and red lysis was performed by adding 3 ml red lysis buffer to 100 µl of blood. After 15 min of lysis at RT cells were washed by adding HANKs buffer. Afterwards, neutrophils were isolated with the Neutrophil Isolation Kit (Miltenyi Biotec, Bergisch Gladbach, Germany) and monocytes were isolated with the CD115 MicroBead Kit (Miltenyi Biotec, Bergisch Gladbach, Germany) according to the manufacturer's instructions. Purity of the resulting neutrophils and monocytes was verified by flow cytometry analysis. Cell pellets were stored at -80°C until further RNA extraction (see section 2.9.2 RNA isolation).

2.9.2 RNA isolation

RNA was extracted using the Quick-RNA^{TM} MicroPrep kit (Zymo Research, Irvine, USA) according to the manufacturer's protocol. RNA concentration was determined using a NanoDrop 2000 (Thermo Fisher Scientific, Waltham, USA). Samples were stored at -80°C until further processing.

2.9.3 cDNA synthesis

cDNA synthesis was carried out with the QuantiNova^{TM} Reverse Transcription Kit (Qiagen, Hilden, Germany) in accordance with manufacturer's instructions.

2.9.4 Quantitative real-time PCR

Quantitative real-time PCR was performed using the QuantiNova^{TM} SYBR® Green PCR kit (Qiagen, Hilden, Germany) on a 7900HT Fast Real-Timer PCR System according to the manufacturer's protocol. The following primers have been used: Mm_Vcam1_1_SG, Mm_Icam1_1_SG, Mm_Selp_1_SG, Mm_Sele_1_SG, Mm_Ccl2_1_SG, and Mm_Rn18s_3_SG (Qiagen, Hilden, Germany). For quantifying the myeloid specific *Bmal1*-knockout the following designed primers were used: Fw_5'-AGA GGT GCC ACC AAC CCA TA-3' and Rv_5'TGA GAA TTA GGT GTT TCA GTT CGT CAT-3' (Metabion, Planegg, Germany). 18S served as a house-keeping gene in all performed mRNA expression analyses. Relative quantification was performed by using the ΔΔCT method which compares

two different experimental RNA samples and normalizes them to a housekeeping gene with the following formula:
Fold change= $2^{-\Delta\Delta CT}$ = [(CT gene of interest – CT internal control) sample A – (CT gene of interest – CT internal control) samples B)]

2.10 Masspectometry

C57Bl/6J mice (Janvier labs, Le Genest Saint Isle, France) were injected i.p. with a single dose of 5 mg/kg CCR2 antagonist (RS102895, Sigma) at ZT1 or ZT13. Plasma was taken after indicated time points and stored at -80°C until pharmacokinetic analysis. Mass spectrometry analysis was performed by Hessel Poelman from the research group of Dr. Gerry A.F. Nicolaes (Department of Biochemistry; Maastricht University) according to an already published protocol by Mitchell et. al. 2013. A concentration step and adaptation to the specific LC-MS setup were added this protocol. A calibration curve ranging from 1 to 500 ng/ml was generated by adding RS102895 into blank samples. Additionally, all samples were spiked with an internal standard (RS504393) to a final concentration of 200 ng/ml and 0.003% DMSO. A volume of 200 µl cold acetonitrile supplemented with 0.1% formic acid was added to 100 µl of each sample to precipitate proteins. Afterwards samples were spun down and 200 µl of supernatant was taken for concentration using SpeedVac™ (Savant SC110, drying rate on low for 2 h). The concentrated solution was spun down again and 50 µl of the supernatant were taken for UPLC-MS measurement, performed using the Waters™ (Milford,MA,USA) XEVOG2QToF system. During this measurement, chromatography was performed with the Acquity UPLC Peptide BEH C18 column 130 Å, 1.7 µm, 2.1mm × 50mm with guard filter. The settings for flow rate were 0.25 ml min^{-1} and the volume for sample injection contained 10 µl. Buffer A (0.1% formic acid) and buffer B (10% water and 0.1% formic acid in acetonitrile) were used for the mobile phase. Buffer B was increased linearly from 10% at 1.5 min to 67% at 11 min. The following settings were used for mass spectrometry operating in ESI+TOF MS/MS mode with a range from 350 kDa to 450 kDa: capillary voltage 2.5kV, sampling cone 30V, extraction cone 4.0V, source temperature 120°C, desolvation temperature 450°C, cone gase 20lh^{-1}, desolvation gas 800lh^{-1}, collision energy off. Acquisition settings were set follows: Polarity Positive, Analyser mode Sensitivity, Dynamic range Normal, Target enhancement 391 Da up until 7 min and 419 Da after, corresponding to the elution times and respective masses of analyte and internal standard. Peak areas were integrated using Waters Quanlyx software (V4.1 SCN802).

2.11 Statistics

Statistical analysis was performed with GraphPad Prism 7 (GraphPad Software Inc.).
All data are expressed as mean ± SEM and statistical parameters including exact value of n, definition of center, statistical analysis and significance are reported in the figure legends. Significance was judged with a $p<0.05$. Normality was tested for each data set by D'Agostino-Pearson omnibus test. Afterwards, Mann-Whitney test, unpaired t test or paired t test were used to compare two samples. For multiple group comparisons, one-way ANOVA analysis was performed followed by Tukey´s multiple comparison tests. Cosinor analyses were performed by using the Matlab 9.4 software.

3. Results

The impact of the circadian clock on myeloid cell recruitment during atherosclerosis was investigated in the well established *Apoe*$^{-/-}$ mouse model. ApoE is present on the surface of most lipoproteins. It functions as a ligand for lipoprotein receptors, thus mediating the uptake of chylomicrons, very low-density lipoprotein (VLDL), and their remnants by hepatic LDL-receptors. Due to the *Apoe* knockout, these mice develop a hyper- and dyslipoproteinemia, severe hypercholesterolemia, and atherosclerotic lesions (Zhang et al. 1992). Furthermore, ApoE is found on the cell surface of hematopoietic stem and multipotential progenitor cells (HSPCs), where it regulates cholesterol efflux pathways (Murphy et al. 2011). HSPCs lacking ApoE accumulate cholesterol intracellularly, thus increasing HSPC proliferation, neutrophilia, monocytosis, and the development of atherosclerosis (Murphy et al. 2011).
Upon high fat diet feeding, the process of atherosclerotic lesion development is accelerated in *Apoe*$^{-/-}$ mouse. In our study, leukocyte recruitment to early atherosclerotic lesions was investigated in *Apoe*$^{-/-}$ mice that were fed with a high fat diet for 4 weeks.

Studies on circadian or diurnal rhythmicity use a specific time system called the Zeitgeber time (ZT) to define the time of day. The Zeitgeber time relates to one of the most important Zeitgebers, namely the light. Zeitgeber time point 0 describes the time point when the light is turned on, while Zeitgeber time point 12 describes the time point when the light is turned off. According to the 12-hour light/ 12-hour dark cycle in our animal facility, the Zeitgeber time is defined as presented by the following graph:

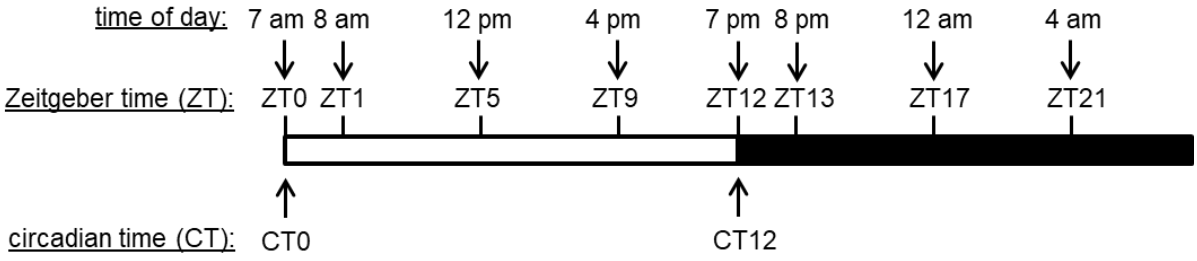

In contrast, the circadian time (CT) is not defined by the Zeitgeber light and represents an estimation of the subjective time under constant darkness. Thus, CT0 defines the beginning of a subjective day and CT12 describes the beginning of a subjective night.

3.1 Myeloid cell recruitment to atherosclerotic lesions oscillates in a time-dependent manner

In the first experiments, we investigated whether arterial myeloid cell recruitment exhibits diurnal rhythmicity during atherogenesis.

3.1.1 Rhythmic myeloid cell adhesion to atherosclerotic prone regions

During atherogenesis leukocytes are released from the bone marrow or spleen into the circulation and transmigrate into atheroprone regions of the carotid artery. In steady state and acute inflammation myeloid cell trafficking exhibits rhythmicity (Scheiermann et al. 2012; Nguyen et al. 2013). To investigate whether myeloid cell recruitment during atherosclerosis appears time-dependent, oscillations in myeloid cell numbers were assessed by flow cytometry in 4 hours-intervals in distinct organs of hypercholesterolemic male *Cx$_3$cr1$^{gfp/WT}$Apoe$^{-/-}$* mice. We observed that numbers of neutrophils and classical monocytes in spleen and bone marrow were at their lowest at ZT17 (Figure 11 A). In contrast, circulating neutrophils and classical monocytes peaked between ZT17 and ZT1 with lowest counts at ZT13 (Figure 11 B). Further experiments aimed to identify rhythmicity in the number of adherent myeloid cells to atherosclerotic prone regions. Thus, intravital microscopy was performed on the carotid artery bifurcation in hypercholesterolemic male *Cx$_3$cr1$^{gfp/WT}$Apoe$^{-/-}$* mice. Rhythmic myeloid cell adhesion to the arterial endothelium peaked between ZT17 and ZT1 and was at their lowest at ZT13 (Figure 11 C). In agreement with oscillatory arterial leukocyte adhesion, aortic myeloid cell numbers analyzed by flow cytometry peaked at ZT1 and exhibited a trough at ZT13 (Figure 11 D), while cell counts of aortic macrophages remained unchanged (Figure 11 H). Furthermore, no rhythmicity was observed for other parameters including platelets, red blood cells, and plasma lipids (Figure 11 E-G).

In summary, numbers of myeloid cells fluctuated in distinct organs under hypercholesterolemia. Furthermore, myeloid cell adhesion to atherosclerotic prone regions in the carotid artery exhibited diurnal rhythmicity. Due to the significant difference of myeloid cell adhesion between ZT1 and ZT13, we focused only on these two time points in further experiments.

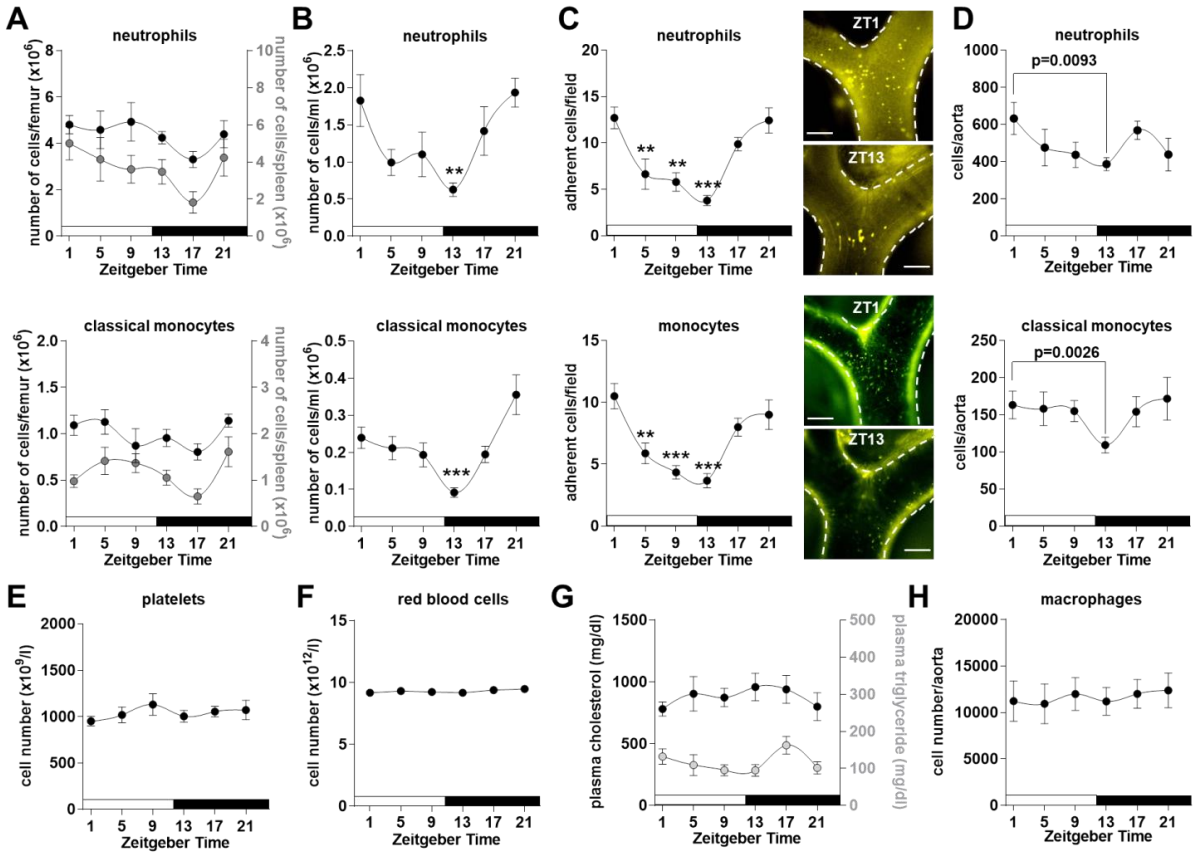

Figure 11: Rhythmic myeloid cell adhesion to atherosclerotic prone regions

(**A-D**) Numbers of myeloid cells in bone marrow and spleen (A), in blood (B), adherent to the carotid artery bifurcation (C) and in aorta (D) were assessed in male hypercholesterolemic *Cx$_3$cr1$^{gfp/WT}$Apoe$^{-/-}$* mice at indicated time points. Representative images illustrate quantification of adherent neutrophils (Ly6G$^+$) or monocytes (gfp$^+$). Scale bar, 100 µm. n=9-18 per time point. Statistical analyses were made by one-way ANOVA. **p<0.001 vs ZT1, ***p<0.0001 vs ZT1. Exact p values in D were calculated by unpaired t-test between indicated groups. Circadian rhythmicity was confirmed in B and C by cosinor analysis with zero-amplitude test. (**E-H**) Numbers of platelets (E), red blood cells (B), plasma lipid levels (G), and aortic macrophages (H) were determined at indicated time points in hypercholesterolemic *Cx$_3$cr1$^{gfp/wt}$Apoe$^{-/-}$* mice**.** n=6-11. Data were analyzed by Kruskal Wallis test. All data are presented as mean±SEM.

3.1.2 Time-dependent myeloid cell entry into atherosclerotic lesions

Our previous results identified elevated myeloid cell adhesion in the carotid artery at ZT1. In addition, higher numbers of myeloid cells were observed in whole aortic tissue at ZT1. However, these results do not reveal whether myeloid cells enter atherosclerotic lesions in a time-dependent manner. To investigate time-dependent myeloid cell transmigration into atherosclerotic lesions, a short-term cell tracking experiment was performed in hypercholesterolemic *Apoe*$^{-/-}$ mice. Intravascular leukocytes were labeled by intravenous administration of a CD45 antibody two hours before harvesting to enable discrimination of vascular derived leukocytes in atherosclerotic lesions. First, the staining efficacy was tested two hours after intravenous injection. More than 95 % of neutrophils and classical monocytes were CD45 positive (Figure 12 A). Second, the specificity of CD45 labeling was investigated by testing the leakage of the antibody through the continuous endothelium of atherosclerotic lesions. Therefore, an antibody to collagen type IV was intravenously injected. Collagen type IV is a component of the basement membrane located underneath endothelial cells, thus providing an optimal target for testing antibody leakage. Fenestrated endothelium of the kidney is permeable and served as a positive control. Indeed, no staining of collagen type IV was observed in the basement membrane of atherosclerotic lesions (Figure 12 B, upper left panel). In contrast, the antibody leaked through the fenestrated endothelium of blood vessels in the kidney, hence being positive for collagen type IV (Figure 12 B, upper right panel). Direct collagen type IV staining confirmed the antibody performance and presence of collagen type IV in the basement membrane of atherosclerotic lesions (Figure 12 B, lower panels).

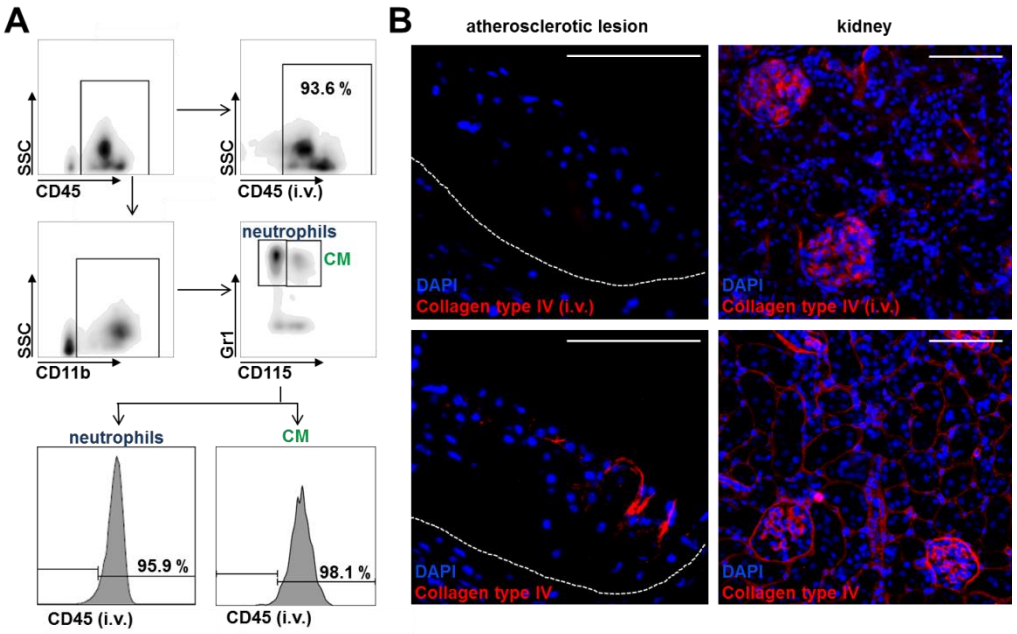

Figure 12: Short-term cell tracking with high efficacy and specificity

Two hours before harvesting, an anti CD45-APC/Cy7 antibody and an anti-collagen type IV antibody were administered intravenously. (A) Labeling efficacy was determined by flow cytometry analysis. (B) No basement membrane staining was detected for the subendothelial matrix in arteries (top left), positive basement membrane staining occurred in fenestrated endothelium of the kidney (top right). Direct staining of aortic root (bottom left) and kidney (bottom right) cross sections served as positive control. Scale bar, 100 µm.

Finally, this experiment setup was used to track intravascular derived leukocytes into atherosclerotic lesions of hypercholesterolemic *Apoe*$^{-/-}$ mice at ZT1 and ZT13. The CD45 antibody was administered two hours before harvesting. Similar staining efficacies assessed by flow cytometry were obtained at ZT1 and ZT13 (Figure 13 A and B). Analysis of intravascular derived leukocytes in whole aortic tissue from hypercholesterolemic *Apoe*$^{-/-}$ mice revealed a higher number of CD45 positive classical monocytes and neutrophils at ZT1 compared to ZT13 (Figure 13 C and D). To investigate the number of transmigrated leukocytes we analyzed the number of CD45 positive cells in atherosclerotic lesions by immunofluorescence. Indeed, a higher number of intravascular derived leukocytes was observed at ZT1 (Figure 13 E). In conclusion, myeloid cell adherence and entry into atherosclerotic lesions peaked at ZT1.

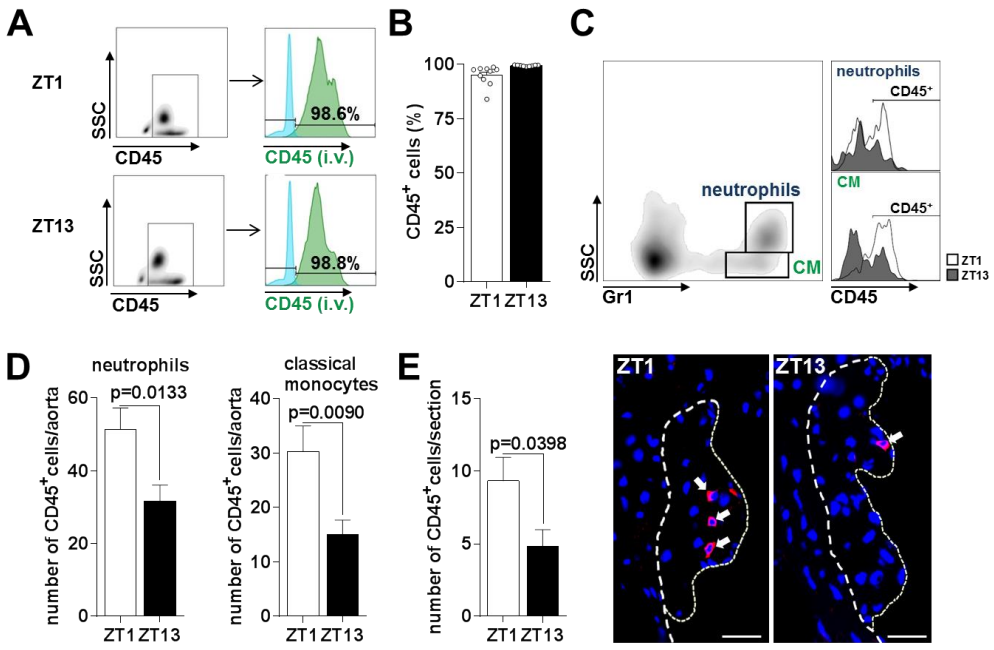

Figure 13: **Time-dependent myeloid cell recruitment into atherosclerotic lesions** (**A-E**) Myeloid cell transmigration into atherosclerotic lesions in hypercholesterolemic *Apoe*$^{-/-}$ mice at ZT1 and ZT13. (A) Representative images of the staining efficacy at ZT1 and ZT13. (B) Percentage of circulating CD45 positive cells at indicated time points. Representative images (C) and quantification of aortic CD45 positive myeloid cells (D) at indicative time points analyzed by flow cytometry. (E) Number of intravascular derived CD45 positive cells (red) counterstained with DAPI (blue) in atherosclerotic lesions analyzed per section. Scale bar, 50 µm. Data were quantified by unpaired t-test. n=14-15 in D and 9-10 in E,B. All data are presented as mean±SEM. CM, classical monocytes; ZT, Zeitgeber time.

3.1.3 Arterial myeloid cell adhesion remained time-dependent under different conditions

In the following experiments we investigated whether rhythmic myeloid cell adhesion to the carotid artery occurred even under different conditions. Therefore, we investigated the number of adherent cells by intravital microscopy in distinct mouse models. First, the influence of gender was assessed by analyzing the number of adherent cells in hypercholesterolemic female *Cx$_3$cr1$^{gfp/WT}$Apoe$^{-/-}$* mice at ZT1 and ZT13. Time-dependent myeloid cell adhesion was maintained with a peak at ZT1, thus indicating that these diurnal differences occur independent of gender (Figure 14 A). Second, time-dependent myeloid cell recruitment was investigated in another mouse model of atherosclerosis, namely hypercholesterolemic *Ldlr$^{-/-}$* mice. The LDL receptor plays a major role in the clearance of ApoB and ApoE containing lipoproteins. LDL receptor deficiency triggers hypercholesterolemia and atherosclerotic lesion development (Ishibashi et al. 1993). Similar results with a peak in the number of adherent myeloid cells at ZT1 were found in female and male hypercholesterolemic *Ldlr$^{-/-}$* mice (Figure 14 B/C). Hence, these results indicate a robust rhythmic myeloid cell recruitment phenotype under hypercholesterolemia. In addition, circadian rhythms oscillate independent of Zeitgebers, thus the endogenous circadian origin was confirmed in different mouse models by keeping the mice in constant darkness (D:D) for two weeks prior harvesting. Indeed, hypercholesterolemic male *Cx$_3$cr1$^{gfp/WT}$Apoe$^{-/-}$* mice and *Ldlr$^{-/-}$* mice of both genders still exhibited time-dependent myeloid cell adhesion under D:D conditions (Figure 14 D-F). These results conclude a time-dependent arterial myeloid cell recruitment phenotype of *bona fide* endogenous circadian nature.

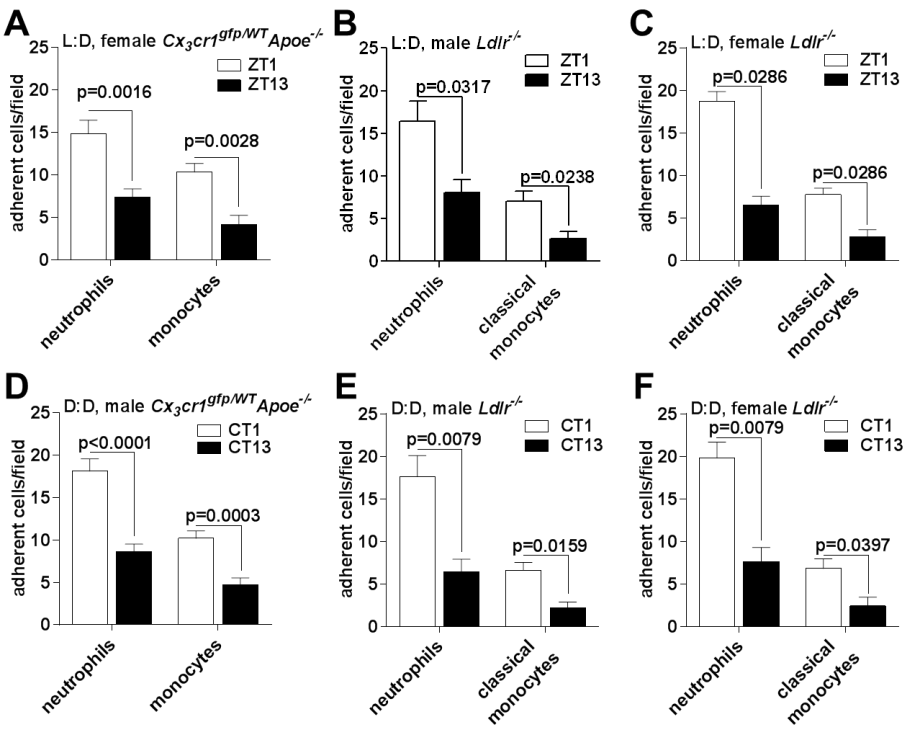

Figure 14: Robust time-dependent arterial myeloid cell adhesion in distinct conditions

Myeloid cell adhesion was studied in female *Cx$_3$cr1$^{gfp/WT}$Apoe$^{-/-}$* (A,D) and male (B,E) or female (C,F) *Ldlr$^{-/-}$* mice by intravital microscopy at ZT1 and ZT13. (**A-C**) Mice were fed with a high fat diet for 4 weeks and kept in L:D conditions. (**D-F**) Mice were fed with a high fat diet for 4 weeks and kept in D:D conditions during the last 2 weeks prior harvesting. Data were analyzed by Mann-Whitney test (A-C and E/F) or Student's t-test (D). n=7-9 in (A), n=5 in (B, E, F), n=4 in (C), n=10 in (D). All data are presented as mean±SEM. L:D, light:dark conditions; D:D, dark:dark conditions; ZT, Zeitgeber time; CT, circadian time.

3.2 Leukocytic expression of adhesion molecules, chemokine receptors, and CCL2 plasma levels exhibit time-dependent differences

Circadian myeloid cell recruitment can be triggered by oscillations in distinct components of the recruitment cascade such as adhesion molecules, chemokines, and chemokine receptors. Furthermore, regulatory mechanisms of the circadian clock such as hormones released from the adrenal gland or the core clock proteins itself might play an important role during circadian myeloid cell recruitment. The following paragraph focuses on identifying the regulatory mechanism that triggers fluctuations in arterial myeloid cell recruitment.

3.2.1 Glucocorticoid or adrenergic receptor signaling does not affect time-dependent myeloid cell recruitment

Rhythms in peripheral clocks are known to be regulated by glucocorticoids or catecholamines, which are released from the adrenal gland into circulation. Glucocorticoids regulate gene transcription by binding to intracellular located glucocorticoid receptors. Upon binding of glucocorticoids, glucocorticoid receptors translocate into the nucleus to function as transcription factors. Catecholamines, such as noradrenaline and adrenaline, bind to adrenergic receptors expressed on the cell surface of different cell types to activate an intracellular signaling cascade.

We tested whether glucocorticoids or catecholamines regulate rhythmic myeloid cell recruitment by blocking their signaling. Hypercholesterolemic *Cx$_3$cr1$^{gfp/WT}$Apoe$^{-/-}$* mice were administered with the glucocorticoid receptor antagonist mifepristone or a cocktail of antagonists blocking α/β adrenergic receptor signaling before performing intravital microscopy at the carotid artery. Inhibition of α/β adrenergic receptor signaling resulted in a reduced number of adherent neutrophils at ZT1 and ZT13, however, time-dependent neutrophil adhesion was maintained (Figure 15 A). No effect of both treatments was observed on monocytes adherence to the carotid artery at ZT1 and ZT13 (Figure 15 B). In summary, these results conclude that glucocorticoid or catecholamine signaling has no impact on the time-dependent differences in arterial myeloid cell adhesion.

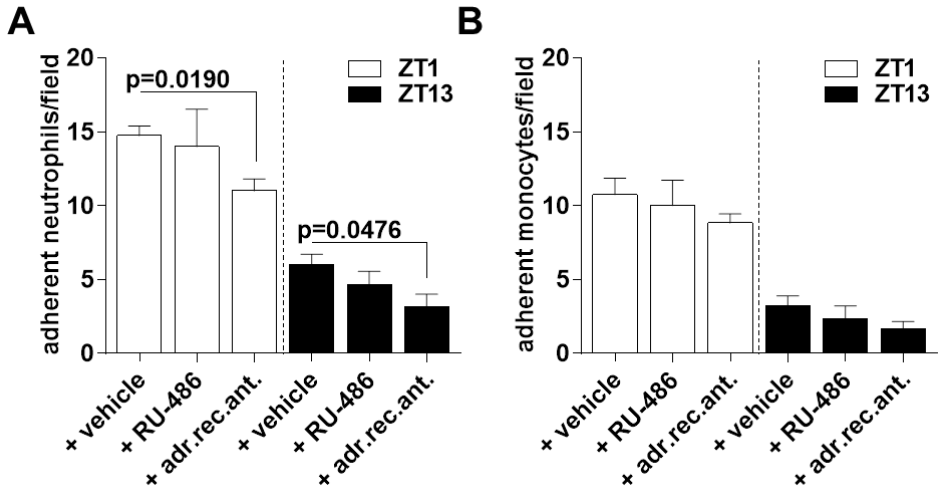

Figure 15: Glucocorticoid and α/β adrenergic receptor signaling does not regulate time-dependent myeloid cell adhesion

(A/B) Glucocorticoid signaling was blocked by the administration of RU-485 (mifepristone), while inhibition of α/β adrenergic receptor signaling was achieved with a cocktail containing a β3-adrenergic

receptor antagonist, a β1/2-adrenergic receptor antagonist propranolol, and α-adrenergic receptor antagonist phentolamine. Data were analyzed by Mann-Whitney test. n=3 (+ RU-486), n=4 (+ vehicle) and n=6 (+ adr.rec.ant.). All data are presented as mean±SEM. adr.rec.ant., α-adrenergic receptor antagonists; ZT, Zeitgeber time.

3.2.2 Arterial endothelial cell adhesion molecules do not exhibit time-dependent differences

Adhesion molecules expressed on endothelial cells regulate leukocyte recruitment to atherosclerotic lesions. Rhythmicity in their expression has previously been reported under steady state (Scheiermann et al. 2012; Gao et al. 2014). To investigate whether time-dependent arterial myeloid cell recruitment is regulated by distinct expression of endothelial cell adhesion molecules at ZT1 and ZT13, we analyzed the expression of VCAM-1, ICAM-1, P-selectin, and E-selectin on endothelial cells of atherosclerotic lesions in hypercholesterolemic *Apoe*$^{-/-}$ mice. These adhesion molecules did not exhibit rhythmic expression on a protein or mRNA level (Figure 16 A-C).

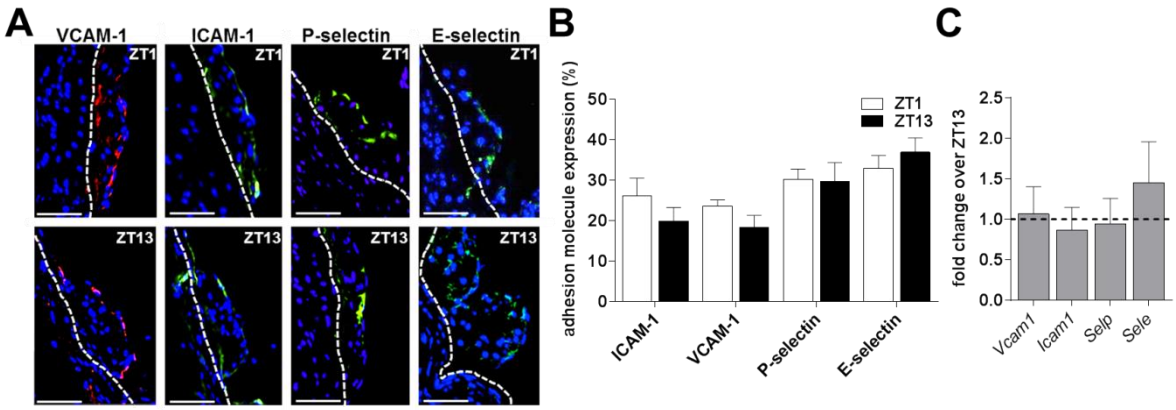

Figure 16: Expression of arterial endothelial cell adhesion molecules does not exhibit time-dependent differences

(A) Representative images of endothelial adhesion molecules vascular cell adhesion molecule-1 (VCAM-1), intercellular cell adhesion molecule-1 (ICAM-1), P-selectin, and E-selectin expressed on lesional endothelium at indicated ZT. Scale bar, 50 µm. (B) Analysis of the expression on endothelial cells of atherosclerotic lesions. n=9-15. Unpaired t-test. (C) mRNA expression analysis of endothelial adhesion molecules *Vcam1*, *Icam1*, *Selp* and *Sele* in isolated aortic tissue from hypercholesterolemic *Apoe*$^{-/-}$ mice. Results were calculated as fold change of ZT1 over ZT13. n=4-11 per analyzed gene. All data are presented as mean±SEM. ZT, Zeitgeber time.

3.2.3 Time-dependent expression of adhesion molecules and chemokine receptors on leukocytes

Next to adhesion molecules expressed on endothelial cells, the leukocyte itself expresses distinct adhesion molecules and chemokine receptors, thus triggering cell adhesion. To investigate whether adhesion molecules and chemokine receptors expressed on circulating classical monocytes and neutrophils exhibit time-dependent differences, their expression was assessed by flow cytometry in hypercholesterolemic *Apoe*$^{-/-}$ mice at ZT1 and ZT13.

Both integrin heterodimers, Mac-1 (CD11b/CD18) and LFA-1 (CD11a/CD18) expressed on leukocytes contribute to cell adhesion on the endothelium (Sumagin et al. 2010). The expression of integrin CD11b (Integrin α-M) on classical monocytes was reduced at ZT13, while its expression on neutrophils remained unchanged (Figure 17 A). In contrast, neutrophils expressed a lower amount of CD11a (Integrin α-L) at ZT13, but its expression on classical monocytes did not change (Figure 17 B). Less expression of CD18 (Integrin β-2) was observed on neutrophils and classical monocytes at ZT13 (Figure 17 C). Additionally, selectins facilitate leukocyte recruitment and indeed less L-selectin was detected on classical monocytes at ZT1 (Figure 17 D).

Furthermore, the expression of distinct chemokine receptors involved in leukocyte recruitment was analyzed on circulating classical monocytes and neutrophils at ZT1 and ZT13. No time-dependent differences were observed for the expression of CXCR2 or CCR5 (Figure 17 E/F). Interestingly, CCR2 expression was increased on neutrophils and classical monocytes at ZT1 (Figure 17 G). Confocal images of monocytes and neutrophils obtained at ZT1 or ZT13 and stained for CCR2 represent a higher expression of CCR2 at ZT1 (Figure 17 H).

In summary, slightly increased expression of distinct integrins on either classical monocytes or neutrophils was observed at ZT1. Less CCR2 expression on both cell types at ZT13 might in combination with oscillatory integrin expression regulate rhythmic myeloid cell recruitment.

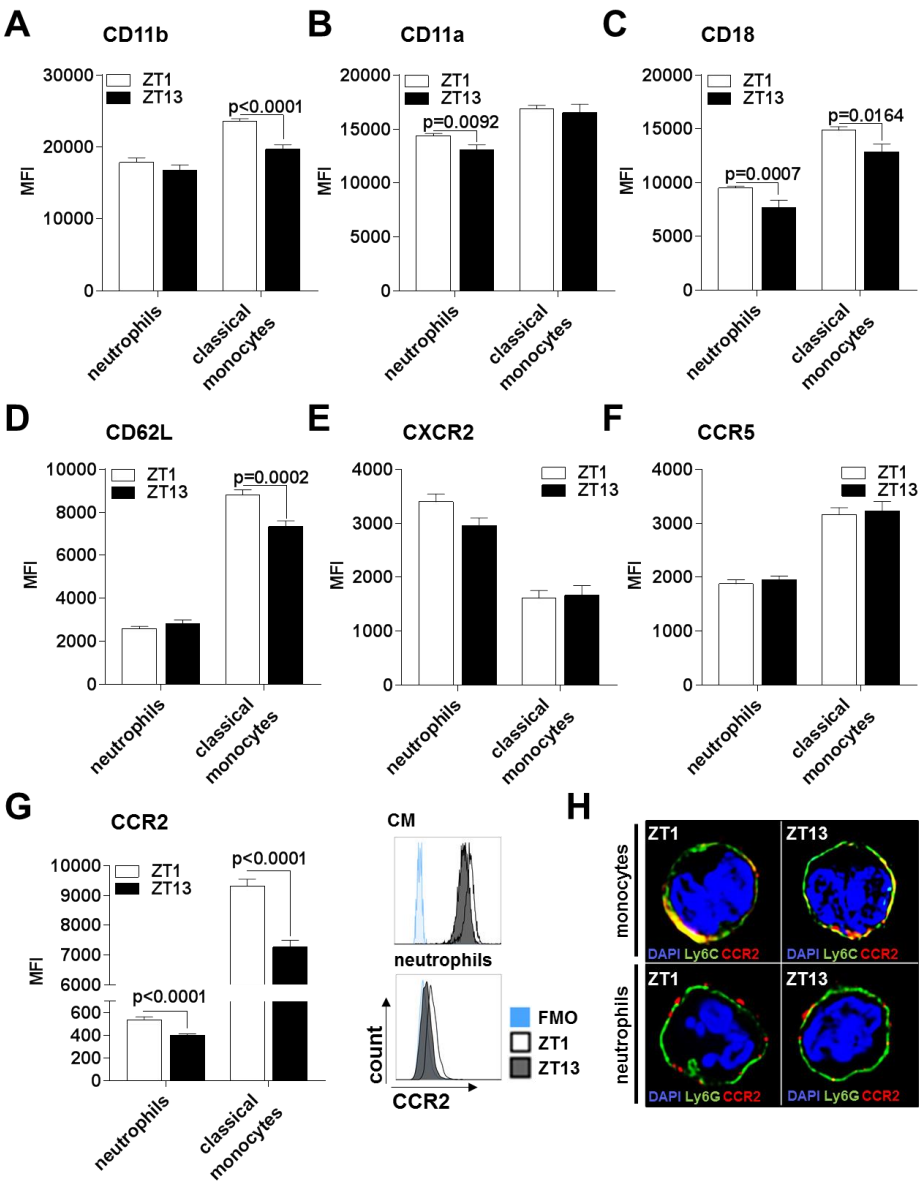

Figure 17: Expression of adhesion molecules on leukocytes exhibit time-dependent differences (**A-D**) Expression of CD11b (A), CD11a (B), CD18 (C), and CD62L (D) on circulating neutrophils and classical monocytes at indicated time points. n>15. Unpaired t-test. (**E-G**) Expression of CXCR2 (E), CCR5 (F), and CCR2 (G) on intravascular myeloid cells. n>15. Unpaired t-test. (**H**) Representative images of classical monocytes and neutrophils from blood stained for CCR2 (red), DAPI (blue) and Ly6G/Ly6C (green) at ZT1 and ZT13. All data are presented as mean±SEM. ZT, Zeitgeber time; FMO, fluorescence minus one; CM, classical monocytes; MFI, mean fluorescence intensity. ZT, Zeitgeber time.

3.2.4 Plasma levels of cytokines

Chemokines and proinflammatory cytokines trigger leukocyte recruitment to sites of inflammation. We investigated whether cytokine levels exhibit time-dependent differences by measuring their protein levels in plasma of hypercholesterolemic *Apoe*$^{-/-}$ mice at ZT1 and ZT13. No differnces in protein levels were observed for CCL5, GM-CSF, TNFα, and IL10 (Figure 18 A-C). A slightly trend of increase of plasma levels of CXCL1, G-CSF, and IL6 was observed at ZT1 (Figure 18 A-C), however, these differences did not reach statistical significance. Interestingly, CCL2 plasma levels were elevated at ZT1 compared to ZT13 (Figure 18 A). Hence, enhanced CCL2 plasma levels might play a role during time-dependent myeloid cell recruitment.

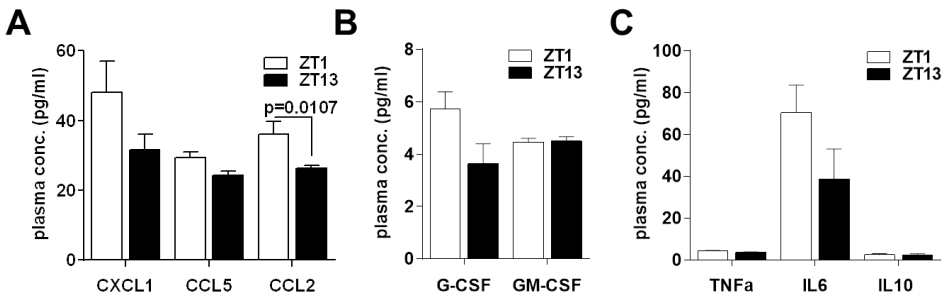

Figure 18: Plasma CCL2 level exhibit diurnal differences

(**A-C**) Protein levels of the chemokines CXCL1, CCL5, and CCL2 (A), the growth factors G-CSF and GM-CSF (B), and the cytokines TNFα, IL6, and IL10 (C) were assessed in plasma obtained from hypercholesterolemic *Apoe*$^{-/-}$ mice at ZT1 and ZT13. ZT. Data were analyzed by Mann-Whitney test or Student's t-test. n=8-15. All data are presented as mean±SEM. ZT, Zeitgeber time.

3.3 Time-dependent arterial myeloid cell adhesion is triggered by the CCL2-CCR2 axis

Previous results revealed higher plasma levels of CCL2, as well as a higher expression of CCR2 on leukocytes at ZT1, indicating that time-dependent myeloid cell recruitment is regulated by the CCR2-CCL2 axis. To further strengthen this hypothesis, we focused on studying CCL2 as the regulatory molecule of time-dependent leukocyte adhesion.

3.3.1 Leukocytes regulate time-dependent differences in CCL2 plasma levels

The chemokine CCL2 guides leukocytes to sites of inflammation by forming a concentration gradient. However, during arterial myeloid cell adhesion, the immobilized CCL2 on endothelial cells is of higher interest for leukocyte arrest. In line with that, we discovered a higher CCL2 coverage on endothelial cells of the carotid artery at ZT1 compared to ZT13 (Figure 19 A). Furthermore, we identified the source of time-dependent CCL2 plasma levels by measuring CCL2 expression in distinct cell types. Bone marrow mesenchymal stem cells (MSCs) express CCL2 upon bacterial infection, thus regulating monocyte trafficking into the blood stream (Shi et al. 2011). Additionally, CCL2 released from lesional macrophages promotes leukocyte recruitment to atherosclerotic lesions (Nazari-Jahantigh et al. 2012). However, expression of CCL2 in both MSCs and lesional macrophages did not exhibit time-dependent differences (Figure 19 B/C). In contrast, we identified time-dependent expression of CCL2 in circulating leukocytes and lymphocytes (Figure 19 D-F). Due to a higher expression of CCL2 in classical monocytes and neutrophils as compared to its expression in lymphocytes, we focused on leukocytes as the source of time-dependent differences in CCL2 plasma levels. In agreement with these findings, depletion of leukocytes by cyclophosphamide (CPM) treatment significantly reduced CCL2 plasma levels at ZT1 to a similar level observed at ZT13 (Figure 19 G/H). In conclusion, time-dependent CCL2 plasma levels derive from circulating leukocytes.

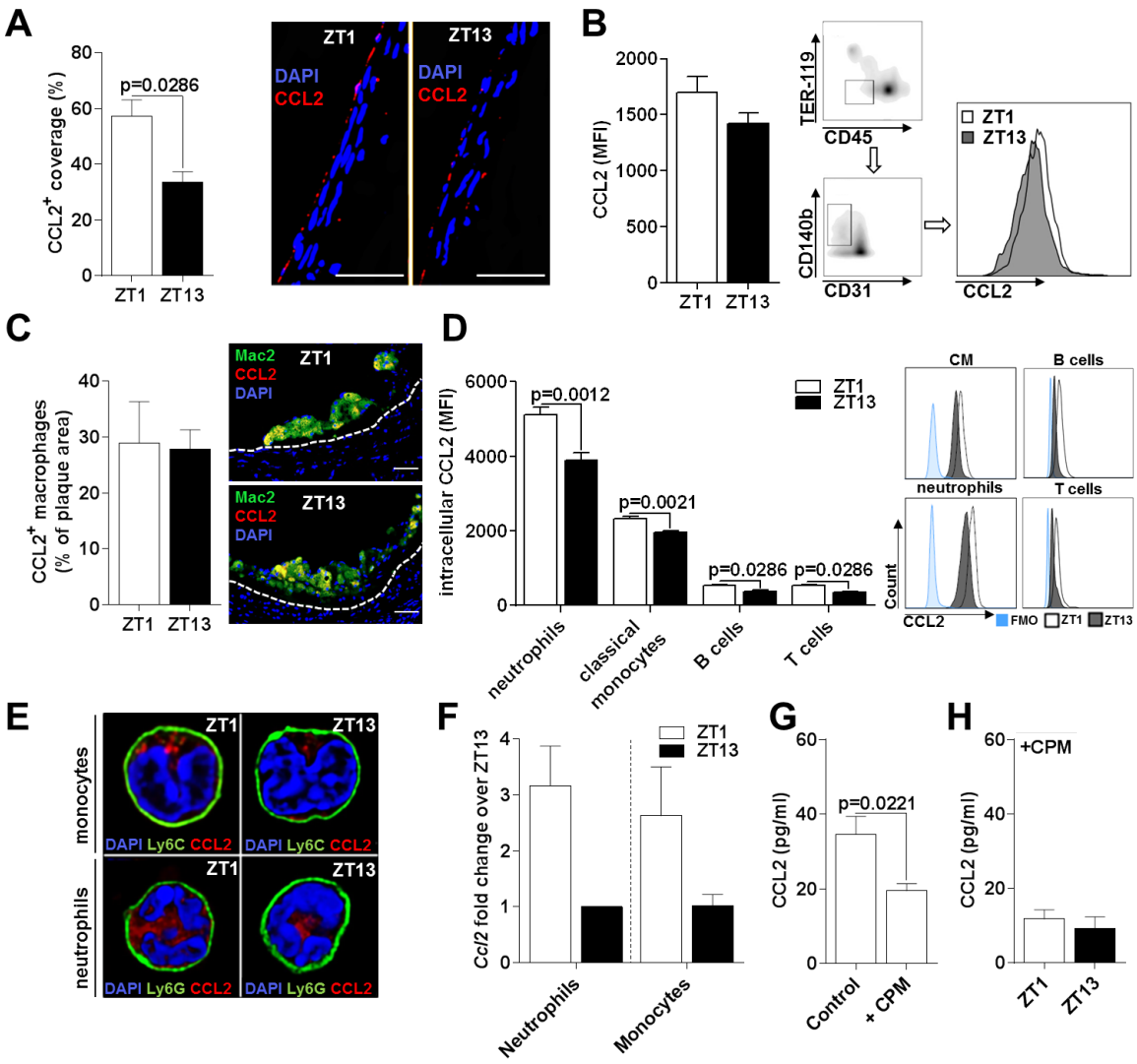

Figure 19: Time-dependent CCL2 plasma levels derive from circulating leukocytes Arterial CCL2 coverage and CCL2 expression in distinct cell types were analyzed in *Apoe*$^{-/-}$ mice after being four weeks on high fat diet. (A) CCL2 coverage on arterial endothelial cells. Scale bar, 50µm. n=4. Mann-Whitney test. (B) Quantification of CCL2 expression in bone marrow mesenchymal stem cells determined by flow cytometry and its gating strategy. n=10. Unpaired t-test. (C) Analysis of CCL2 expression in lesional macrophages in aortic root sections. n=12-13. Unpaired t-test. (D) Intracellular CCL2 content in distinct cell types assessed by flow cytometry and representative histograms. n=4-7. Mann-Whitney test. (E) Representative confocal images stained for Ly6G/Ly6C (green), CCL2 (red) and DAPI (blue) at ZT1 and ZT13. (F) Relative mRNA expression of CCL2 in neutrophils and monocytes. n=6. No signal was detected in 5 out of 6 samples for neutrophils and 4 out of 6 samples in monocytes at ZT13. (G/H) CCL2 plasma levels in leukopenic hypercholesterolemic *Apoe*$^{-/-}$ mice at ZT1 and ZT13. n=6-7. Mann-Whitney test. All data are presented as mean±SEM. CPM, cyclophosphamide. ZT, Zeitgeber time.

3.3.2 Time-dependent myeloid cell recruitment depends on a leukocyte intrinsic effect

Our previous data indicate that rhythmic myeloid cell recruitment depends on a leukocyte intrinsic effect, rather than an endothelial cell triggered phenotype. In order to confirm these findings, *Apoe*$^{-/-}$ mice with a specific deletion of the core clock gene *Bmal1* in arterial endothelial cells or myeloid cells were used. BMAL1 (brain and muscle ARNT [arylhydrocarbon receptor nuclear translocator]-like) is one of the core clock proteins controlling circadian gene expression at a molecular level. Hence, its deficiency leads to a disruption of the molecular circadian clock. Here, we used hypercholesterolemic *Lyz2CreBmal1*$^{fl/fl}$*Apoe*$^{-/-}$ mice carrying a myeloid-specific *Bmal1* knockout and hypercholesterolemic *BmxCre*^{ERT2}*Bmal1*$^{fl/fl}$*Apoe*$^{-/-}$ mice with a specific *Bmal1* deficiency in arterial endothelial cells. While time-dependent myeloid cell adhesion was maintained in hypercholesterolemic *BmxCre*^{ERT2}*Bmal1*$^{fl/fl}$*Apoe*$^{-/-}$ and the respective control mice, time-dependent differences in myeloid cell adhesion were abolished in hypercholesterolemic *Lyz2CreBmal1*$^{fl/fl}$*Apoe*$^{-/-}$ mice (Figure 20 A-E). Interestingly, oscillations in circulating leukocyte numbers remained time-dependent in hypercholesterolemic *Lyz2CreBmal1*$^{fl/fl}$*Apoe*$^{-/-}$ mice (Figure 20 F). Deficiency of *Bmal1* in neutrophils and classical monocytes was confirmed by mRNA expression analyses (Figure 20 G). Furthermore, plasma CCL2 levels were reduced at ZT1 to a similar level as observed at ZT13 in *Lyz2CreBmal1*$^{fl/fl}$*Apoe*$^{-/-}$ mice (Figure 20 H), suggesting that CCL2 could indeed function as regulator of rhythmic arterial leukocyte recruitment.

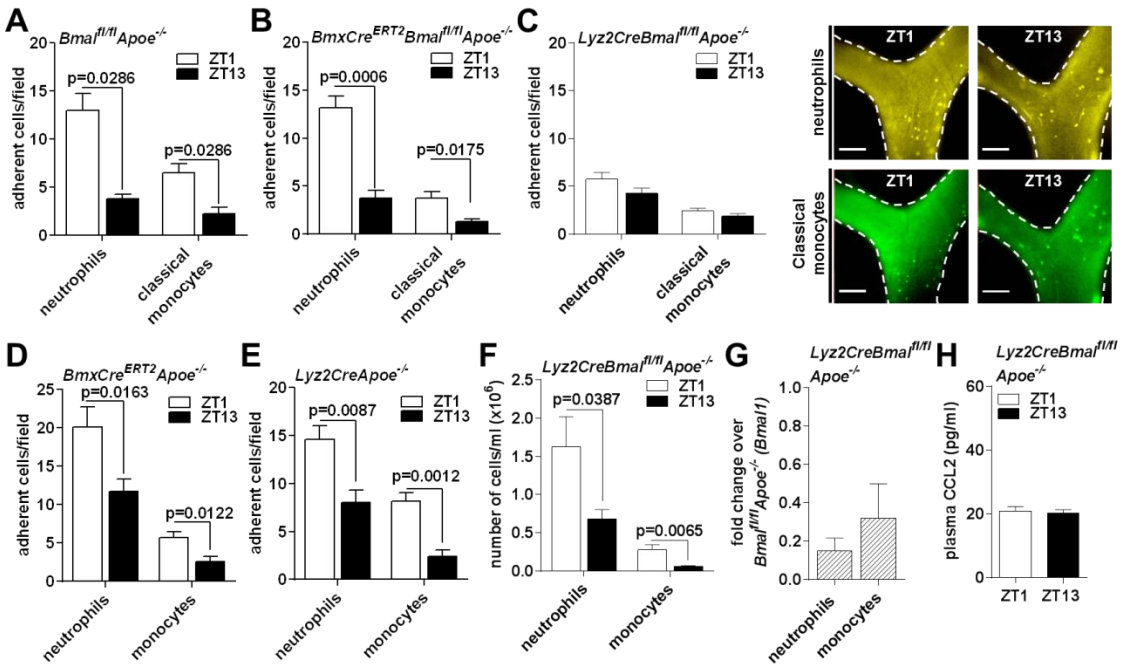

Figure 20: Time-dependent myeloid cell recruitment depends on a leukocyte intrinsic effect (**A-C**) Analysis of myeloid cell adhesion to the carotid artery by intravital microscopy in hypercholesterolemic *Bmal1*$^{fl/fl}$*Apoe*$^{-/-}$ (A), *BmxCre*^{ERT2}*Bmal1*$^{fl/fl}$*Apoe*$^{-/-}$ (B), *Lyz2CreBmal1*$^{fl/fl}$*Apoe*$^{-/-}$ mice (C), *BMXCre*^{ERT2}*Apoe*$^{-/-}$ mice (D), and *Lyz2Cre*^{I}*Apoe*$^{-/-}$ mice at ZT1 and ZT13. Images in C represent arterial leukocyte adhesion in *Lyz2CreBmal1*$^{fl/fl}$*Apoe*$^{-/-}$ mice. Scale bar, 100 µm. n=4 in (A), n=7 in (B/D/E), n=15-17 in (C). Statistical analyses were made with Mann-Whitney test (A/B/D/E) or unpaired t-test (C). (F) Number of circulating neutrophils and monocytes in *Lyz2CreBmal1*$^{fl/fl}$*Apoe*$^{-/-}$ mice. n=12-16. unpaired t-test (G) Bmal1 expression in circulating neutrophils and monocytes of hypercholesterolemic *Lyz2CreBmal1*$^{fl/fl}$*Apoe*$^{-/-}$ mice. n=4-5 (H) Plasma CCL2 levels in hypercholesterolemic *Lyz2CreBmal1*$^{fl/fl}$*Apoe*$^{-/-}$ mice at ZT1/ZT13. n=4-7. Mann-Whitney test. All data are presented as mean±SEM. ZT, Zeitgeber time.

3.3.3 CCL2-CCR2 signaling triggers time-dependent myeloid cell adhesion

The hypothesis of CCL2 as the regulator of time-dependent leukocyte adhesion was confirmed by studying the impact of CCL2 on leukocyte adhesion *in vivo* and *ex vivo* at different time points. In previous experiments, time-dependent myeloid cell adhesion and differences in CCL2 plasma levels between ZT1 and ZT13 were abolished in hypercholesterolemic *Lyz2CreBmal*$^{fl/fl}$*Apoe*$^{-/-}$ mice. Therefore, we investigated whether the time-dependent myeloid cell adhesion phenotype could be rescued by inducing an enhanced

CCL2 plasma level at ZT1. During the experiment the number of adherent myeloid cells was determined by intravital microscopy in hypercholesterolemic *Lyz2CreBmal$^{fl/fl}$Apoe$^{-/-}$* mice at ZT1 before and after intravenous administration of a low dose of CCL2 (Figure 21 A). As expected, intravenous delivery of CCL2 into *Lyz2CreBmal$^{fl/fl}$Apoe$^{-/-}$* mice at ZT1 enhanced myeloid cell adhesion (Figure 21 A). A similar experiment setup was used to study whether myeloid cell recruitment can be enhanced in hypercholesterolemic *Cx$_3$cr1$^{gfp/WT}$Apoe$^{-/-}$* mice at ZT13, when CCL2 plasma levels were low as observed in previous experiments. And indeed, CCL2 delivery to *Cx$_3$cr1$^{gfp/WT}$Apoe$^{-/-}$* mice at ZT13 resulted in a higher number of adherent myeloid cells (Figure 21 B).

In further *ex vivo* experiments myeloid cell adhesion to equally coated surfaces was investigated at ZT1 and ZT13. *Ex vivo* adhesion of monocytes and neutrophils obtained at ZT1 or ZT13 was similar, hence leukocyte adhesion is not regulated through a cell intrinsic pathway (Figure 21 C). To study the impact of plasma on myeloid cell adhesion, monocytes and neutrophils isolated from hypercholesterolemic *Apoe$^{-/-}$* mice at ZT1 were treated with plasma obtained from hypercholesterolemic *Apoe$^{-/-}$* mice at ZT1 or ZT13. Interestingly, myeloid cell adhesion was reduced in the presence of plasma obtained from hypercholesterolemic *Apoe$^{-/-}$* mice at ZT13 (Figure 21 D). Moreover, plasma obtained from *Lyz2CreBmal$^{fl/fl}$Apoe$^{-/-}$* mice at ZT1 reduced the number of adherent myeloid cells, which were isolated from hypercholesterolemic *Apoe$^{-/-}$* mice at ZT1, more efficiently than plasma obtained from *Apoe$^{-/-}$* mice at ZT1 (Figure 21 E). These results indicate the importance of a soluble factor in guiding time-dependent cell adhesion. Finally, we identified CCL2 as the regulating soluble factor by blocking its signalling via CCR2. Neutralization of CCR2 signaling with a small molecule CCR2 antagonist RS102895 in myeloid cells obtained from hypercholesterolemic *Apoe$^{-/-}$* mice at ZT1 resulted in less myeloid cell adhesion *ex vivo* (Figure 21 F). Consistent with these observations, *in vivo* disruption of CCL2-CCR2 signaling in *Apoe$^{-/-}$Ccr2$^{-/-}$* mice abolished time-dependent myeloid cell adhesion by reducing the number of adherent myeloid cells to the carotid artery at ZT1 (Figure 21 G), although oscillations in numbers of circulating cells were maintained (Figure 21 H). In summary, CCR2-CCL2 signaling triggers rhythmic myeloid cell adhesion to the carotid artery.

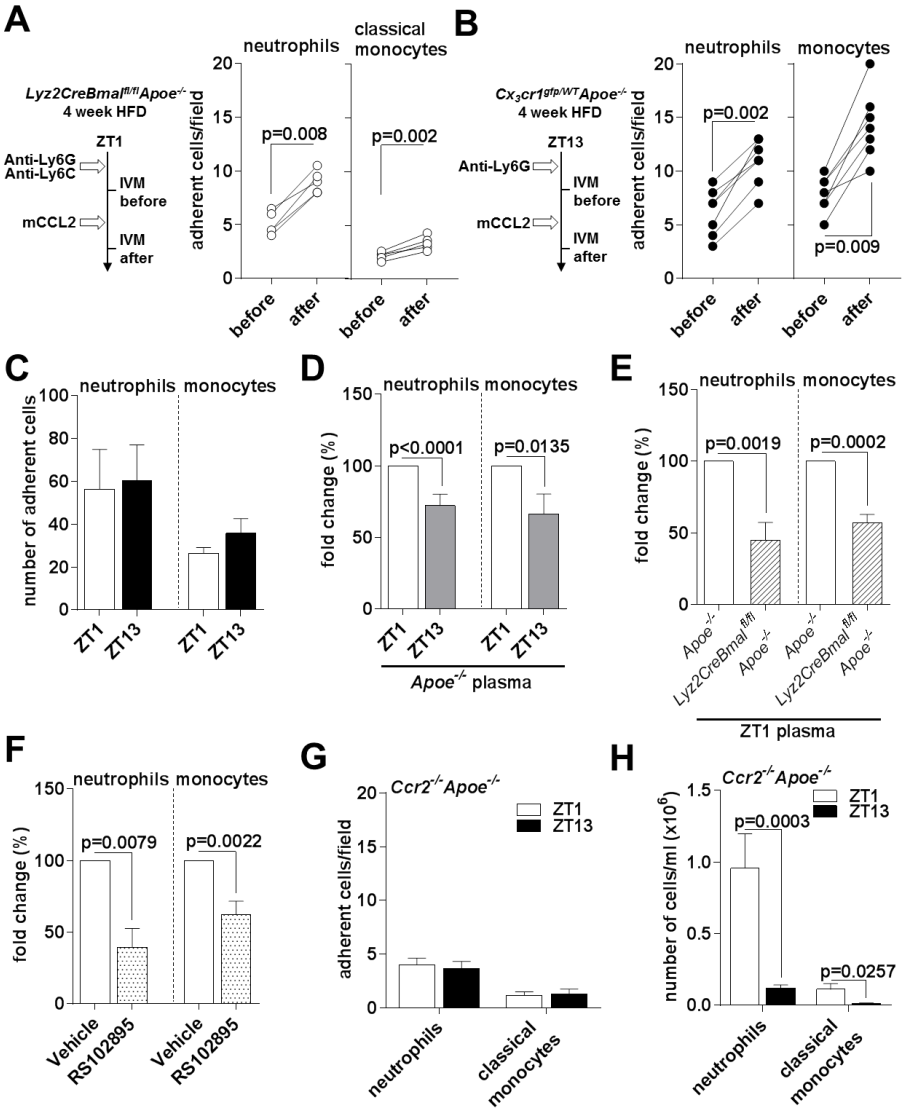

Figure 21: CCR2-CCL2 signaling impacts on time-dependent myeloid adhesion

(A/B) Numbers of adherent monocyte and neutrophil in hypercholesterolemic *Lyz2CreBmal1*$^{fl/fl}$*Apoe*$^{-/-}$ at ZT1 (A) or hypercholesterolemic *Cx*$_3$*cr1*$^{gfp/WT}$*Apoe*$^{-/-}$ mice at ZT13 (B) before and after administration of CCL2. n=4. Paired t-test. (C) Analysis of e*x vivo* adhesion of myeloid cells from hypercholesterolemic *Apoe*$^{-/-}$ mice obtained at ZT1 or ZT13 in the presence of static adhesion buffer. n=4-10. Mann-Whitney test. (D) *Ex vivo* adhesion of myeloid cells from hypercholesterolemic *Apoe*$^{-/-}$ mice obtained at ZT1 in the presence of plasma isolated at ZT1 or ZT13. n=10-16. Unpaired t-test. (E) *Ex vivo* myeloid cell adhesion obtained from hypercholesterolemic *Apoe*$^{-/-}$ mice at ZT1 in presence of plasma from *Apoe*$^{-/-}$ mice or *Lyz2CreBmal1*$^{fl/fl}$*Apoe*$^{-/-}$ mice isolated at ZT1. n=8-9. Unpaired t-test. (F) Number of adherent myeloid cells isolated from hypercholesterolemic *Apoe*$^{-/-}$ mice at ZT1 in the presence of *Apoe*$^{-/-}$ plasma obtained at ZT1 and with an inhibitor to CCR2 (RS102895, 100 ng/ml) or the respective control. n=5-6. Mann-Whitney test. (G) Number of adherent cells to the carotid artery of hypercholesterolemic *Ccr2*$^{-/-}$*Apoe*$^{-/-}$mice at ZT1 and ZT13. n=7-8. Mann-Whitney test. (H) Number of circulating myeloid cells in *Ccr2*$^{-/-}$*Apoe*$^{-/-}$mice at ZT1 and ZT13. n=7-8. Mann-Whitney test. All data are presented as mean±SEM. IVM, intravital microscopy; HFD, high fat diet; ZT, Zeitgeber Time.

3.3 Chrono-pharmacological treatment strategy prevents early lesion development

In light of the observed importance of the CCL2-CCR2 axis during time-dependent myeloid cell adhesion to atheroprone regions, we designed a chrono-pharmacological treatment strategy to prevent the development of atherosclerosis by targeting CCL2 signaling in a time-dependent manner.

3.3.1 Diverse time-dependent recruitment patterns in the macro- and microcirculation

Due to proposed side effects and failed attempts to inhibit chemokine driven lesional leukocyte recruitment in the past, we defined the site- and time-specificity of leukocyte recruitment by performing near-simultaneous intravital microscopy in the carotid artery (macrocirculation) and cremaster muscle (microcirculation) in hypercholesterolemic *Apoe*$^{-/-}$ mice. In contrast to the leukocyte recruitment pattern in the macrocirculation, an opposing recruitment phenotype with a peak at ZT13 and a trough at ZT1 was observed in the cremasteric microcirculation (Figure 22 A-E).

Next, we investigated whether pharmacological disruption of CCL2 signaling affects leukocyte adhesion in macro- and microcirculation in the same manner. In the macrocirculation, less adherent monocytes and neutrophils occurred after CCR2 blockage at ZT1, while treatment at ZT13 had no impact on myeloid cell adhesion (Figure 22 B-C). In contrast, disruption of CCL2-CCR2 signaling in the microcirculation reduced the number of adherent monocytes at ZT13, but was without effect on neutrophil adhesion (Figure 22 D/E). Numbers of circulating myeloid cells were not changed upon pharmacological CCR2 blockage (Figure 22 F/G). Furthermore, the comparable decay of the CCR2 antagonist in plasma at ZT1 and ZT13 confirmed a similar drug metabolism at both time points (Figure 22 H).

Taken together, these results propose timed CCR2 blockage as a promising chrono-pharmacological treatment strategy in atherosclerosis, possibly with only minor side effects.

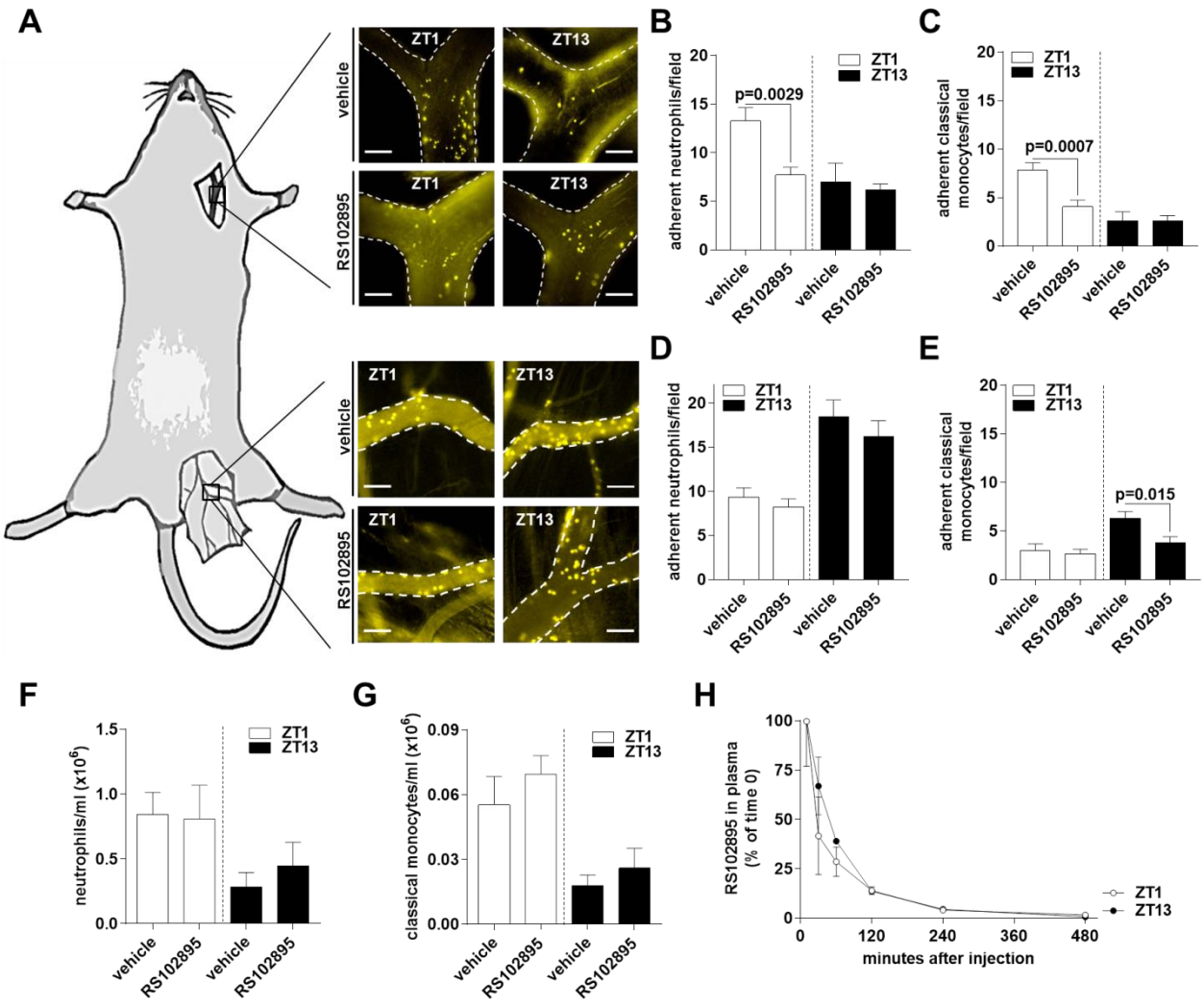

Figure 22: Diverse effect of CCR2 blockage on time-dependent cell adhesion in the macro- and microcirculation

(**A-E**) Number of myeloid cell adhesion in the cremaster muscle and the carotid artery. (A) Near-simultaneous intravital microscopy in hypercholesterolemic *Cx$_3$cr1$^{gfp/WT}$Apoe$^{-/-}$* mice treated with the CCR2 antagonist (RS102895, 5 mg/kg) or vehicle control 30 min before recording at indicated ZT. (B/C) Number of adherent neutrophils (B) and classical monocytes (C) in the macrocircuation. (D/E) Number of adherent neutrophils (D) and classical monocytes (E) in the microcirculation. Scale bar, 100 µm in (B/C) and 50 µm in (D/E). n=5-13 in (B/C) and n=9-15 in (D/E). Statistical analyses were made with Mann-Whitney test (B/C) or unpaired t-test (D/E). (F/G) Number of circulating neutrophils (F) and classical monocytes (G) in hypercholesterolemic *Cx$_3$cr1$^{gfp/WT}$Apoe$^{-/-}$* mice treated with the CCR2 antagonist (RS102895, 5 mg/kg) or vehicle control. (H) Pharmacokinetic analysis of the CCR2 antagonist RS102895 (5 mg/kg) injected i.p. at indicated ZT. Plasma levels of RS102895 were assessed by mass spectrometry. n=3 per time point. All data are presented as mean±SEM. ZT, Zeitgeber time.

3.3.2 Chrono-pharmacological treatment strategy prevents early lesion development

We designed a chrono-pharmacological treatment strategy with timed blockage of CCL2-CCR2 signaling. *Apoe*$^{-/-}$ mice were treated daily with the CCR2 antagonist at ZT5 or ZT17 while being on HFD for 4 weeks. The small molecules CCR2 antagonist RS102895 has a short half-life and is not detectable in plasma 9 hours after i.p. administration of 5 mg/kg (Mitchell et al., 2013). Therefore, administration of RS102895 at ZT5 blocked CCL2-CCR2 signaling when arterial leukocyte adhesion was low, whereas administration of RS102895 at ZT17 blocked CCL2-CCR2 signaling when arterial leukocyte adhesion was at its highest (Figure 23 A).

After four weeks of HFD and daily timed CCR2 blockage, *Apoe*$^{-/-}$ mice were sacrificed at ZT1 and ZT13 for further leukocyte adhesion and atherosclerotic lesion analyses. The number of adherent myeloid cells to the carotid artery was reduced at ZT1 after treating these mice with the CCR2 antagonist at ZT17 (Figure 23 B/C). In contract, no difference in the number of adherent myeloid cells was observed at ZT13 after CCR2 antagonist treatment at ZT5 (Figure 23 B/C). Circulating leukocyte counts and time-dependent differences in CCL2 plasma levels were not affected by prolonged CCR2 neutralization (Figure 23 D-F). Atherosclerotic lesion analyses revealed less atherosclerotic lesion formation and less lesional macrophage content after prolonged CCR2 antagonist treatment at ZT17, while treatment at ZT5 had no impact on early atherosclerotic lesion development (Figure 23 G/H). Hence, timed blockage of CCL2 signaling during the phase of elevated leukocyte adhesion successfully reduced atherosclerotic lesion development.

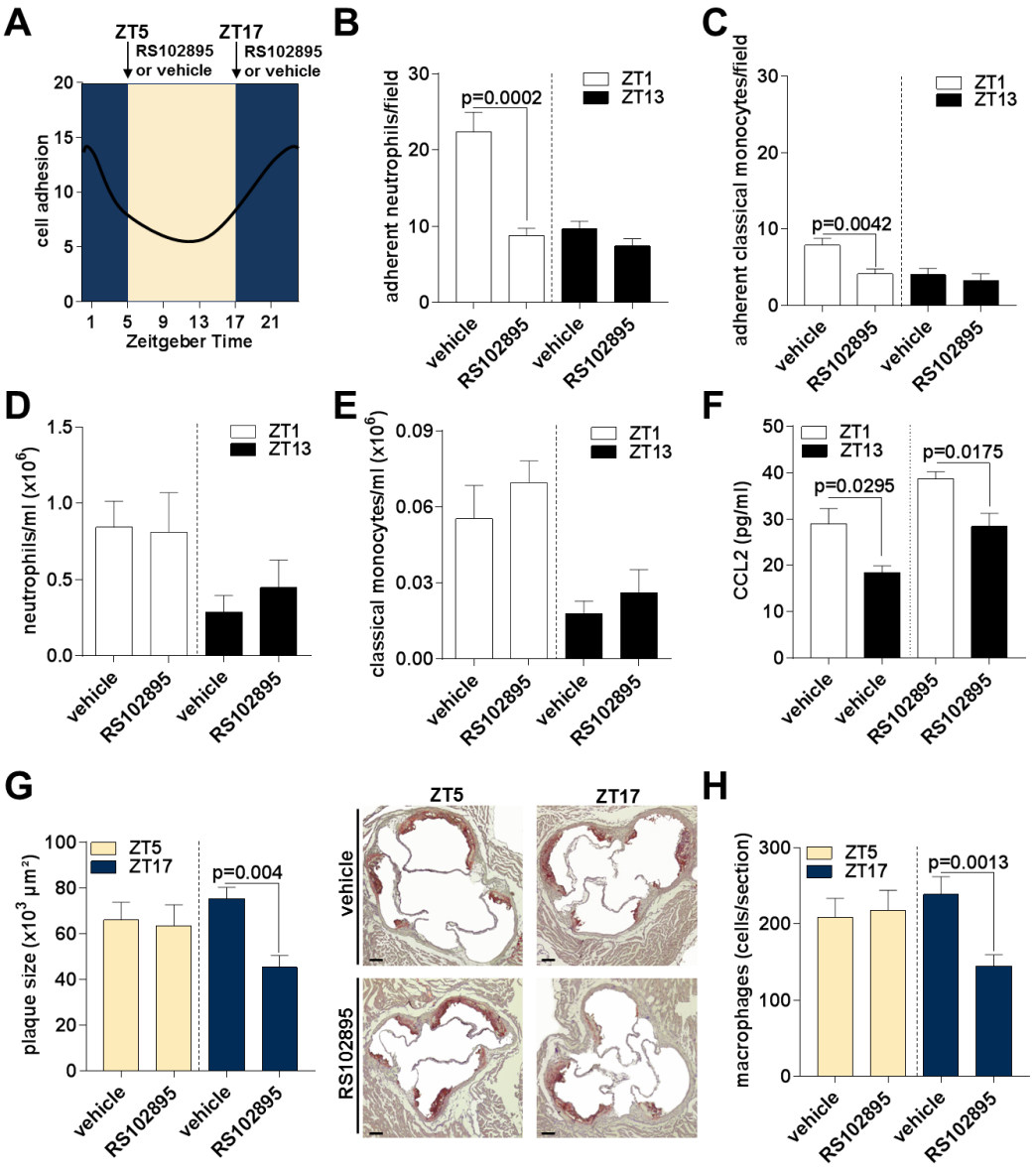

Figure 23: Timed CCR2 blockage reduces atherosclerotic lesion development without affecting time-dependent differences in blood cell counts and CCL2 plasma levels

Apoe$^{-/-}$ mice were treated daily with a CCR2 antagonist (5 mg/kg) or vehicle control at ZT5 or ZT17 while being on HFD for four weeks. (A) Experimental setup (B/C) Analysis of adherent neutrophils (B) and adherent classical monocytes (C) to the carotid artery assessed by intravital microscopy. (D/E) Quantification of circulating neutrophils (D) and classical monocytes (E) in *Apoe*$^{-/-}$ mice was determined by flow cytometry. n=8. Unpaired t-test. (F) Quantification of plasma CCL2 levels. n=5-8. Mann-Whitney test. (G) Quantification of atherosclerotic lesion size. Representative images of oil red O staining are displayed. Scale bar, 100 µm. (H) Amount of lesional Mac2^{+} macrophages. n=8 per group, 3 sections were analyzed per mouse. Unpaired t-test. All data are presented as mean±SEM. ZT, Zeitgeber time.

3.3.3 Impact of the established chronotherapy on acute lung inflammation

Although chrono-pharmacological treatment of atherosclerosis successfully prevented early lesion development, its therapeutic relevance was further proven by assessing the impact of timed CCR2 blockage on a disease model occurring in the microcirculation, such as bacterial pneumonia. Bacterial pneumonia mainly occurs in the elderly and leads to acute lung injury characterized by lung edema and rapid neutrophil influx (Grommes et al. 2011). The influence of CCR2 neutralization was tested in a mouse model of acute lung inflammation to investigate whether timed chrono-pharmacological treatment of early lesion development impacts on bacterial pneumonia. After administration of the CCR2 antagonist at ZT5 or ZT17, C57BL/6J mice were exposed to aerosolized LPS to induce acute lung injury (Figure 24 A/C). The number of infiltrated cells into the lung was assessed at ZT1 and ZT13 by flow cytometry. Interestingly, administration of the CCR2 antagonist at ZT1 was without effect on myeloid cell infiltration into the lungs at ZT1, however, neutrophil infiltration was reduced at ZT13 (Figure 24 A-D). Hence, chrono-pharmacological treatment of early lesion development could be of important therapeutic relevance due to its reduced side effects and increased efficacy.

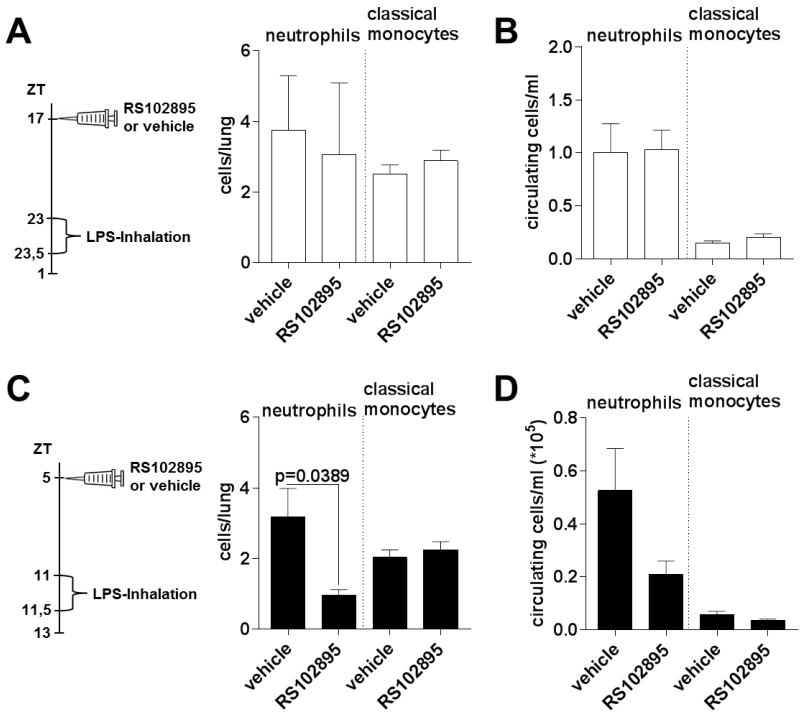

Figure 24: Myeloid cell recruitment to lungs at ZT1 is not affected by timed CCR2 neutralization (A/C) C57BL/6J mice received a single dose of CCR2 antagonist (5 mg/kg) or vehicle control at ZT5 or ZT17. Afterwards, mice were exposed to aerosolized LPS (500 µg/ml) at ZT23 or ZT11. Myeloid cell influx into the lungs was determined by flow cytometry. (A/C) Quantification of infiltrated myeloid cells into lungs at ZT1 (A) and ZT13 (C). (B/D) Number of circulating myeloid cells of the same mice at ZT1 (B) and ZT13 (D). n=7-8 per group. Mann-Whitney test. All data are mean±SEM. ZT, Zeitgeber time.

4. Summary

Leukocyte recruitment to sites of activated arterial endothelium plays a major role during initiation of atherosclerotic lesion development. In regard that distinct components of the immune system exhibit circadian rhythmicity, thus modulating leukocyte recruitment during inflammation in a time-dependent manner, we questioned whether rhythmic leukocyte recruitment occurs during atherosclerosis (Scheiermann et al. 2012; Nguyen et al. 2013). With the importance of the circadian clock in immune responses, previous studies focused on investigating the impact of the core clock proteins BMAL1 and CLOCK on the development of atherosclerosis (Pan et al. 2013; Yang et al. 2016; Huo et al. 2017). However, little was known about the influence of the circadian clock on inflammatory processes during early atherosclerotic lesion development. Therefore, the aim of this study was to investigate to what extent the circadian clock orchestrates time-dependent leukocyte recruitment during atherogenesis and to identify its regulatory mechanisms for generating a chronopharmacological treatment strategy.

In this current study, leukocyte infiltration into atherosclerotic lesions was monitored for the first time in hypercholesterolemic *Apoe*$^{-/-}$ mice over a time period of 21 hours. Leukocyte recruitment to atherosclerotic lesions peaked at ZT1, while leukocyte recruitment was at its lowest at ZT13. Rhythmic leukocyte recruitment also occurs to peripheral organs under physiological conditions or to sites of acute injury (Scheiermann et al. 2012; Nguyen et al. 2013). Under these conditions, endothelial cell adhesion molecules or chemokines expressed in a time-dependent manner guide time-dependent differences in leukocyte trafficking. However, we did not observe differences in the expression of cell adhesion molecules on endothelial cells of atherosclerotic lesions at different time points. Moreover, time-dependent activation of the CCR2-CCL2 axis regulated differences in the infiltration of leukocytes into atherosclerotic lesions at ZT1 and ZT13. Elevated plasma levels of leukocyte derived CCL2 were observed at ZT1, thus increased immobilized CCL2 on the endothelium of atherosclerotic prone regions triggers enhanced leukocyte adhesion. In light of the importance of the CCR2-CCL2 axis on time-dependent lesional leukocyte recruitment, blockage of CCR2 signaling via treatment with a CCR2 antagonist abolished time-dependent leukocyte recruitment in the macrocirculation, but had only minor effects in the microcirculation. These new insights lay the foundation for a novel chronopharmacological treatment therapy to ameliorate atherosclerosis. Subsequently, timed disruption of CCL2-CCR2 signaling reduced the development of atherosclerosis without causing side effects during acute lung injury.

In summary, our extended understandings of time-dependent inflammatory mechanisms during atherogenesis illustrate the necessity for developing novel chrono-pharmacotherapies to improve drug efficacy and to reduce side effects.

5. Discussion

5.1 Rhythmic leukocyte recruitment to atherosclerotic lesions

Rhythmicity in the recruitment of leukocytes into distinct tissues has already been investigated under steady state and acute inflammation (Scheiermann et al. 2012; Nguyen et al. 2013). Previous studies also indicate that the circadian clock modulates chronic inflammatory diseases, such as atherosclerosis (Pan et al. 2013; Yang et al. 2016; Huo et al. 2017). Myeloid cell specific deletion of the core clock protein BMAL1 worsens diet-induced obesity and insulin resistance (Nguyen et al. 2013). Furthermore, *Bmal1* deficiency in myeloid cells promotes atherosclerosis due to enhanced recruitment of Ly6C^{hi} monocytes to atherosclerotic lesions (Huo et al. 2017). The entry of leukocytes into atherosclerotic lesions is of crucial importance to the development of atherosclerosis. Consequently, the influence of cell adhesion molecules, chemokines, and their respective chemokine receptors on arterial leukocyte recruitment has been intensively studied. However, nothing was known so far about the rhythmic recruitment of leukocytes during early atherosclerotic lesion formation, thus, this is the first study describing time-dependent leukocyte recruitment during atherogenesis.

Next to time-dependent myeloid cell recruitment to atherosclerotic lesions, we investigated oscillations in the number of myeloid cells in bone marrow and spleen of hypercholesterolemic *Apoe*$^{-/-}$ mice. Previous studies have demonstrated rhythmic circulating leukocyte numbers with a peak at ZT5 in C57B/L6 mice under steady state (Scheiermann et al. 2012). Opposing cell numbers were observed in the bone marrow, whereas cell numbers in the spleen showed almost similar rhythmic patterns as observed in blood (Scheiermann et al. 2012; Nguyen et al. 2013). These results conclude that elevated circulating cell numbers derive from the bone marrow during the resting phase. In the experimental study presented here, a drop of leukocyte counts occurred in the bone marrow and spleen, when numbers of circulating cells begin to increase. Furthermore, time-dependent changes in the number of leukocytes in bone marrow and spleen were similar, which is in contrast to observations made in recent studies (Scheiermann et al. 2012; Nguyen et al. 2013). Overall, our results indicate that circulating myeloid cells derive from the spleen and bone marrow in hypercholesterolemic *Apoe*$^{-/-}$ mice. Circulating monocytes and neutrophils develop from HSCs, whose number undergoes circadian changes in human bone marrow with a peak at daytime (Abrahamsen et al. 1998). Furthermore, rhythmic modulation of the hematopoietic niche in bone marrow has been observed in mice (Casanova-Acebes et al. 2013, Méndez-Ferrer et al. 2008). Previous studies point out that hypercholesterolemia induces monocytosis and neutrophilia due to enhanced hematopoiesis in the spleen and the bone marrow (Swirski et al. 2012; Drechsler et al. 2010). In addition, Robbins et al. identified the

spleen as an extramedullary site that contributes to the production of circulating inflammatory cells during chronic inflammation (Robbins et al. 2012). Hypercholesterolemia enhances hematopoiesis by increasing the accumulation of cholesterol in HSPCs (Murphy et al. 2011). The accumulation of cholesterol elevates the expression of the common β-subunit of the interleukin-3 receptor and granulocyte/macrophage colony-stimulating factor receptor, thus enhancing HSPCs proliferation (Murphy et al. 2011). Up to date, it is not known whether one of those receptors is expressed in a time-dependent manner to regulate rhythmicity in myeloid cell proliferation. However, it provides a possible mechanism how hypercholesterolemia could interfere with the rhythmic production of neutrophils and monocytes. Furthermore, the peak in the number of circulating leukocytes was observed earlier in hypercholesterolemic *Apoe*$^{-/-}$ mice as compared to observations made for circulating leukocytes under steady state (Scheiermann et al. 2012; Nguyen et al. 2013). Endothelial cells in the bone marrow regulate rhythmic release of leukocytes by time-dependent expression of *Selp*, *Sele* and *Vcam1* in endothelial cells (Scheiermann et al. 2012). Furthermore, hypercholesterolemia is known to cause a reprogramming of the rhythmic transcriptome in hepatic tissue (Eckel-Mahan et al. 2013). Whether high fat diet feeding also changes the rhythmic transcriptome in endothelial cells of the bone marrow and spleen, thus modifying the egress and homing of leukocytes from and to the bone marrow under hypercholesterolemia, has not been studied so far. In summary, indications are given that the phase shifted phenotype observed in the number of circulating leukocytes and the diverse phenotype observed in spleen and bone marrow according to previous studies relate to the possible influence of hypercholesterolemia on immune cell production and trafficking.

In follow up experiments, we investigated the influence of external factors on time-dependent myeloid cell adhesion. Entrainment of circadian rhythms by light or food intake ensures synchronization of the internal circadian clock with the environment. Disruption of the circadian clock by shift work results in an increased risk for an acute cardiovascular event (Knutsson et al. 1986). Furthermore, misalignment of the rest/activity phases with metabolic processes due to chronic circadian disruption enhances the susceptibility for metabolic disorders (Feng et al. 2012). Therefore, it is important to investigate the influence of entrainment factors on inflammatory processes. Here, we confirmed *bona fide* circadian rhythmicity for time-dependent leukocyte recruitment in hypercholesterolemic *Apoe*$^{-/-}$ mice that were kept in constant darkness for two weeks. In previous studies, similar results were observed for circadian oscillations of lymphocyte numbers in lymph nodes and leukocyte trafficking into tissues, which were sustained in constant darkness and entrained by photic cues (Druzd et al., 2017; Scheiermann et al. 2012). We did not investigate the influence of

the entrainment factor light on leukocyte recruitment during chronic inflammation. Nevertheless, determining the effect of photic cues on rhythmic myeloid cell recruitment during atherogenesis will draw further conclusions, how jetlag or shift work impacts on atherosclerotic lesion development. Next to changes in the environmental light/dark cycle, changes in meal times represent another consequence of shift work or time-zone transition. Previous studies observed that feeding periods entrain circadian gene expression in peripheral clocks, while having no impact on the circadian rhythmicity in the SCN (Damiola et al. 2000). One study demonstrates that restricted feeding during the day results in a phase shifted diurnal gene expression of clock genes in liver (Nguyen et al. 2013). However, restricted feeding had no impact on circadian gene expression in peritoneal macrophages, thus diurnal monocyte trafficking remained unchanged (Nguyen et al. 2013). Although feeding restriction had no effect on diurnal monocyte oscillations in steady state, its influence might have a bigger impact during chronic inflammation induced by hypercholesterolemia (Nguyen et al. 2013). Follow up studies are necessary to reveal the influence of food intake on rhythmic leukocyte recruitment to atherosclerotic lesions. Besides the time of food intake, the type of diet represents an additional factor that is known to influence circadian rhythmicity. Hypercholesterolemia induced in *Ldlr*$^{-/-}$ mice with a high fat diet containing 42.7% kcal carbohydrate, 20.4% kcal protein, and 36.9% kcal fat leads to circadian abnormalities in their behavior (Akashi et al. 2017). Another study with a similar diet provides evidence that a high caloric diet alters the expression and cycling of canonical circadian clock genes in the hypothalamus, liver, and adipose tissue (Kohsaka et al. 2007). Moreover, high fat diet characterized by containing 60% kcal from fat generates a reorganization of specific metabolic pathways, thus modulating transcriptional reprogramming in the circadian clock (Eckel-Mahan et al. 2013). According to the impact of specific diets on circadian rhythmicity and metabolic pathways, the impact of our high fat diet (containing 21% fat and 0.15% cholesterol) and especially of the feeding period on rhythmic leukocyte recruitment is of interest for future investigations.

Besides entrainment factors, catecholamines and glucocorticoids contribute to the regulatory branch of the circadian clock machinery by modulating peripheral clocks. Levels of glucocorticoids and catecholamines oscillate within 24 hours (Ikeda et al. 2013; Prinz et al. 1979). Moreover, activation of the sympathetic nervous system guides leukocyte recruitment to peripheral tissues through adrenergic receptor signaling (Scheiermann et al. 2012). Therefore, it was tempting to investigate whether glucocorticoid and adrenergic receptor signaling affects rhythmic myeloid cell recruitment. However, blocking of glucocorticoid

signaling had no impact on rhythmic myeloid cell adhesion, whereas blocking of adrenergic receptors had only minor effects on the number of adherent neutrophils.

5.2 CCL2-CCR2 axis guides time-dependent leukocyte adhesion

Myeloid cell recruitment during atherogenesis is regulated through distinct adhesion molecules expressed on lesional endothelial cells, but also by many chemokines and its respective receptors. The CCL2-CCR2 axis has been determined in the past to play a major role in early lesion development (Boring et al. 1998; Gu et al. 1998). Here, we identified the CCL2-CCR2 axis as the trigger for rhythmic myeloid cell recruitment during atherogenesis.

By investigating the regulatory mechanism of rhythmic myeloid cell recruitment, we studied the expression of adhesion molecules on endothelial cells of atherosclerotic lesions. Adhesion molecules guide leukocytes to activated arterial endothelial cells. Rhythmic expression of endothelial E-selectin, P-selectin, VCAM1, and CXCL12 regulates time-dependent recruitment of leukocytes to the bone marrow, while ICAM1 and CCL2 drive rhythmic leukocyte recruitment in the skeletal muscle (Scheiermann et al. 2012). Under acute inflammation in cremaster-muscle tissue, ICAM1 expression was increased and its circadian oscillation remained unchanged, thus still promoting rhythmic leukocyte recruitment (Scheiermann et al. 2012). In our study, we did not observe any rhythmic expression of adhesion molecules on endothelial cells of atherosclerotic lesions. According to the distinct rhythmic gene expression of adhesion molecules in the bone marrow, cremasteric muscle and cardiac tissue, our investigations in arterial endothelial cells could represent a tissue specific phenotype (Scheiermann et al. 2012; Schloss et al. 2016). These tissues specific phenotypes might derive from the impact of different shear stresses on the phenotype of endothelial cells in distinct tissues. Shear stress regulates NF-κB transcriptional pathways or endothelial gene expression, thus modifying the circadian clock and its rhythmic transcriptome (Dai et al. 2004; Baratchi et al. 2017). Furthermore, distinct rhythmic gene expression in lesional endothelial cells might relate to a disturbed circadian clock caused by chronic inflammation within the atherosclerotic lesion. Indications for chronic inflammation as a disturbing factor of the circadian clock are already given by another chronic inflammatory disease model, namely rheumatoid arthritis (RA). Synovial fibroblasts from RA patients display altered circadian expression of clock components triggered by inflammatory stimuli (Kouri et al. 2013).

Besides the unchanged expression of adhesion molecules on endothelial cells under hypercholesterolemia, we observed controversial CCL2 plasma levels in

hypercholesterolemic *Lyz2CreBmal1*$^{fl/fl}$*Apoe*$^{-/-}$ mice. A previous study reported that the heterodimer BMAL1/CLOCK recruits the polycomb repressive complex 2 (PRC2) to silence chemokine gene expression (Nguyen et al. 2013). Surprisingly, we observed low CCL2 plasma levels in hypercholesterolemic *Lyz2CreBmal1*$^{fl/fl}$*Apoe*$^{-/-}$ mice, although its repressor BMAL1 was deactivated. Nevertheless, increased expression of *Ccl2* does not directly modify plasma CCL2 protein levels due to the involvement of further regulatory mechanisms in chemokine release. However, our observations in endothelial and myeloid cells indicate a different rhythmic gene expression pattern under chronic inflammation induced by hypercholesterolemia as compared to observations that were made under steady state or acute inflammation. Next to chronic inflammatory processes, hypercholesterolemia represents another disturbing factor of the circadian clock. Specific diets are known to change the circadian gene expression in hepatic tissue, thus raising the question whether hypercholesterolemia also leads to a reprogramming of the rhythmic transcriptome in endothelial cells and myeloid cells (Eckel-Mahan et al. 2013*)*. High fat diet feeding causes phase-shifted or reduced recruitment of the BMAL1/CLOCK complex to its target promoters, thus causing a reprogramming of circadian expressed genes (Eckel-Mahan et al. 2013). Furthermore, high fat diet changes the presence and pattern in oscillations as well as the recruitment of other transcription factors, thus providing additional transcriptional pathways to regulate circadian rhythmicity (Eckel-Mahan et al. 2013). The circadian clock is also directly coupled with metabolism by the SIRT1 NAD-dependent deacetylase, which plays a major role during energy metabolism and gets modified under high fat diet feeding (Chalkiadaki et al. 2012). SIRT1 modulates the circadian clock by directly modulating the gene expression of core clock proteins, hence providing another possible mechanism how high fat diet interferes with the rhythmic transcriptome (Chang et al. 2013; Nakahata et al. 2008; Asher et al. 2008). Overall, the rhythmic expression profile under hypercholesterolemia differs and could explain our observations according to the expression of adhesion molecules and chemokines in hypercholesterolemic *Apoe*$^{-/-}$ mice. Nevertheless, the regulatory mechanism of the circadian clock and its outcomes under hypercholesterolemia and chronic inflammation in different cell types has to be further investigated in detail.

According to the importance of BMAL1 in leukocyte recruitment during steady state and acute inflammation, it was tempting to speculate that BMAL1 regulates rhythmic leukocyte recruitment during atherogenesis (Scheiermann et al. 2012; Nguyen et al. 2013). Here, hypercholesterolemic *Lyz2CreBmal1*$^{fl/fl}$*Apoe*$^{-/-}$ mice carrying a myeloid-specific *Bmal1* knockout exhibited an abolished rhythmicity in leukocyte recruitment with a low number of adherent cells at ZT1 similar to the number of adherent cells observed at ZT13. In contrast, a

previous study identified diurnal oscillations for Ly6C^{high} inflammatory monocytes and observed a pro-inflammatory phenotype in *Lyz2CreBmal1$^{fl/fl}$* mice (Nguyen et al. 2013). In detail, *Lyz2CreBmal1$^{fl/fl}$* mice infected with *Listeria monocytogenes* in the peritoneum exhibit an increased recruitment of Ly6C^{high} monocytes to the inflamed tissue, thus amplifying the inflammatory response by a significant increase in CCL2, CCL8, IL1β and IL6 expression. In agreement with this previous study, we also observed an increase in the number of circulating myeloid cells in hypercholesterolemic *Lyz2CreBmal1$^{fl/fl}$Apoe$^{-/-}$* mice. However, according to the enhanced pro-inflammatory phenotype in *Lyz2CreBmal1$^{fl/fl}$* mice, we expected to observe an elevated number of recruited myeloid cells to atherosclerotic lesions. But we discovered a reduced number of adherent cells in hypercholesterolemic *Lyz2CreBmal1$^{fl/fl}$Apoe$^{-/-}$* mice. These controversial results highlight diverse regulatory mechanisms of rhythmic myeloid cell recruitment in two distinct disease models, namely chronic and acute inflammation. In addition, both studies focused on different tissues. While our study investigated inflammation in atheroprone regions of aortic tissue, the study of Nguyen et al. focused on inflammatory processes in the peritoneum. Nevertheless, future studies investigating tissue and model specific differences in the circadian modulation of immune responses will provide further insights.

In addition, distinct leukocyte recruitment patterns have been described in the macro- and microcirculation. For instance, cathepsin G is a chemotactic protein stored in neutrophil azurophil granules and controls myeloid cell adhesion in the carotid artery, but not in the microcirculation of the cremaster muscle (Ortega-Gomez et al. 2016). Furthermore, the expression of distinct endothelial adhesion molecules differs between different organs, thus regulating cell recruitment in a tissue-specific manner (Rossaint et al. 2013). Here, we observed a different rhythmic leukocyte recruitment pattern in the macro- and microcirculation in hypercholesterolemic *Apoe$^{-/-}$* mice. The CCL2-CCR2 axis plays an important role in myeloid cell recruitment in the carotid artery, but it is less important in microvessels of the cremaster muscle. CCL2 coverage on endothelial cells in the carotid artery was higher at ZT1, but we did not observe a difference in endothelial CCL2 coverage between ZT1 and ZT13 in the microcirculation of cremasteric tissue (data not shown). Thus, our results highlight the CCR2-CCL2 axis as another factor that differs in the macro- and microcirculation and regulates tissue specific leukocyte recruitment patterns. These results also raise the questions to what extent glycosaminoglycans regulate tissue specific or rhythmic leukocyte recruitment. Glycosaminoglycans are located on the cell-surface and bind selectively to chemokines via electrostatic interactions (Middleton et al. 2002). Side specific glycosaminoglycan patterns define distinct chemokine presentations, thus controlling

functionality and hierarchy of chemokines and their receptors during leukocyte arrest (Witt et al. 1994; Kuschert et al. 1999; de Paz et al. 2007; Weber et al. 1999). However, time-dependent differences of endothelial glycosaminoglycans in the macro- and microcirculation have not been studied so far. Nevertheless, our findings provide further evidence of distinct leukocyte recruitment patterns in the macro- and microcirculation and underline the diverse importance of the CCR2-CCL2 axis in leukocyte recruitment.

5.3 Chronopharmacological treatment strategy ameliorates atherosclerosis

Chronopharmacological treatment strategies describe timed drug administration according to the rhythmic appearance or activity of its target, thus leading to enhanced efficacy and less side effects. The majority of best-selling drugs targets circadian expressed proteins (Zhang et al. 2014). In detail, current attempts to reduce the risk of cardiovascular diseases aim at proteins with circadian rhythmicity such as angiotensin II receptor blockers, β-adrenoreceptor antagonists, and aldosterone receptor blockers (Zhang et al. 2014). There are several examples, where the time of administration resulted in improved drug efficacies. For example, statins taken in the evening, when cholesterol synthesis is increased, revealed a significantly lower cholesterol level as compared to the effect of statins taken in the morning (Saito et al. 1991). Furthermore, a delayed delivery system of verapamil provides the optimal plasma concentration in the early morning, when blood pressure is at its highest (White et al. 1995). Similar experiences are observed with a new chronotherapeutic formulation of propranolol, Innopran XL^{TM}, which was designed to be taken at night and to release propranolol after a lag phase of 4-5 hours (Sica et al. 2003). Importantly, the wrong timing of administration can even result in unintended effects as shown by a clinical study on the time-dependent effect of aspirin in hypertensive patients. The blood pressure of hypertensive patients, who received aspirin in the evening, was significantly reduced (Hermida et al. 2005). In contrast, administration of aspirin in the morning slightly elevated blood pressure in hypertensive patients (Hermida et al. 2005). In summary, chronotherapy improves drug efficacy and is already used in clinic to successfully reduce the effect of risk factors for cardiovascular diseases. However, timed treatment strategies targeting the underlying cause of cardiovascular diseases, namely atherosclerosis, are still missing in clinic. Here, we present a novel chronopharmacological treatment strategy, which ameliorates atherosclerosis in a mouse model by efficiently reducing arterial leukocyte recruitment. Previous approaches targeting leukocyte recruitment during inflammation by blocking adhesion molecule interactions largely failed due to severe side effects (Ulbrich et al. 2003).

Furthermore, treatment strategies blocking CCR2 showed promising results in rheumatoid arthritis and multiple sclerosis, however, clinical trials failed (Karpus et al. 1997; Ogata et al. 1997; Beaulieu et al. 2006). Another study aimed at reducing atherogenesis by prolonged blocking of CCR2 signaling with the CCR2 antagonist 15a (Bot et al. 2017). This treatment strategy successfully reduced atherosclerotic lesion development (Bot et al. 2017). But, the prolonged blockage of CCR2 signaling resulted in reduced numbers of circulating monocytes, thus enhancing the risk of side effects (Bot et al. 2017). In the established chronotherapy presented here, timed treatment with the CCR2 antagonist RS102895 at ZT17 only targeted the period, when leukocyte recruitment was at its highest, due to the short half-life of the antagonist. Timed administration of the CCR2 antagonist reduced atherosclerotic lesion development without affecting the number of circulating cells or CCL2 plasma levels. Furthermore, we reduced unwanted secondary effects by considering distinct recruitment patterns in other tissues. Therefore, we determined the time- and side specificity of rhythmic myeloid cell recruitment in the macro- and microcirculation. The number of adherent myeloid cells peaked in the macrocirculation at ZT1, while an opposing phenotype with a peak at ZT13 occurred in the microcirculation. This data is in agreement with previous studies and highlights distinct rhythmic leukocyte recruitment patterns in diverse tissues, which are beneficial for reducing side effects and defining treatment specificity (Scheiermann et al. 2012). In our study, the time- and side specificity of rhythmic myeloid cell recruitment already proposed minor side effects and indeed, timed CCR2 blockage had no severe effects on acute lung injury, a disease model involving microcirculation. Hence, the results of our study underline the importance of defining circadian rhythmicity of drug targets to enhance drug efficacy and to reduce the magnitude of side effects.

Next to considering the rhythmic presence or activity of the drug target, time-dependent drug absorption, distribution, metabolism, and excretion play an important role in chronotherapeutic trials by influencing the drug effective period. Genome-wide analysis of gene expression revealed a circadian rhythm in the expression of many genes encoding proteins responsible for drug metabolism, thus resulting in time-dependent bioavailability and chronotoxicity (Panda et al. 2002; Gachon et al. 2006). We confirmed a similar pharmacokinetic of the CCR2 antagonist RS102895 at ZT1 and ZT13. In contrast, other drugs such as benzodiazepines, paracetamol, and antidepressants revealed a chronopharmacokinetic effect with an enhanced drug absorption and metabolism early in the morning (Nakano et al. 1983; Kamali et al. 1987; Müller et al. 1987). These examples emphasize the existence of time-dependent fluctuations not only at the level of drug targets but also in drug distribution, metabolism, and elimination.

The successful establishment of a chronotherapy to ameliorate atherosclerosis with only minor side effects in mice leads to the question whether this treatment strategy can be transferred into humans. Circadian rhythmicity was observed for CCR2 on circulating classical monocytes in humans (Schloss et al. 2017). However, transferring chronotherapy into humans is practically difficult due to distinct rhythmic gene expression in individuals mediated by the influence of distinct life styles. Shift work, type of diet, mealtimes or stress impact on the circadian clock and affect the life of an individual person to a different extent (Leone et al. 2015; Zarrinpar et al. 2014; Eckel-Mahan et al. 2013). Although examples for timed treatment strategies as mentioned above are already used in clinic, each chronotherapy has to be taken with caution before applying it to an individual person. Furthermore, patients in clinic already suffer from clinical outcomes caused by advanced atherosclerotic lesions. But our treatment strategy targets leukocyte recruitment during the early development of atherosclerosis, hence our established pharmacotherapy would only be useful for patients who did not developed atherosclerotic lesions so far. Future research on circadian rhythmicity in advanced atherosclerotic lesions and in humans will provide a new platform for possible chronotherapies, which might be more beneficial to be transferred into clinic. Taken together, our novel chronopharmacological treatment strategy to prevent the development of atherosclerosis highlights the importance and benefits of timed therapies. However, limitations are given by transferring this chronotherapy into humans.

5.4 Outlook

Integral parts of the immune system display circadian rhythmicity, thus modulating immune responses (Keller et al. 2009; Scheiermann et al. 2012; Nguyen et al. 2013; Gibbs et al. 2014). Previous studies identified the influence of core clock proteins on the development of atherosclerosis (Pan et al. 2013; Yang et al. 2016; Huo et al. 2017). However, little is known about to what extent inflammatory processes in atherosclerosis exhibit circadian rhythmicity, thus providing targets for chronopharmacological treatment strategies. Due to the novelty of this study that rhythmic leukocyte recruitment in early lesion development is guided through the CCL2-CCR2 axis, a chronopharmacological treatment strategy was generated to ameliorate atherosclerosis. Hence, these results comprehensively expend our knowledge about circadian rhythmicity during chronic inflammation and highlight the success of timed chronotherapy. But, our study also raises further questions for future research projects.

With the identification of circadian rhythmicity in components of the immune system, which play a major role during the early stage of atherosclerosis, our study indicates a complex

regulatory mechanism of the circadian clock during distinct disease models. Due to controversial results observed during leukocyte recruitment in steady state or acute inflammation as discussed above, the influence of diet, tissue specificity or chronic inflammation on the rhythmic transcriptome and leukocyte recruitment needs to be further investigated in detail.

While our study focused on the impact of the circadian clock on early atherosclerotic lesion development, it also attracts attention to investigate circadian rhythmicity in further stages of atherosclerosis. In a later stage of atherosclerosis, an advanced atherosclerotic lesion has been established. Advanced atherosclerotic lesions contain a necrotic core surrounded by a fibrous cap that prevents the lesion from breaking apart. The main cell types controlling inflammation and stability within this lesion are macrophages and smooth muscle cells, while leukocyte recruitment is less important. After a period of time, continuous inflammation with enhanced cell death and fibrous cap thinning causes instability and finally lesion rupture with severe clinical outcomes, such as myocardial infarction or stroke. Previous studies describe circadian rhythmicity in distinct inflammatory processes such as pro-inflammatory cytokine release, cell death, and resolution of inflammation, which also play an important role in advanced atherosclerotic lesions (Young et al. 1995; Spengler et al. 2012; Wang et al. 2015; Huo et al. 2017). However, these rhythmic inflammatory processes might differ in distinct cell types and in a chronic inflammatory environment. Therefore, further research on identifying rhythmicity in inflammatory processes in different cell types within an advanced atherosclerotic lesion will provide new insights into the relation of the circadian clock and atherosclerosis. Overall, identifying peaks in inflammatory processes within 24 hours could also give conclusions why the incidence of myocardial infarction or stroke peaks early in the morning (Mueller et al. 1985). Furthermore, determining rhythmic inflammatory processes will provide a new platform for possible pharmacological targets.

The generation of a novel chronopharmacological treatment strategy that ameliorates early atherosclerotic lesion development in an animal model, questions whether this chronotherapy can be transferred into humans. Therefore, future investigations in humans are necessary to provide conclusions about similarities in rhythmic inflammatory processes. However, most patients in clinic already suffer from advanced atherosclerotic lesions. Thus, the established chronopharmacological treatment strategy presented here could only be beneficial for patients with a high risk for cardiovascular diseases, who did not development atherosclerosis so far. To avoid the inconveniences of a prolonged pharmacotherapy to prevent early atherosclerotic lesion development, future studies on circadian rhythmicity in advanced atherosclerotic lesions are adjuvant to generate a novel chronotherapy for

patients, who are already in clinic. Furthermore, the concept of chronotherapy can also be transferred to other oscillating targets including PPARγ and TNF, whose pharmacological targeting has thus far failed, or evoked serious side effects under untimed regimes (Ryan et al., 2011; Nissen et al., 2007).

Taken together, future research focusing on rhythmic inflammatory processes during the pathogenesis of atherosclerosis and on chronopharmacology will improve therapeutic strategies for cardiovascular diseases.

References

Abrahamsen, J.F. et al. Variation in cell yield and proliferative activity of positive selected human CD34+ bone marrow cells along the circadian time scale. *Eur. J. Haematol.*, 60:7-15 (1998).

Aiello, R.J. et al. Monocyte chemoattractant protein-1 accelerates atherosclerosis in apolipoprotein E-deficient mice. *Arterioscler. Thromb. Vasc. Biol.*, 19:1518-1525 (1999).

Akashi, M. et al. Hypercholesterolemia causes circadian dysfunction: a potential risk factor for cardiovascular disease. *EBioMedicine*, 20:127-136 (2017).

Alard, J.E. et al. Recruitment of classical monocytes can be inhibited by disturbing heteromers of neutrophil HNP1 and platelet CCL5. *Sci Transl Med.*, 7(317):317ra196 (2015).

Arjona, A. et al. Circadian rhythms of granzyme B, perforin, IFN-γ, and NK cell cytolytic activity in the spleen: effects of chronic ethanol. *J. Immunol.*, 172:2811-2817 (2004).

Asher, G. et al. SIRT1 regulates circadian clock gene expression through PER2 deacetylation. *Cell*, 134:317-328 (2008).

Auffray, C. et al. Blood monocytes: development, heterogeneity, and relationship with dendritic cells. *Annu. Rev. Immunol.*, 27:669-92 (2009).

Auffray, C. et al. Monitoring of blood vessels and tissues by a population of monocytes with patrolling behavior. *Science*, 317:666-670 (2007).

Baratchi, S. et al. Molecular sensors of blood flow in endothelial cells. *Trends Mol. Med.*, (9):850-868 (2017).

Barnes, P.J. et al. Anti-inflammatory actions of glucocorticoids: molecular mechanisms. *Clin. Sci. (Lond),* 94(6):557-72 (1998).

Barreiro O. et al. Dynamic interactions of VCAM-1 and ICAM-1 with moesin and ezrin in a novel endothelial docking structure for adherent leukocytes. *J. Cell Biol.*, 157:1233-1245 (2002).

Bdeir, K. et al. Defensin promotes the binding of lipoprotein(a) to vascular matrix. *Blood*, 94:2007-2019 (1999).

Beaulieu, A. et al. The efficacy and safety of a CCR2 receptor antagonist in the treatment of rheumatoid arthritis. *Ann. Rheum. Dis.*, 65(Suppl II):175 (2006).

Bellet, M.M. et al. Mammalian circadian clock and metabolism – the epigenetic link. *J. of Cell Sci.*, 123:3837-3848 (2010).

Bollinger, T. et al. Circadian clocks in mouse and human CD4+ T cells. *PLoS One*, 6(12):e29801 (2011).

Boring, L. et al. Decreased lesion formation in CCR2-/- mice reveals a role for chemokines in the initiation of atherosclerosis. *Nature*, 394:894-897 (1998).

Bot, I. et al. A novel CCR2 antagonist inhibits atherogenesis in apoE deficient mice by achieving high receptor occupancy. *Sci. Rep.,* 7(1):52 (2017).

Brown, S.A. et al. Rhythms of mammalian body temperature can sustain peripheral circadian clocks. *Curr. Biol.*, 12(18):1574-1583 (2002).

Bunger, M.K. et al. Mop3 is an essential component of the master circadian pacemaker in mammals. *Cell*, 103(7):1009-1017 (2000).

Campdell, I.D. et al. Integrin structure, activation, and interactions. *Cold Spring Harb. Perspect. Biol.,* 3,a004994 (2011).

Casanova-Acebes, M. et al. Rhythmic modulation of the hematopoietic niche through neutrophil clearance. *Cell*, 153:1025-1035 (2013).

Chalkiadaki, A. et al. High-fat diet triggers inflammation-induced cleavage of SIRT1 in adipose tissue to promote metabolic dysfunction. *Cell Metab.*, 16(2):180-188 (2012).

Chalmers, J.A. et al. Vascular circadian rhythms in a mouse vascular smooth muscle cell line (Movas-1). *Am. J. Physiol. Requl. Integr. Comp. Physiol.*, 295(5):R1529-38 (2008).

Chaly, Y.V. et al. Neutrophil alpha-defensin human neutrophil peptide modulates cytokine production in human monocytes and adhesion molecule expression in endothelial cells. *Eur. Cytokine Netw.*, 11:257-266 (2000).

Chang, H.C. et al. SIRT1 mediates central circadian control in the SCN by a mechanism that decays with aging. *Cell*, 153:1448-1460 (2013).

Cheng, B. et al. Tissue-intrinsic dysfunction of circadian clock confers transplant arteriosclerosis. *Proc. Natl. Acad. Sci. U S A*, 108(41):17147-52 (2011).

Chiu, J.J. and Chien S. Effects of disturbed flow and vascular endothelium: pathophysiological basis and clinical perspectives. *Physiol. Rev.,* 91:327-387 (2011).

Clarke, M.C. et al. Apoptosis of vascular smooth muscle cells induces features of plaque vulnerability in atherosclerosis. *Nat Med.*, 12:1075-1080 (2006).

Cosentino, M. et al. Adrenergic regulation of innate immunity: A review. *Front Pharmacol.*, 6:171 (2015).

Curtis, A.M. et al. Circadian clock proteins and immunity. *Immunity*, 40(2):178-186 (2014).

Da Costa Martins, P. et al. P-Selectin glycoprotein ligand-1 is expressed on endothelial cells and mediates monocyte adhesion to activated endothelium. *Arterioscler. Thromb. Vasc. Biol.*, 27:1023-1029 (2007).

Dai, G. et al. Distinct endothelial phenotypes evoked by arterial waveforms derived from atherosclerosis-susceptible and -resistant regions of human vasculature. *Proc. Natl. Acad. Sci. U S A.*, 101(41):14871-14876 (2004).

Damiola, F. et al. Restricted feeding uncouples circadian oscillators in peripheral tissues from the central pacemaker in the suprachiasmatic nucleus. *Genes Dev.*, 14:2950-2961 (2000).

de Mairan, JJO. "Observation Botanique", *Histoire de l'Academie Royale des Science,* 35-36 (1729).

de Paz, J.L. et al. Profiling heparin-chemokine interactions using synthetic tools. *ACS Chem. Biol.*, 2:735-744 (2007).

Dimitrov, S. et al. Cortisol and epinephrine control opposing circadian rhythms in T cell subsets. *Blood*, 113(21):5134-43 (2009).

Doeing, D. C. et al. Gender dimorphism in differential peripheral blood leukocyte counts in mice using cardiac, tail, foot, and saphenous vein puncture methods. *BMC Clin. Pathol.* 3,3 (2003).

Doering, Y. et al. Lack of neutrophil-derived CRAMP reduces atherosclerosis in mice. *Circ. Res.*, 110:1052-1056 (2012).

Dong, Z.M. et al. The combined role of P- and E-selectins in atherosclerosis. *J. Clin. Invest.*, 102(1):145-152 (1998).

Drechsler, M. et al. Hyperlipidemia-triggered neutrophilia promotes early atherosclerosis. *Circulation,* 122:1837-1845 (2010).

Drechsler, M. et al. The complexity of arterial classical monocyte recruitment. *J. Innate Immun.*, 5:358-366 (2013).

Druzd, D. et al. Lymphocyte circadian clocks control lymph node trafficking and adaptive immune responses. *Immunity*, 46:120-132 (2017).

Eckel-Mahan, K.L. et al. Reprogramming of the circadian clock by nutritional challenge. *Cell*, 155:1464-1478 (2013).

Feng, D. et al. Clocks, metabolism, and the epigenome. *Mol. Cell.*, 47:158-167 (2012).

Fernandes, G. et al. Circadian rhythm in activity of lympholytic natural killer cells from spleens of fischer rats. *J. Immunol.*, 123:622-625 (1979).

Gachon, F. et al. The circadian PAR-domain basic leucine zipper transcription factors DBP, TEF, and HLF modulate basal and inducible xenobiotic detoxification. *Cell Metab.,* 4(1):25-36 (2006).

Gao, Y. et al. Clock upregulates intercellular adhesion molecule-1 expression and promotes mononuclear cells adhesion to endothelial cells. *Biochem. Biophys. Res. Commun.,* 443:586-591 (2014).

Gauchon, F. et al. The mammalian circadian timing system: from gene expression to physiology. *Chromosoma*, 113:103-112 (2004).

Gibbs, J. et al. An epithelial circadian clock controls pulmonary inflammation and glucocorticoid action. *Nat. Med.*, 20(8):919-926 (2014).

Ginhoux, F. et al. Monocytes and macrophages: developmental pathways and tissue homeostasis. *Nat. rev. Immunol.*, 14(6):392-404 (2014).

Grommes, J. et al. Contribution of neutrophils to acute lung injury. *Mol. Med.*, 17(3-4):293-307 (2011).

Gu, L. et al. Absence of monocyte chemoattractant protein-1 reduces atherosclerosis in low density lipoprotein receptor-deficient mice. *Mol. Cell.*, 2:275-281 (1998).

Guo, H. et al. Differential control of peripheral circadian rhythms by suprachiasmatic-dependent neural signals. *PNAS*, 102(8):3111-3116 (2005).

Hansson, G.K. and Hermansson, A. The immune system in atherosclerosis. *Nat. Immunol.,* 12:204-212 (2011).

Hermida, R.C. et al. Aspirin administered at bedtime, but not on awakening, has an effect on ambulatory blood pressure in hypertensive patients. *J. Am. Coll. Cardiol.*, 20;46(6):975-83 (2005).

Herzog, E.D. et al. Neurons and networks in daily rhythms. *Nat. Rev. Neurosci.*, 8:790-802 (2007).

Hou, L. et al. Effect of hyperlipidemia on the expression of circadian genes in apolipoprotein E knock-out atherosclerotic mice. *Lipids Health Dis.*, 8:60 (2009).

Huo, M. et al. Myeloid Bmal1 deletion increases monocyte recruitment and worsens atherosclerosis. *FASEB J.*, 31(3):1097-1106 (2017).

Huo, Y. et al. Circulating activated platelets exacerbate atherosclerosis in mice deficient in apolipoprotein. *Nat. Med.*, 9(1):61-7 (2003).

Iiyama, K. et al. Patterns of vascular cell adhesion molecule-1 and intercellular adhesion molecule-1 expression in rabbit and mouse atherosclerotic lesions and at sites predisposed to lesion formation. *Circ. Res.*, 85:199-207 (1999).

Ikeda, Y. et al. Modulation of circadian glucocorticoid oscillation via adrenal opiod-CXCR7 signaling alters emotional behavior. *Cell*, 155:1323-1336 (2013).

Ishibashi, S. et al. Hypercholesterolemia in low density lipoprotein receptor knockout mice and its reversal by adenovirus-mediated gene delivery. *J. Clin. Invest.*, 92:883-893 (1993).

Kamali, F. et al. Temporal variations in paracetamol absorption and metabolism in man. *Xenobiotica.*, 17(5):635-41 (1987).

Karpus, W. et al. MIP-la and MCP-1 differentially regulate acute and relapsing autoimmune encephalomyelitis as well as Thl/1h2 lymphoctye differentiation. *J. Leukoc. Biol.*, 62:681-687 (1997).

Keller, M. et al. A circadian clock in macrophages controls inflammatory immune responses. *Proc. Natl. Acad. Sci. U S A*, 106(50):21407-21412 (2009).

Kiessling, S. et al. The circadian clock in immune cells controls the magnitude of Leishmania parasite infection. *Sci. Rep.*, 7(1):10892 (2017).

King, D.P. et al. Positional cloning of the mouse circadian clock gene. *Cell*, 89:641-653 (1997).

Knutsson, A. et al. Increased risk of ischaemic heart disease in shift workers. *Lancet.,* 2:89-92 (1986).

Kohsaka, A. et al. High-fat diet disrupts behavioral and molecular circadian rhythms in mice. *Cell Met.*, 6:414-421 (2007).

Kolaczkowska, E. et al. Neutrophil recruitment and function in health and inflammation. *Nat. Rev. Immunol.*, 13(3):159-75 (2013).

Kornmann, B. et al. System-driven and oscillator-dependent circadian transcription in mice with a conditionally active liver clock. *PLoS Biol.*, 5(2):e34 (2007).

Kouri, V.P. et al. Circadian timekeeping is disturbed in rheumatoid arthritis at molecular level. *PLoS One*, 8(1):e54049 (2013).

Kunjathoor, V.V. et al. Scavenger receptors class A-I/II and CD36 are the principal receptors responsible for the uptake of modified low density lipoprotein leading to lipid loading in macrophages. *J. Biol.Chem.*, 277(51):49982-8 (2002).

Kuschert, G. S. et al. Glycosaminoglycans interact selectively with chemokines and modulate receptor binding and cellular responses. *Biochemistry*, 38:12959-12968 (1999).

Kyaw, T. et al. Cytotoxic and proinflammatory $CD8^+$ T lymphocytes promote development of vulnerable atherosclerotic plaques in ApoE-deficient mice. *Circulation*, 127:1028-1039. (2013).

Leone, V. et al. Effects of diurnal variation of gut microbes and high-fat feeding on host circadian clock function and metabolism. *Cell Host Microbe*, 17(5):681-9 (2015).

Ley, K. et al. Getting to the site of inflammation: the leukocyte adhesion cascade updated. *Nat. Rev. Immunol.,* 7:678-689 (2007).

Lin, C. et al. The rhythmic expression of clock genes attenuated in human plaque-derived vascular smooth muscle cells. *Lipids Health Dis.*, 13:14 (2014).

Liyama, K. et al. Patterns of vascular cell adhesion molecule-1 and intercellular adhesion molecule-1 expression in rabbit and mouse atherosclerotic lesions and at sites predisposed to lesion formation. *Circ. Res.*, 85:199-207 (1999).

Llogan, R.W. et al. Chronic shift-lag alters the circadian clock of NK cells and promotes lung cancer growth in rats. *J. Immunol.*, 188(6):2583-91 (2012).

Long, J.E. et al. Morning vaccination enhances antibody response over afternoon vaccination: A cluster-randomised trial. *Vaccine*, 34(24):2679-85 (2016).

Lutshumba, J. et al. Deletion of BMAL1 (Brain and Muscle ARNT-Like Protein-1) in smooth muscle cells protects mice from abdominal aortic aneurysms. *Arterioscler. Thromb. Vasc. Biol.,* 2018;38:00-00 (2018).

Ma, H. et al. Increased atherosclerotic lesions in LDL receptor deficient mice with hematopoietic nuclear receptor rev-erbα knock- down. *J. Am. Heart Assoc.*, 2:e000235 (2013).

Marcovecchio, P.M. et al. Scavenger receptor CD36 directs nonclassical monocyte patrolling along the endothelium during early atherogenesis. *Arterioscler. Thromb. Vasc. Biol.*, 37:2043-2052 (2017).

Méndez-Ferrer, S. et al. Haematopoietic stem cell release is regulated by circadian oscillation. *Nature*, 452:442-447 (2008).

Middleton, J. et al. Leukocyte extravasation: chemokine transport and presentation by the endothelium. *Blood*, 100:3853-3860 (2002).

Mitchell, L.A. et al. Optimized dosing of a CCR2 antagonist for amplification of vaccine immunity. *Int. Immunopharmacol.*, 15(2):357-63 (2013).

Mohawk, J.A. et al. Central and peripheral circadian clocks in mammals. *Annu. Rev. Neurosci.*, 35:445-62 (2012).

Moore, K.J. and Tabas, I. Macrophages in the pathogenesis of atherosclerosis. *Cell*, 145:341-355 (2011).

Mordelet, E. et al. Chemokine transport across human vascular endothelial cells. *Endothelium*, 14(1):7-15 (2006).

Mueller, J.E. et al. The MILIS study group: Circadian variation in the frequency of onset of acute myocardial infarction. *N. Engl. J. Med.*, 313:1315-1322 (1985).

Müller, F.O. et al. Pharmacokinetics of temazepam after day-time and night-time oral administration. *Eur. J. Clin. Pharmacol.*, 33(2):211-4 (1987).

Murphy, A.J. et al. ApoE regulates hematopoietic stem cell proliferation, monocytosis, and monocyte accumulation in atherosclerotic lesions in mice. *J. Clin. Invest.*, 121(10):4138-4149 (2011).

Murray, D.B. et al. Clock control of ultradian respiratory oscillation found during yeast continuous culture. *J. Bacteriol.*, 183(24):7253-7259 (2001).

Nader, N. et al. Circadian rhythm transcription factor CLOCK regulates the transcriptional activity of the glucocorticoid receptor by acetylating its hinge region lysine cluster: potential physiological implications. *FASEB J.*, 23:1572-1583 (2009).

Nahrendorf, M. et al. The healing myocardium sequentially mobilizes two monocyte subsets with divergent and complementary functions. *J. Exp. Med.*, 204:3037-3047 (2007).

Nakahata, Y. et al. The NAD+-dependent deacetylase SIRT1 modulates CLOCK-mediated chromatin remodeling and circadian control. *Cell*, 134:329-340 (2008).

Nakano, S. et al. Chronopharmacology of amitriptyline. *Clin. Pharmacol. Ther.*, 33(4):453-9 (1983).

Nakashima, Y. et al. Upregulation of VCAM-1 and ICAM-1 at atherosclerosis-prone sites on the endothelium in the ApoE-deficient mouse. *Arterioscler. Thromb. Vasc. Biol.,* 18:842-851 (1998).

Napoli, F.C. et al. Fatty streak formation occurs in human fetal aortas and is greatly enhanced by maternal hypercholesterolemia. Intimal accumulation of low density lipoprotein and its oxidation precede monocyte recruitment into early atherosclerotic lesions. *J. Clin. Invest.*, 100(11):2680-2690 (1997).

Nguyen, K.D. et al. Circadian gene Bmal1 regulates diurnal oscillations of Ly6C^{hi} inflammatory monocytes. *Science*, 341(6153):1481-8 (2013).

Nissen, S.E. et al. Effect of rosiglitazone on the risk of myocardial infarction and death from cardiovascular causes. *N. Engl. J. Med.*, 356:2457-2471 (2007).

Ogata, H. et al. The role of monocyte chemoattractant protein-1 (MCP-1) in the pathogenesis of collagen-induced arthritis in rats. *J. Pathol.*, 182:106-114 (1997).

Ortega-Gomez, A. et al. Cathepsin G controls arterial but not venular myeloid cell recruitment. *Circulation*, 134:1176-1188 (2016).

Pan, X. et al. Impaired cholesterol metabolism and enhanced atherosclerosis in clock mutant mice. *Circulation*, 128(16):1758-1769 (2013).

Panda, S. et al. Coordinated transcription of key pathways in the mouse by the circadian clock. *Cell*, 109(3):307-20. (2002).

Phillipson, M. et al. Intraluminal crawling of neutrophils to emigration sites: a molecularly distinct process from adhesion in the recruitment cascade. *J. Exp. Med.*, 203(12):2569-75 (2006).

Poupel, L. et al. Pharmacological inhibition of the chemokine receptor, CX3CR1, reduces atherosclerosis in mice. *Arterioscler. Thromb. Vasc. Biol.*, 33:2297-2305 (2013).

Preitner, N. et al. The orphan nuclear receptor REV-ERB controls circadian transcription within the positive limb of the mammalian circadian oscillator. *Cell*, 110:251-260 (2002).

Prinz, P.N. et al. Circadian variation of plasma catecholamines in young and old men: relation to rapid eye movement and slow wave sleep. *J. Clin. Endocrinol. Metab.*, 49(2):300-4 (1979).

Ralph, M.R. et al. Transplanted suprachiasmatic nucleus determines circadian period. *Science*, 247(4945):975-8 (1990).

Reape, T.J. et al. Chemokines and atherosclerosis. *Atherosclerosis*, 147:213-225 (1999).

Robbins, C.S. et al. Extramedullary hematopoiesis generates Ly-6Chigh monocytes that infiltrate atherosclerotic lesions. *Circulation*, 125:364-374 (2012).

Rorvig, S. et al. Proteome profiling of human neutrophil granule subsets, secretory vesicles, and cell membrane: correlation with transcriptome profiling of neutrophil precursors. *J. Leukoc. Biol.*, 94:711-721 (2013).

Rossaint, J. et al. Tissue-specific neutrophil recruitment into the lung, liver, and kidney. *J. Innate Immun.*, 5:348-357 (2013).

Roth, G.A. et al. Global and regional patterns in cardiovascular mortality from 1990 to 2013. *Circulation*, 132:1667-1678 (2015).

Rudic, R.D. et al. Bioinformatic analysis of circadian gene oscillation in mouse aorta. *Circulation*, 112:2716-2724 (2005).

Ryan, C. et al. Association between biologic therapies for chronic plaque psoriasis and cardiovascular events: a meta-analysis of randomized controlled trials. *JAMA.,* 306:864-871 (2011).

Saederup, N. et al. Fractalkine deficiency markedly reduces macrophage accumulation and atherosclerotic lesion formation in CCR2$^{-/-}$ mice. *Circulation*, 117:1642-1648 (2008).

Saito, Y. et al. Comparison between morning and evening doses of simvastatin in hyperlipidemic subjects. *Arterioscler. Thromb.*, ll:816-826 (1991).

Sakai, A. et al. P-Selectin and vascular cell adhesion molecule-1 are focally expressed in aortas of hypercholesterolemic rabbits before intimal accumulation of macrophages and T lymphocytes. *Arterioscler. Thromb. Vasc. Biol.*, 17:310-316 (1997).

Sato, T.K. et al. A Functional genomics strategy reveals rora as a component of the mammalian circadian clock. *Neuron*, 43:527-537 (2004).

Scheiermann, C. et al. Adrenergic nerves govern circadian leukocyte recruitment to tissues. *Immunity*, 37(2):290-301 (2012).

Scheiermann, C. et al. Circadian control of the immune system. *Nat. Rev. Immunol.*, 13(3): 190-198 (2013).

Schenkel, A.R. et al. Locomotion of monocytes on endothelium is a critical step during extravasation. *Nat. Immunol.*, 5:393-400 (2004).

Schloss, J.M. et al. The time-of-day of myocardial infarction onset affects healing through oscillations in cardiac neutrophil recruitment. *EMBO Mol. Med.*, 8:937-948 (2016).

Shih, P.T. et al. Blocking very late antigen-4 integrin decreases leukocyte entry and fatty streak formation in mice fed an atherogenic diet. *Circ. Res*., 84:345-351 (1999).

Sica, D. et al. Pharmacokinetics of propranolol after single and multiple dosing with sustained release propranolol or propranolol CR (innopran XL) , a new chronotherapeutic formulation. *Heart Dis.*, 5(3):176-81 (2003).

Silver, A.C. et al. Circadian expression of clock genes in mouse macrophages, dendritic cells, and B cells. *Brain Behav. Immun.*, 26(3):407-413 (2012).

Silver, C.S. et al. The circadian clock controls toll-like receptor 9-mediated innate and adaptive immunity. *Immunity*, 36:251-261 (2012).

Sitaula, S. et al. Suppression of atherosclerosis by synthetic REV-ERB agonist. *Biochem. Biophys. Res. Co*mmun., 460(3):566-571 (2015).

Soehnlein, O. et al. Distinct functions of chemokine receptor axes in the atherogenic mobilization and recruitment of classical monocytes*. EMBO Mol. Med.*, 5:471-481 (2012).

Soehnlein, O. et al. Mechanisms underlying neutrophil-mediated monocyte recruitment. *Blood*, 114(21):4613-23 (2009).

Soehnlein, O. et al. Neutrophil primary granule proteins HBP and HNP1–3 boost bacterial phagocytosis by human and murine macrophages. *J. Clin. Invest.*, 118:3491-3502 (2008b).

Soehnlein, O. et al. Neutrophil secretion products pave the way for inflammatory monocytes. *Blood,* 112:1461-1471 (2008).

Soehnlein, O. et al. Neutrophil secretion products regulate anti-bacterial activity in monocytes and macrophages. *Clin. Exp. Immunol.*, 151:139-145 (2008c).

Soehnlein, O. et al. Phagocyte partnership during the onset and resolution of inflammation. *Nat. Rev. Immunol.,* 10:427-439 (2010).

Somanath, P.R. et al. Deficiency in core circadian protein Bmal1 is associated with a prothrombotic and vascular phenotype. *J. Cell Physiol.*, 226(1):132-140 (2011).

Spengler, M.L. et al. Core circadian protein CLOCK is a positive regulator of NF-κB–mediated transcription. *PNAS,* 109(37):E2457-2465 (2012).

Spertini, O. et al. P-selectin glycoprotein ligand 1 is a ligand for L-selectin on neutrophils, monocytes, and $CD34^+$ hematopoietic progenitor cells. *J. Cell Biol.*, 135(2):523-531 (1996).

Sumagin, R. et al. LFA-1 and Mac-1 define characteristically different intralumenal crawling and emigration patterns for monocytes and neutrophils in situ. *J. Immunol.*, 185:7057-7066 (2010).

Swirski, F.K. et al. Identification of splenic reservoir monocytes and their deployment to inflammatory sites. *Science*, 325(5940):612-616 (2009).

Swirski, F.K. et al. Ly-6Chi monocytes dominate hypercholesterolemia-associated monocytosis and give rise to macrophages in atheromata. *J. Clin. Invest.*, 117(1):195-205 (2007).

Tabas, I. et al. Subendothelial lipoprotein retention as the initiating process in atherosclerosis. *Circulation*, 116:1832-1844 (2007).

Tacke, F. et al. Monocyte subsets differentially employ CCR2, CCR5, and CX3CR1 to accumulate within atherosclerotic plaque. *J. Clin. Invest.*, 117:185-194 (2007).

Taekema-Roelvink, M.E. et al. Proteinase 3 enhances endothelial monocyte chemoattractant protein-1 production and induces increased adhesion of neutrophils to endothelial cells by upregulating intercellular cell adhesion molecule-1. *J. Am. Soc. Nephrol.*, 12:932-940 (2001).

Thomas, G. et al. Nonclassical patrolling monocyte function in the vasculature. *Arterioscler. Thromb. Vasc. Biol*., 35:1306-1316 (2015).

Ulbrich, H. et al. Leukocyte and endothelial cell adhesion molecules as targets for therapeutic interventions in inflammatory disease. *Trends Pharmacol. Sci.*, 24(12):640-647 (2003).

Vestweber, D. How leukocytes cross the vascular endothelium. *Nat. Rev. Immunol.,* 15:692-704 (2015).

Viswambharan, H. et al. Mutation of the circadian clock gene Per2 alters vascular endothelial function. *Circulation*, 115:2188-2195 (2007).

Wang, Y. et al. Circadian gene hClock enhances proliferation and inhibits apoptosis of human colorectal carcinoma cells in vitro and in vivo. *Mol. Med. rep.*, 11:4204-4210 (2015).

Wantha, S. et al. Neutrophil-derived cathelicidin promotes adhesion of classical monocytes. *Circ. Res.*, 112(5):792-801 (2013).

Watanabe, T. et al. Atherosclerosis and inflammation mononuclear cell recruitment and adhesion molecules with reference to the implication of ICAM-1/LFA-1 pathway in atherogenesis. *Int. J. Cardiol.*, 66(Suppl 1):S45-S53 (1998).

Weber, C. et al. The multifaceted contributions of leukocyte subsets to atherosclerosis: lessons from mouse models. *Nat. Rev. Immunol.*, 8:802-815 (2008).

Weber, K.S. et al. Differential immobilization and hierarchical involvement of chemokines in monocyte arrest and transmigration on inflamed endothelium in shear flow. *Eur. J. Immunol.* 29:700-712 (1999).

Weber, KS. et al. Differential immobilization and hierarchical involvement of chemokines in monocyte arrest and transmigration on inflamed endothelium in shear flow. *Eur. J. Immunol.*, 29(2):700-12 (1999).

White, W.B. et al. Nocturnal dosing of a novel delivery system of verapamil for systemic hypertension. *Am. J. Cardiol.*, 76:375-380 (1995).

Winter, C. et al. Chrono-pharmacological targeting of the CCL2-CCR2 axis ameliorates atherosclerosis. *Cell Metab.,* 28(1):175-182.e5 (2018).

Witt, D.P. et al. Differential binding of chemokines to glycosaminoglycan subpopulations. *Curr. Biol.*, 4:394-400 (1994).

Yang, G. et al. Timing of expression of the core clock gene Bmal1 influences its effects on aging and survival. *Sci. Transl. Med.*, 8(324):324ra16 (2016).

Yang, L. et al. Overexpression of CRY1 protects against the development of atherosclerosis via the TLR/NF-κB pathway. *Int. Immunopharmacol.*, 28(1):525-30 (2015).

Yoo, S.H. et al. PERIOD2::LUCIFERASE real-time reporting of circadian dynamics reveals persistent circadian oscillations in mouse peripheral tissues. *PNAS*, 101(15):5339-5346 (2004).

Young, M.R.I. et al. Circadian rhythmometry of serum interleukin-2, interleukin-10, tumor necrosis factor-α, and granulocyte-macrophage colony-stimulating factor in men. *Chronobiol. Int,,* 12(1):19-27 (1995).

Zarrinpar, A. et al. Diet and feeding pattern affect the diurnal dynamics of the gut microbiome. *Cell Metab.*, 20(6):1006-17 (2014).

Zernecke, A. et al. Chemokines in atherosclerosis: an update*. Arterioscler. Thromb. Vasc. Biol.,* 28:1897-1908 (2008).

Zernecke, A. et al. Deficiency in CCR5 but not CCR1 protects against neointima formation in atherosclerosis-prone mice: involvement of IL-10. *Blood*, 107:4240-4243 (2006).

Zhang, R. et al. A circadian gene expression atlas in mammals: Implications for biology and medicine. *PNAS*, 111:16219-16224 (2014).

Zhang, S.H. et al. Spontaneous hypercholesterolemia and arterial lesions in mice lacking apolipoprotein E. Science, 258:468-71 (1992).

Zhou, Z. et al. Lipoprotein-derived lysophosphatidic acid promotes atherosclerosis by releasing CXCL1 from the endothelium. *Cell Met.*, 13(5):p592-600 (2011).

Acknowledgments

I would like to express my special appreciation to my supervisor Univ.-Prof. Dr. Dr. med. Oliver Soehnlein for his extensive support in the past years. Furthermore, my thesis advisory committee members Dr. Christoph Scheiermann and Dr. Andrés Hidalgo helped me to successfully accomplish my PhD project.

In addition, I would like to thank my colleagues. The project would have not been so successful without your help, the awesome team spirit, and willingness to work irrespective of the time of day. I thank Patricia Lemnitzer, Janine Winter and Ariane Schumski for never hesitating helping me, Carlos Silvestre-Roig and Almudena Ortega for being helpful with their excellent advices and scientific suggestions; Laura Perez-Olivares, Pan Chang and Sanne Maas for keeping the team spirit; Quinte for providing the background music, Giovanna Leonie and Bartolo Ferrero for the italian spirit.

Furthermore, I would like to thank my family for their faith and their support during my whole life. They encouraged me to work hard without losing passion and fun. Thanks for supporting my education, my travel plans, and internships abroad in the past. Furthermore, I would like to especially thank my sisters, Merle and Finja, for your friendship. Thank you for being such a wonderful family.

And finally I would like to thank my best friends Christin, Anika, Esther, Annika, Steffi, Anso, Iris and Sara for each exciting day that I spent with you the past years. Thanks and cheers to many further seasons and experiences together.

Appendix

Publications arising from this work

Cell Metab. 2018 Jul 3;28(1):175-182.e5.

Chrono-pharmacological targeting of the CCL2-CCR2 axis ameliorates atherosclerosis.

Winter C, Silvestre-Roig C, Ortega-Gomez A, Lemnitzer P, Schumski A, Winter J, Drechsler M, de Jong R, Immler R, Sperandio M, Hristov M, Zeller T, Weber C, R. Viola J, Hidalgo A, Scheiermann C, Soehnlein O

Curr Opin Lipidol. 2018

The potential of chronopharmacology for treatment of atherosclerosis

Winter C and Soehnlein O

Arterioscler Thromb Vasc Biol. 2018 May;38(5):982-983.

TIMPing the aorta: smooth muscle cell specific deletion of BMAL1 limits murine abdominal aortic aneurysm development.

Winter C, Soehnlein O, Maegdefessel L

J Innate Immun. 2018 Apr 18. doi: 10.1159/000488091

The in and out of myeloid cells in atherosclerosis.

Schumski A, Winter C, Döring Y, Soehnlein O

Arterioscler Thromb Vasc Biol. 2017 Jun;37(6):1022-1028.

Circadian Control of Inflammatory Processes in Atherosclerosis and Its Complications.

Steffens S, Winter C, Schloss MJ, Hidalgo A, Weber C, Soehnlein O